



Andriy Sheremet

Graduated in Biology

**Bioinspired polyethersulfone-based
hollow fiber membranes as the
scaffolds in renal assist device for
protein-bound toxins removal from
blood**

Dissertation for obtaining the Master degree in Membrane
Engineering

Erasmus Mundus Master in Membrane Engineering

Advisor: D. Stamatialis, Professor, UTwente
Co-advisors: Isabel Coelho, Professor, FCT-UNL
João G. Crespo, Professor, FCT-UNL

Jury:

President: Isabel Coelho, Professor, FCT-UNL
Examiners: Damien Quemener, Professor, Montpellier University II
Vlastimil Fila, Professor, ICT-Prague
C. Portugal, Researcher, IBET
Member: João G. Crespo, Professor, FCT-UNL



FACULDADE DE
CIÊNCIAS E TECNOLOGIA
UNIVERSIDADE NOVA DE LISBOA

July 2014

Andriy Sheremet

Graduated in Biology

**Bioinspired polyethersulfone-
based hollow fiber membranes
as the scaffolds in renal assist
device for protein-bound toxins
removal from blood**

Dissertation presented to Faculdade de
Ciências e Tecnologia, Universidade Nova
de Lisboa for obtaining the master degree in
Membrane Engineering

July 2014

Bioinspired polyethersulfone-based hollow fiber membranes as the scaffolds in renal assist device for protein-bound toxins removal from blood



The EM3E Master is an Education Programme supported by the European Commission, the European Membrane Society (EMS), the European Membrane House (EMH), and a large international network of industrial companies, research centres and universities (<http://www.em3e.eu>).

Copyright @ Name, FCT/UNL

A Faculdade de Ciências e Tecnologia e a Universidade Nova de Lisboa têm o direito, perpétuo e sem limites geográficos, de arquivar e publicar esta dissertação através de exemplares impressos reproduzidos em papel ou de forma digital, ou por qualquer outro meio conhecido ou que venha a ser inventado, e de a divulgar através de repositórios científicos e de admitir a sua cópia e distribuição com objectivos educacionais ou de investigação, não comerciais, desde que seja dado crédito ao autor e editor.

Projecto financiado com o apoio da Comissão Europeia. A informação contida nesta publicação vincula exclusivamente o autor, não sendo a Comissão responsável pela utilização que dela possa ser feita.

ACKNOWLEDGMENTS

First of all I would like to acknowledge all EM3E team, and thank them for high quality education they offer.

I would like to express special thanks to UNL staff who created outstanding learning environment and made it possible for me to work on this project.

I express my sincere gratitude to my supervisors at BST group of UTwente – prof. D. Stamatialis and N. Chevtchik for their support, advice and cooperation.

Also I thank BST group members for their friendly and professional attitude.

ABSTRACT

Using bioartificial kidney is the promising approach for removal of non-dializable, protein-bound uremic toxins, which are responsible for high mortality and morbidity in treating kidney failure related conditions. Additionally, bioartificial kidney device could perform the physiological roles of the kidney such as metabolic replacement, endocrine function and immunomodulation.

In the current work two commercial polyethersulfone-based membranes, Gambro HCO 1100 and Membrana MicroPES TF10 used in haemofiltration and plasma separation applications respectively were investigated. To provide adequate cytocompatibility of the membrane biomimetic, biomimetic double layer coating was developed. First, the membranes were coated with mussel-inspired synthetic polydopamine film, following with the coating of Collagen Type IV.

Transport properties of the coated and native membranes were investigated. Increase in pure water permeability of the coated HCO 1100 membranes was observed. Membrane surface hydrophilization was assumed as the major factor responsible for the effect. Membrane permeabilities for bovine serum albumin and immunoglobulin G solutions were studied. Significant increase in protein rejection was observed for double coated HCO 1100 membranes with small or no effect of the double coated MicroPES TF10 membranes.

Next, formation of confluent monolayers of the renal epithelial cells on the membrane scaffolds was studied. Cell seeding strategy was developed and two seeding conditions were tested. Specifically, the cells were allowed to adhere to the biomimetic membranes passively, and the negative pressure was applied to facilitate cell adhesion. After cultivation in semi-batch conditions the monolayer formation was examined. Confluent monolayers were observed for the conditions with passive cell adherence for the both membranes. Cell contacts formation and cell polarization were confirmed with the staining for ZO-1 protein. Applying the pressure to facilitate cell adhesion, on the contrary, resulted in the loss of cell ability to form functional monolayers.

Keywords

Uremic toxins, Bioartificial kidney, Renal assist device, Human proximal tubule epithelial cells, ZO-1, Biomimetic surface

TABLE OF CONTENTS

ACKNOWLEDGMENTS.....	IV
Abstract	V
Table of contents	VI
Index of figures	VIII
Index of tables	X
Abbreviations	XI
1. Introduction	1
1.1. Background and motivation.....	1
1.2. Objectives	2
2. Literature review	3
2.1 Acute kidney injury overview	3
2.2 Uremic toxins in acute kidney injury	5
2.3 Traditional management of the uremic toxins	7
2.4 Protein-bound uremic toxins and their treatment	9
2.5. State of the art of bioartificial kidney development	10
2.5.1. Cell line selection.....	11
2.5.2. Membranes for bioartificial kidney applications	12
2.5.3. Biomimetic surface modification.....	13
3. Materials and methods	18
3.1. Reagents, materials and the supplies	18
3.2. Assembly of the mini-modules.....	19
3.3. Modification of PES-based hollow fiber membranes.....	19
3.4. Hollow fiber membranes characterization.....	20
3.4.1. Hydraulic permeability experiments.....	20
3.4.2. Protein permeation and apparent sieving coefficient determination.....	20
3.4.3. Scanning electron microscopy	21
3.4.4. Coating characterization by ATR-FTIR	21
3.5. Cell culture <i>in vitro</i>	21
3.5.1. Initiating the culture.....	21
3.5.2. Subculturing.....	21
3.6. Bioreactor conditions.....	22
3.6. Direct and indirect fluorescent staining.....	22
3.7. Attachment of cells to hollow fiber membranes.....	23
3.8. Cell imaging	23
3.9 Statistical analysis.....	23

4. Results and discussion.....	24
4.1. Surface characterization of hollow fiber membranes	24
4.2 Transport properties of the membranes	26
4.3 Cells attachment and proliferation.....	32
4.3.1. Preliminary characterization of the cell line	32
4.3.2 Cell attachment in hollow fiber bioreactors.....	34
4.3.3 Investigation of monolayer formation in batch bioreactor conditions.....	36
5. Conclusions and future perspectives	42
6. REFERENCES.....	43
APPENDICES.....	50
Appendix A.....	50
Comparison between the parameters of RIFLE and AKIN criteria [6]	50
Appendix B.....	51
Different groups of uremic toxins [12]	51
Appendix C.....	53
HCO 1000 membrane specification [100,118]	53
Dextran sieving curve of HCO 1100 membrane [118].....	53
Selective skin layer pore size distribution of several hemodialysis membranes [118]...	54
Appendix D.....	55
MicroPES TF10 membrane specification [99,98]	55
Latex beads sieving curve of MicroPES TF10 membrane [99].....	55
Appendix E.....	56
Membranes, mini-modules and the setub used in the current work	56
Appendix F	58
Morphology and growth patterns of subconfluent (a), near confluent (b) and superconfluent (c) human proximal tubular cells	58

INDEX OF FIGURES

Fig. 2.1. Causes of acute kidney injury [9].	4
Fig. 2.2. Acute kidney injury progress. GFR, glomerular filtration rate. NGAL, neutrophil gelatinase-associated lipocalin. Cys C, cystatin C. KIM-1, kidney injury molecule 1. IL-18, interleukin 18. GST, glutathione-S-transferase. L-FABP, liver fatty-acid-binding protein. CRP, C reactive protein. IL-6, interleukin 6 [8].....	5
Fig. 2.3. Indoxyl sulfate transport by organic anion transporters in kidney tubular cells [22,22].	7
Fig. 2.4. Effect of serum albumin modifications in uremic conditions [29].	9
Fig. 2.5. Schematic structure of the nephron [23].	11
Fig. 2.6. Schematic representation of cellular junctional complexes [47,56].	12
Fig. 2.7. Schematic representation of an integrin receptor [23].	13
Fig. 2.8. Structural formula of L-3,4-dihydroxyphenylalanine or L-DOPA.	15
Fig. 2.9. Proposed mechanism of L-DOPA oxidative self-polymerization [84].	15
Fig. 2.10. Immunostaining for tight junction ZO-1 protein (green) of renal cells after one week incubation on coated flat synthetic membranes: a – HK-2 cells on PES/PVP flat L-DOPA coated membrane; b – HPTC on L-DOPA coated PES/PVP membrane; c – HPTC on double coated with L-DOPA and collagen IV PSF/PVP membrane [54].	17
Fig. 4.1. Scanning electron microscopy images of lateral surface (a, b, c) and the cross sections (d, e, f) of HCO 1100 hollow fiber membranes.	24
Fig. 4.2. Scanning electron microscopy images of lateral surface (a, b, c) and the cross sections (d, e, f) of MicroPES hollow fiber membranes.	25
Fig. 4.3. ATR-FTIR spectra of HCO 1100 (a) and MicroPES TF10 (b) membranes: 1 – virgin membrane; 2 – L-DOPA coated membrane; 3 – L-DOPA and Col IV coated membrane.	26
Fig. 4.4. Pure water flux of HCO 1100 membranes.	27
Fig. 4.5. Pure water flux of MicroPES TF10 membranes.	28
Fig. 4.6. Hydraulic permeabilities of virgin and coated HCO 1100 (a) and MicroPES TF10 (b) membranes.	29
Fig. 4.7. Operational curve of HCO 1100 membrane for filtration of BSA (a) and IgG (b) solutions.	29
Fig. 4.8. Permeate flux of MicroPS TF10 membranes during filtration of BSA(a) and IgG (b) solutions.	30
Fig. 4.9. BSA (a) and IgG (b) sieving coefficients of HCO 1100 membranes.	31

- Fig. 4.10. BSA (a) and IgG (b) sieving coefficients of MicroPES TF10 membranes. 31
- Fig. 4.11. Human proximal tubular cells growth curve. 32
- Fig. 4.12. Immunostaining for tight junction ZO-1 protein (red) of primary tubular proximal cells after one week incubation on unmodified (a), L-DOPA coated (b) and double coated with L-DOPA and Col IV flat PES membranes. Staining for rabbit ZO-1 antibody was performed with goat anti-rabbit Texas Red labeled secondary antibody. 34
- Fig. 4.13. DAPI fluorescent staining for the nuclei of cells attached to the surface of HCO 1100 (a, c, e) and MicroPES TF10 (b, d, f) membranes: a, b – negative pressure applied, double coated membranes; c, d – passive adsorption, double coated membranes; e, f – passive adsorption, unmodified membranes. 35
- Fig. 4.14. DAPI fluorescent staining for the nuclei of cells attached to the surface of HCO 1100 (a, c, e) and MicroPES TF10 (b, d, f) membranes after 7 days of culture: a, b – negative pressure applied, double coated membranes; c, d – passive adsorption, double coated membranes; e, f – passive adsorption, unmodified membranes. 37
- Fig. 4.15. Immunostaining for tight junction ZO-1 protein (green) of primary tubular proximal cells after one week incubation on double coated with L-DOPA and Col IV hollow fiber HCO 1100 membranes. Staining for rabbit ZO-1 antibody was performed with goat anti-rabbit Alexa 488 labeled secondary antibody. 38
- Fig. 4.16. Immunostaining for tight junction ZO-1 protein (green) of primary tubular proximal cells after one week incubation on double coated with L-DOPA and Col IV hollow fiber MicroPES membranes. Staining for rabbit ZO-1 antibody was performed with goat anti-rabbit Alexa 488 labeled secondary antibody. 39
- Fig. 4.17. Immunostaining for tight junction ZO-1 protein (green) of primary tubular proximal cells after one week incubation on double coated with L-DOPA and Col IV HCO 1100 (a) and MicroPES (b) membranes. Negative pressure applied for the seeding. 39
- Fig. 4.18. Immunostaining for tight junction ZO-1 protein (green) of primary tubular proximal cells after one week incubation on virgin HCO 1100 (a) and MicroPES (b) membranes. 40

INDEX OF TABLES

Table 2.1. Toxicity profiles of selected uremic solutes.....	6
Table 3.1. Cell subculture parameters	22
Table 4.1. Cell densities on the hollow fiber membranes 24 h after the seeding.....	36
Table 4.2. Cell densities on the hollow fiber membranes after 7 days in culture	36

ABBREVIATIONS

AKI	- acute kidney injury
ATR-FTIR	- attenuated total reflectance Fourier transform infrared spectroscopy
BAK	- bioartificial kidney
BSA	- bovine serum albumin
CKD	- chronic kidney disease
C_L	- solute clearance
CMFP	- 3-carboxy-4-methyl-5-propyl-2-furanpropionate
Col IV	- collagen type IV
DAPI	- 4',6-diamidino-2-phenylindole
DPBS	- Dulbecco's phosphate buffered saline
ECM	- extracellular matrix
FBS	- fetal bovine serum
FESEM	- field emitting scanning electron microscopy
HAS	- human serum albumin
HBSS	- Hank's balanced salt solution
HD	- hemodialysis
HPTC	- human proximal tubular cells
IgG	- immunoglobulin G
IS	- indoxyl sulfate
J_v	- permeate volumetric flux
L-DOPA	- 3,4-dihydroxyphenethylamine
LFH	- laminar fume hood
L_p	- hydraulic permeability
OAT	- organic anion transporter
PA	- polyamide
PBS	- phosphate buffered saline
PES	- polyethersulfone
PVP	- polyvinylpyrrolidone
PWF	- pure water flux
RAD	- renal assist device
RCF	- relative centrifugal force
REGM	- renal epithelial growth medium
ROS	- reactive oxygen species
RRT	- renal replacement therapy
S_o	- apparent sieving coefficient
TMP	- transmembrane pressure
Tris	- tris(hydroxymethyl)aminomethane
UT	- uremic toxins
ZO-1	- zonula occludens protein-1

1. INTRODUCTION

1.1. Background and motivation

Several million people die per year worldwide from a severe condition with limited understanding of its pathophysiology and the methods of its treatment called acute kidney injury. Much more people require permanent hospitalization for treatment of its complications such as tubular necrosis, hepatorenal syndrome, rhabdomyolysis, sepsis, cardiorenal syndrome etc. Acute kidney injury is a syndrome which is related to unexplainably high mortality rates, high morbidity for which no effective commonly accepted treatment exists today.

Understanding of the acute kidney injury is limited first of all because of its extremely fast progression in patients. Most information on the mechanisms of the syndrome was obtained from animal models and from a condition called chronic kidney disease. However, the information obtained from both sources may not be extrapolated on the acute kidney injury conditions.

Uremic toxins are proposed to link kidney failure with high mortality rates and various renal and non-renal pathologies. Specific cluster of non-dializable, protein-bound uremic toxins comprises the group of 25 solutes requires the special attention due to their diverse and severe toxicity. The removal of such solutes from the bloodstream is obscured owing to their protein bound state. Numerous traditional strategies exist to overcome these limitations. Examples of such approaches are an increase in duration and frequency of haemodialysis and / or increase of the mass transfer coefficient of the dialyzer. However only below 20 % toxin removal improvement was reported. Therefore there is the strong necessity of developing novel successful strategy to remove protein-bound uremic toxins.

Such novel approaches include using protein-leaking membranes and various adsorption strategies (polymethylmethacrylate membranes, hemoperfusion, mixed matrix membranes, albumin dialysis). Another promising strategy in treating kidney failure related condition is in using bioartificial kidney. Organic anion and cation transporters present in renal proximal epithelial cells are capable of specific, unidirectional transport of protein-bound uremic toxins. Moreover, in addition to the toxin removal bioartificial kidney device could perform other physiological roles of the kidney such as metabolic replacement, endocrine function and immunomodulation.

Bioartificial kidney is a bioreactor system, typically consisting of hollow fiber membranes and is seeded with functional epithelial cells from kidney proximal tubules. The specified cells are of the major interest since they perform the most of the active reabsorption in the nephron. Moreover, the cells are able to replace other physiological functions of kidney. The bioreactor seeded with the proximal tubular cells is traditionally called renal assist device.

Positive results were obtained in bioartificial kidney development using human and animal derived immortalized cell lines. However, only limited success was achieved when using human primary tubular cells, which are preferred for clinical applications. The nature of these cells is more demanding to the chemical or mechanical signals that triggers their growth and differentiation. It became evident that successful transport of the uremic toxins by the epithelial cells could only be possible in case of formation of polarized monolayer. In such polarized cells apical and basal parts are performing different functions. Formation of tight junctions is one of the keys that triggers cell polarization and impaired tight junction formation corresponds to the loss of the transport properties of the cells.

Therefore, membrane properties plays critical role in bioartificial kidney development. Being used in contact with blood requires sufficient hemocompatible properties of the membrane. Sufficient membrane transport should be assured for the duration of at least 100 h. And finally the membrane should promote and facilitate cell attachment differentiation and proliferation.

Using commercial membranes currently applied in hemodialysis/hemofiltration in development of bioartificial kidney is the common strategy, considering the membrane requirements. However, in most of the membrane surface modification is required to promote cell performance. The parameters of membrane topography such as roughness, porosity and the pore size also must be considered.

1.2. Objectives

Therefore, taking into account all of above two types of commercial membranes (Gambro HCO 1100 and Membrana MicroPES TF10) used in hemofiltration and plasma separation were selected to be tested as scaffolds for human primary tubular cells. To perform the study on the basis of the literature data the following objectives were established:

- Develop and biomimetic coating the outer surface of the membrane hollow fibers using mussel-inspired synthetic coating with poly-L-DOPA and the components of extracellular matrix;
- Characterize transport properties of the coated membranes;
- Establish confluent functional monolayer of primary human tubular cells on the outer surface of the fibers.

2. LITERATURE REVIEW

2.1 Acute kidney injury overview

Acute kidney injury (AKI), formerly known as acute renal failure, is a syndrome with the complex etiology and it is generally characterized as an abrupt loss of kidney function, which develops within the time up to one week. Due to the numerous causes of the syndrome, no commonly accepted definition exists nowadays.

The concept of the syndrome have been evolving in the last 50 years and various attempts were made to standardize and classify renal dysfunction. The first consensus definition of acute renal failure that was broadly supported had been developed by Acute Dialysis Quality Initiative group [1] and published in 2004 [2]. The concept was called RIFLE using such categories as: Risk, Injury, Failure, Loss of function, and End-stage renal disease as the stages of AKI severity. The concept was designated to diagnose the presence or absence of AKI in patients, as well as for determining the severity of the condition. It is worth mentioning that the system neither aimed to predict the mortality or the outcome nor intended to recommend the specific therapeutic treatment of the patients.

However, since even the small rises in serum creatinine levels corresponded to elevated mortality in patients, the term acute kidney injury has later been used to emphasize the importance of whole range of renal dysfunction from its onset to the long-term failure and not only the stage of failure itself. Therefore, in order to overcome some of the existing limitations, AKI Network [3] developed another classification based on the RIFLE system in 2007 [4]. The both RIFLE and AKIN systems are common for clinical practice and use the sudden increase of serum creatinine levels and/or oliguria as main diagnostic criteria (Detailed specifications of the criteria used for RIFLE and AKIN classifications are given in Appendix A). But in spite of relative simplicity of the diagnostics, the above approaches have some limitations. The both systems use alterations in urea output and creatinine levels from hypothetical baseline, the symptoms which emerge relatively late after injury had occurred. Also, neither of the approaches addresses the question about the nature nor the site of the injury. Therefore, more research is required for investigation of the new biomarkers of AKI for the more specific diagnostics [4–7].

Incidence and severity of AKI vary among populations and communities of people. Accordingly, occurrence of AKI when no dialysis treatment is required is estimated as 5000 cases per million per year. Whereas about 300 cases per million per year are reported for dialysis-required patients worldwide. Prevalence of AKI varies also geographically. Thus, in developing countries AKI is often induced with hypovolaemia secondary to diarrhea. Whereas in developed countries major surgeries, especially open heart surgeries, are common cause of the disease [8].

Among the general triggers of the disease are such conditions as: inflammatory process in the kidney, renal ischemia (restriction of blood supply), nephrotoxins exposure etc.. Occurrence of AKI is common in hospitalized patients, especially the ones undergoing major surgery and is very common in critically ill patients.

Overall, two different group of patients with AKI could be distinguished. In the first case, AKI usually originates from using nephrotoxins such as steroidal anti-inflammatory drugs, some antibiotics vasoconstrictors or of such conditions as glomerulonephritis or rhabdomyolysis. In all of above patients, AKI is restricted to the single organ and the overall prognosis is positive with the mortality rate of 8 %.

On the other hand, tremendous difference is observed in patients with AKI when multiple organ failure is present. The presence of AKI in this case could be regarded as an indicator of severity of underlying pathology. It is this form of acute kidney injury, triggered generally by prerenal factors, which is the most common form of the disease in the developed countries and among critically ill patients. Here, the mortality rates remain at extremely high levels of higher than 60% in the intensive care units worldwide. The overview of AKI epidemiology is shown in Fig. 2.1. [5,7–9].

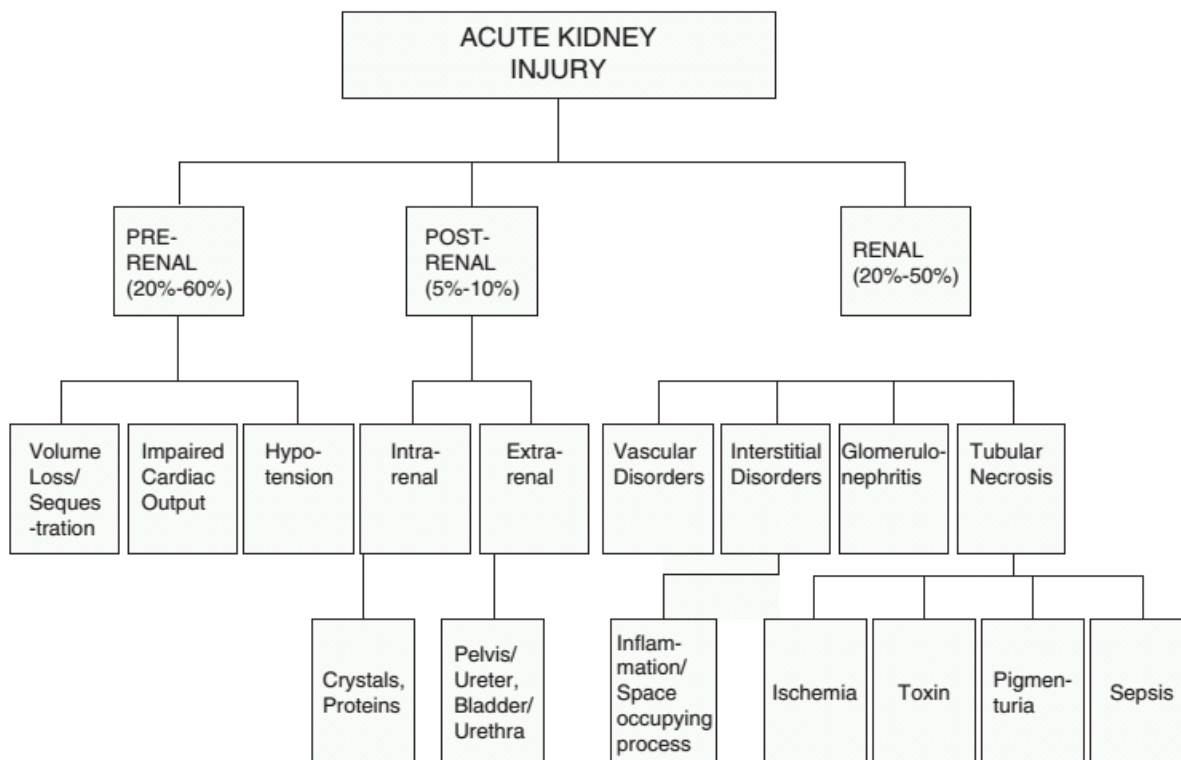


Fig. 2.1. Causes of acute kidney injury [9].

Limited understanding of the mechanisms of AKI, and as a result, the of the methods of its treatment, results in high morbidity and mortality rates. The main progress of understanding concerning the mechanisms of AKI is obtained from works on animals. There are three main types of animal models that are used to investigate AKI. Namely they are ischemia, sepsis and toxins models. The strong discussion is present concerning relevance, applicability and reproducibility of these models in critically ill patients [2].

Nonetheless, it is becoming clear that renal injury is able to cause in the injury of other organs through yet unclear pathways, which are still have to be investigated. The phenomenon is called organ cross-talk, which underlines the complexity of the condition. Such complications can be further categorized in the following conditions:

- Hepatorenal syndrome
- Rhabdomyolysis
- Sepsis
- Cardiorenal syndrome [8,10].

As it could be seen from above, that even short-term kidney injury could result in the prolonged morbidity and mortality. Bellomo at al.[8] in their work attempted to summarize the evolution of AKI, which could be schematically represented in Fig. 2.2.

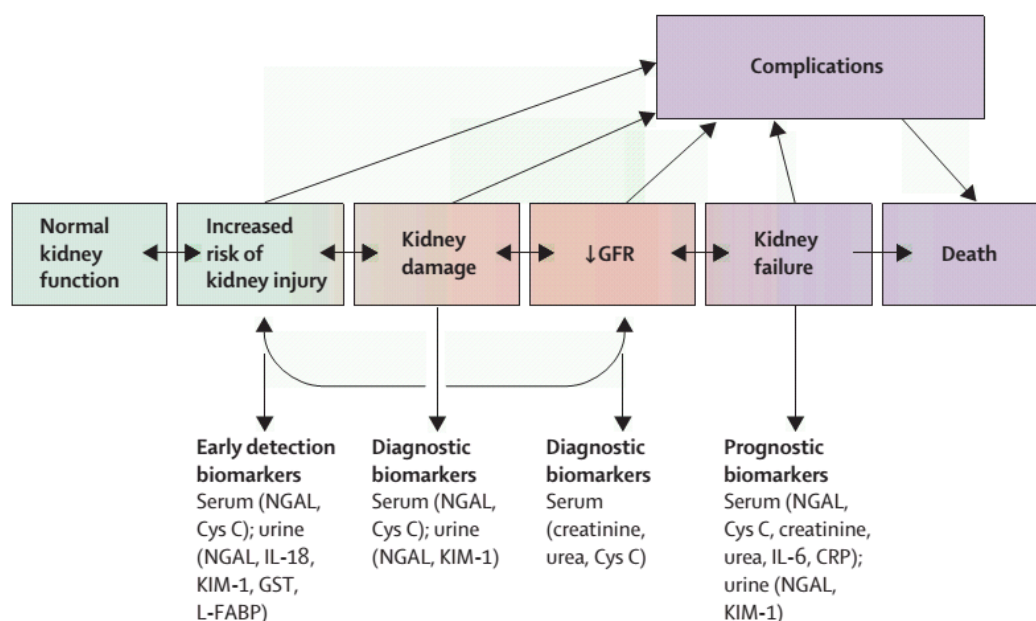


Fig. 2.2. Acute kidney injury progress. GFR, glomerular filtration rate. NGAL, neutrophil gelatinase-associated lipocalin. Cys C, cystatin C. KIM-1, kidney injury molecule 1. IL-18, interleukin 18. GST, glutathione-S-transferase. L-FABP, liver fatty-acid-binding protein. CRP, C reactive protein. IL-6, interleukin 6 [8].

2.2 Uremic toxins in acute kidney injury

As it could be seen from above, the most severe form of AKI is associated with the increased mortality in patients. The condition is related with non-renal pathologies such as lung, liver and heart failure, sepsis etc. Uremic toxins could represent the connection between the renal and non-renal manifestations of AKI, since the damage to the non-renal organs can be explained by their action [11].

In the both cases of AKI and chronic kidney disease (CKD), uremia initially results from decrease of glomerular filtration rate and urine output, which in turn leads to the retention of the nitrogenous and non-nitrogenous waste products, metabolic acidosis, hyperkalemia and hypervolemia. It should be mentioned, that most of the uremic toxins were previously studied and characterized for chronic kidney disease and the investigation of the uremic toxins in AKI is still in its infancy. Investigations are mainly obscured due to the fact of the specificity of the toxins types according to the form of AKI and the transient, rapidly changing nature of uremic toxins levels. Whereas, in CKD the steady-state conditions could be observed [9,11].

Traditionally uremic toxins for both AKI and CKD fall into the following categories:

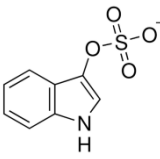
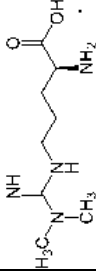
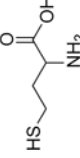
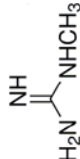
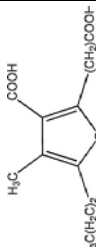
- Small water-soluble molecules, MW < 500 Da
- Protein-bound molecules
- Middle molecules, MW > 500 [9,11].

More refined view on the toxins was proposed by Uremic Toxin Work Group (EUTox) in 2003 [12]. In the extensive study 90 uremic solutes were investigated. Majority of toxins investigated (68 solutes) were small molecules with molecular weight <500 Da. The second largest group of the toxins were protein-bound solutes, comprising of 25 molecules (~ 30 %), with all but two toxins having MW<500 Da. Concentrations of these substances ranged from 32.0 ng/L for methionine-enkephalin up to 2.3 g/L for urea. Moreover, inorganic substances such as PO_4^{3-} , SO_4^{2-} , Cl^- , K^+ , Na^+ , Ca^{2+} etc., can also be regarded as toxic substances in uremic conditions. Specifically increase of NaCl concentration results in dramatic effect on cardiovascular system, whereas accumulation of calcium phosphates results in vascular blockage. The extensive lists of the investigated toxins and their physiological parameters are given in Appendix B [12,13].

As it could be seen from above, low molecular weight compounds comprise the vast majority of the uremic toxins. But the importance of this group of compounds lies not only in the abundance but also in its diverse toxicity. Distinctive feature of this group of molecules is their action on several or

multiple systems of the organism. To illustrate the above statement, the following table summarizes selected low molecular weight uremic toxins and the main of investigated actions on the specific systems.

Table 2.1. Toxicity profiles of selected uremic solutes

Uremic Toxin	Structural Formula	Toxicity	Reference
Indoxyl Sulfate		<ul style="list-style-type: none"> • Nephrotoxicity (tubular fibrosis and glomerular sclerosis) • Promotion of transforming growth factor beta expression • Induction of oxidative stress in tubular cells, mesangial cells, vascular smooth muscle cells, endothelial cells and osteoblasts as well as stimulating aortic calcification • Promotion of cardiovascular disease and osteodystrophy • Central nervous system toxicity 	Niwa 2010, [14] D'Hooge et al., 2003 [15]
Asymmetric Dimethylarginine (ADMA)		<ul style="list-style-type: none"> • Promotes inflammation • Kidney enzymes inhibition • Endothelial and vascular damage, vasoconstriction, increased blood pressure through endothelial NO synthase inhibition 	Cardounel et al., 2007, [16]
Homocysteine		<ul style="list-style-type: none"> • Oxidative stress via producing of reactive oxygen species • Protein binding and modification and enzyme inhibition • Arterial occlusion and vascular damage 	Perna et al., 2003, [17]
Guanidines, (Methylguanidine)		<ul style="list-style-type: none"> • Proinflammatory effects on leukocytes • Stimulation of production of Tumor necrosis factor alpha • Central nervous system toxicity (Guanidinosuccinate) 	Glorieux et al., 2004 [18] D'Hooge et al., 2003 [15]
3-carboxy-4-methyl-5-propyl-2-furanpropionate (CMPF)		<ul style="list-style-type: none"> • Oxidative damage in renal tubular cells • Inhibition of organic acid transport at brain/blood barrier, uremic ecelophaty • Toxicity to mitochondria, liver enzymes and erythroid blood cells 	Miyamoto et al., 2012, [19]

Action on multiple systems of the organisms generally characteristic for middle molecules with molecular weight of 500 – 12.000 Da. Typically these compounds are of the peptide nature and often interfere with immune and cardiovascular functions. Specifically, elevated concentrations of various potent proinflammatory cytokines such as: Interleukins -6, -1, -18, Tumor necrosis factor α were observed in the conditions of uremia. Which in turn, result in inflammation in such organs and systems as lung, kidney tubules, central nervous system [11].

Decrease of immune defense, through different mechanisms, in uremic patients is linked the increased levels of such molecules as: Granulocyte-inhibiting protein I, κ - and λ -Light chains of immunoglobulins etc [9].

Low levels K^+ and high PO_4^{3-} levels in kidney failure conditions result in the production of excess of Parathyroid hormone. Which, in turn, triggers the systemic uptake of calcium into the cells and further modifications of critical physiological functions [9,13].

Another, well studied uremic peptide is β_2 -Microglobulin. The molecule is related to late stages of renal injury and amyloidosis. This peptide of 11.8 kDa is often used as a marker of large molecules removal with dialysis treatment [9,13].

As it was mentioned previously, AKI and CKD manifestation results in the damage of kidney tubular cells, namely tubular necrosis through complex interrelated mechanisms. In the normal physiology, renal tubules are exposed to approximately 150 L/day of glomerular ultrafiltrate. Consequently, in the renal tubules takes place reabsorption of low molecular weight proteins, amino acids, glucose, up to 90% of phosphate and 80% and 60% of bicarbonate and chloride respectively. Additionally there are also being removed the numerous endogenous and exogenous substances and performed endocrine and paracrine functions. Therefore, proximal and distal tubular cells are responsible for active secretion of uremic toxins from blood into urine and have numerous specialized secretion and enzymatic systems expressed on their surface. Specifically, organic anions and cations, which represent the largest group of uremic toxins, are transported with unidirectional transcellular transport. Namely, toxin uptake takes place by the transporter at the basolateral membrane at the blood side with its consecutive secretion into urine by the transporter at the brush border membrane [5,20,21].

The example of indoxyl sulfate elimination from bloodstream could be used to illustrate the toxin transport in the proximal tubular cells. Indoxyl sulfate could only be transported in these cells by the organic anion transporters (OAT) since it is almost exclusively bound to the albumin in the blood. These transporters are responsible for the uptake and/or secretion of the specified uremic toxin and the other endogenous and exogenous organic anions, including various drugs. Therefore, since indoxyl sulfate is a physiological ligand for OATs, its increased levels in uremic conditions leads to the accumulation of the toxin within renal tubular cells and their subsequent damage. Schematic representation of unidirectional indoxyl sulfate transport is given in the following graph [13,21,22].

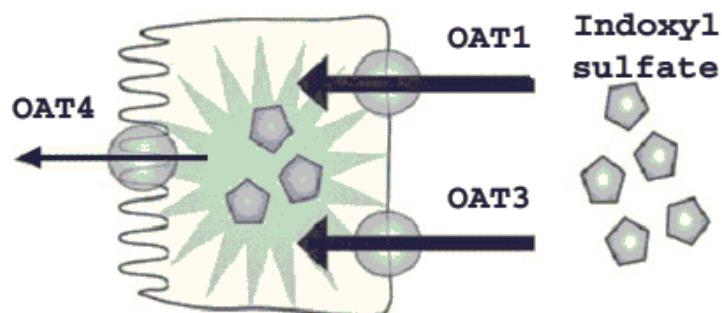


Fig. 2.3. Indoxyl sulfate transport by organic anion transporters in kidney tubular cells [22,22].

To conclude, as it could be seen from above that uremic toxins showed strong involvement in the progression and pathology of acute kidney injury and chronic kidney disease. Renal tubular cells serve as the organism's primary defense line against toxic uremic substances. Consequently, such conditions as glomerular and tubular necrosis and tubular fibrosis are diagnostic conditions generally present in AKI or CKD.

2.3 Traditional management of the uremic toxins

Wide range of metabolic diversity is performed by the kidney. One of the most crucial role of the kidney for the organism is its excretory function where kidney is responsible for removal of thousands of different chemicals from the bloodstream. Therefore, as it was discussed before, loss of

the function of the kidney results in the toxins accumulation in the blood. The toxins produced during nitrogen metabolism, such urea, are of particular importance since the large amounts they are produced and their high toxicity [23].

Extracorporeal devices, therefore, are often applied to eliminate the toxins from the blood. In such devices, normally small flow of blood is removed continuously from the patient and returned back to the patient after treatment. Normally toxin molecules are removed from blood to the dialysate side by diffusion through semipermeable membrane. Flow rates of blood are usually 100 – 500 mL/min and the total volume of the extracorporeal blood circuit is usually several hundred milliliters . Dialysate circuit is usually applied in the counter current mode. For optimal blood purification the ratio between dialysis fluid and blood flow rates must be around 1.5 – 2. For higher ratios result in little increase of toxin removal and for lower ratios significant reduction of clearance rates was observed. Most dialysis machines work in fixed dialysate flow rate of 500 mL/min, which require 120 L of dialysate for 4 h of operation. Normally this amount of fluid is prepared by dilution of concentrated electrolyte and buffer solution with purified water [23,24].

Chemical extraction from blood is controlled by the permeability characteristics of the membrane and the flow rates of blood and dialysate Q_b and Q_d respectively. Applying mass balance to the blood and dialysate compartments it is possible to describe overall effect of the dialyzer [23]:

$$N_t = Q_b(C_b^{in} - C_b^{out}) = Q_d(C_d^{out} - C_d^{in}) \quad (2.1)$$

where:

N_t – total removal rate of the solute, mol/min);

Q_b, Q_d – blood and dialysate flow rate, mL/min;

C_b, C_d – molar concentration of the component in blood and dialysate compartments .

The effectiveness of separation of the compounds in hemodialysis is normally described by the term “clearance,” which describes removal rate in ml/min. The expression of clearance in three different modes of operation – hemodialysis (2.2), hemofiltration (2.3) and hemodiafiltration (2.4) are described using following equations [25]:

$$C_L = \frac{Q_b(C_b^{in} - C_b^{out})}{C_b^{in}} = \frac{N_t}{C_b^{in}} \quad (2.2)$$

$$C_L = \frac{C_f}{C_b^{in}} Q_f \quad (2.3)$$

$$C_L = \frac{Q_b(C_b^{in} - C_b^{out}) + Q_f \cdot C_b^{out}}{C_b^{in}} \quad (2.4)$$

where:

C_L – solute clearance;

Q_f – filtrate flow rate;

C_f – molar concentration of the compound in the filtrate.

Common indicator of dialysis efficiency is the clearance of uremic toxins. Using the membrane with ~60 kDa cutoff urea is classified as low molecular weight substance and can be completely removed by dialysis. For higher molecular weight compounds, such as vitamin B₁₂ (1355 Da) or inulin (5200 Da) lower clearances have been observed. Blood flow is the one of the most important characteristics for the clearance of compounds. At low blood flows clearance increases linearly with the blood flow and reaches plateau for higher flows. Also, it is worth mentioning, that at low blood flows the clearance is fully controlled by dialysate flow [25].

Two groups of materials are used in modern dialyzers:

- cellulose based
- synthetic.

Cellulose membranes are made of reconstituted cellulose and are relatively inexpensive. The main drawback of this type of material is the significant levels of complement activation due to the presence of high amount of hydroxyl residues. Cellulose OH group substitution can result in less

amount of complement activation but on the other hand results in increased blood coagulation which requires increase of anticoagulant treatment [24].

The main fraction of the dialyzers used worldwide is represented by synthetic materials. Variety of polymers and their mixtures are used to obtain optimal performance. Specifically, ultrafiltration coefficient or hydraulic permeability are the parameters that divide HD membranes into the two categories: low- and high-flux. Application of either type of the membrane depends on the case, but, for example, in Europe high-flux membranes are normally applied for the patients with chronic renal failure [26]. High-flux dialyzers are typically made of synthetic membranes and achieve ultrafiltration coefficients ~ 60 mL/Min-mmHg. They have higher molecular weight cutoff and greater convective permeability to the middle molecules 5 – 25 kDa. As a materials for such membranes are commonly used PMAA, PAN, PES etc [24,25].

The membrane materials used in the current work are based on the mixtures of PES/PVP/PA and PES/PVP for Gambro HCO 1100® (Gambro Dialysatoren GmbH, Hechingen, Germany) and MicroPES® TF10 (Membrana GmbH, Germany) respectively. Specifications of the specified membranes are given in Appendices C and D.

2.4 Protein-bound uremic toxins and their treatment

Special group of uremic toxins comprises protein-bound solutes. Protein binding of these molecules results in major limitations for their effective clearance through hemodialysis. Traditional hemodialysis becomes inefficient at high toxin binding ratios, since only small part of toxins is able to diffuse through the membrane. Performing hemofiltration with the membranes having higher cut-off values, could improve clearances, by increasing convective component of the transport, but still efficiency of the process is low due to the high protein binding [27].

Comprehensive list of 25 protein-bound solutes is given in Appendix B. For such molecules as 3-Deoxyglucosone, N-(carboxymethyl)lysine, indoxyl sulfate, leptin, and 3-carboxy-4-methyl-5-propyl-2-furanpropionic acid (CMPF) more than 5-fold increase of concentrations was observed in uremic conditions [13].

In uremic conditions, human serum albumin serves a major ligand for protein-bound toxins. In normal physiology, albumin, being predominant protein in serum, acts as circulating ligand and free radical scavenger. In uremic conditions, however, albumin is subjected to various post translational modifications. Most common examples are thiolation, carbonylation, glycation and oxidation. Generally, such modifications result in the increase of the negative charge of serum albumin and the exposure of its hydrophobic regions. Functionally, it results in impaired ligand binding capability and decreased antioxidant activity. Above considerations are presented schematically in Fig. 2.4 [28–32].

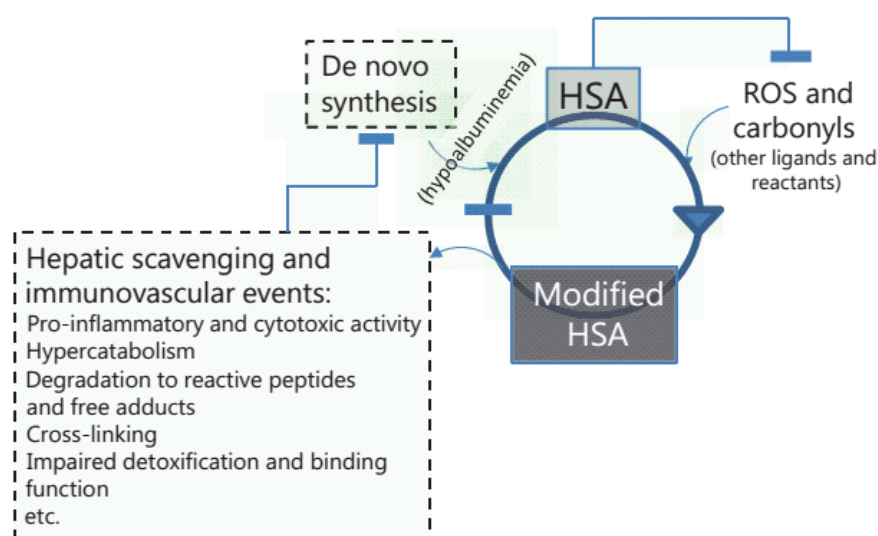


Fig. 2.4. Effect of serum albumin modifications in uremic conditions [29].

Whereas the most of the protein-bound toxins interact with albumin, retinol-binding protein, could be an example of the exception to general rule. Retinol-binding protein is a protein of 21 kDa and 90% of it is bound to a carrier of thyroid hormone – transthyretin [13].

As it can be deduced, therapeutic difficulty to remove bound substances in HD is directly linked to the binding ratio of the toxins. Such molecules as indoxyl sulfate, p-cresyl sulfate, CMPF, and 4-ethylphenyl sulfate exhibit especially high protein-binding ratios of more than 90%. As a result, less than 35% of the specified toxins could be removed with conventional therapy. Interestingly, that for such potent uremic toxin as CMPF, with exceptionally high albumin binding ratios of more than 95%, after HD treatment in patients was observed 15% increase in its concentration. Therefore, CMPF removal is impossible with HD due to its strong albumin binding [33,34].

Several approaches have been used to overcome the specified limitation. Traditional therapy involves an increase in duration and frequency of HD. Another approach implies an increase of dialysate flow rate Q_d and improvement of the membrane mass transfer coefficient. However, only minor improvement in removal efficiency could be achieved with the traditional therapy, which in turn results in the strong necessity for alternative, more efficient strategies [29].

One of the first examples of such untraditional therapy was using of protein-leaking membranes for HD treatment. Such effect could be achieved by using larger pore size and high porosity materials. Specifically, protein-leaking hemodialysis when using BK-F polymethylmethacrylate membrane (Toray Medical Co., Chiba, Japan) is shown to decrease CMPF serum levels by 50%. Also, using such membranes let significantly improve removal of middle molecules, such as pro-inflammatory cytokines, light chains of immunoglobulins, β_2 -microglobulin etc. Another example of such protein leaking membranes, successfully used in therapy is Gambro HCO 1100® (Gambro Dialysatoren GmbH, Hechingen, Germany) dialyzer, which is reported to successfully remove immunoglobulins light chains in variety of the therapeutic conditions, including AKI [34,35].

Alternative approach involves the use of various adsorption methods. Such effects could be obtained by the action of membrane itself, as it was reported in case of polymethylmethacrylate [36,37]. Different variations of this approach involving applications of natural or synthetic adsorbents for protein-bound toxin trapping were also reported in the literature. Direct adsorption from blood in packed columns (hemoperfusion) is still in its underdeveloped stage mainly due to the low hemocompatibility of such treatment [38,39]. Similarly, Meyer et al. report the increase in protein-bound toxin clearances when using synthetic adsorbent (activated charcoal) in the dialysate fluid [40]. Using mixed matrix membranes could combine the advantages of using the adsorbent and have excellent hemocompatibility properties. Recent work of Tijink et al. [41] could be regarded as an example for this approach. Yet another strategy for protein-bound toxins trapping, is in using natural adsorbents. In analogy to the synthetic adsorbents, albumin dialysis therapy, used in liver failure could be applied for bound solutes displacement from uremic albumin, therefor preventing undesirable protein modifications. Successful examples of such treatments are Molecular Adsorbent Recirculation System (MARS), Single-Pass Albumin Dialysis (SPAD) and the Prometheus systems [29,39].

Yet another approach to overcome uremic solutes related conditions, as it was demonstrated by Kikuchi et al. [42] is in using of oral sorbents. Since such potent uremic toxins as IS originate from colon microflora, therefore such therapy could be regarded as very attractive approach.

However, it is worth mentioning, that all of above examples of protein bound toxins treatments are generally supportive in their nature. Despite of the numerous attempts to overcome the limitations for the protein bound toxins removal, existing techniques still demonstrate to fail in preventing severe medical conditions related to kidney injury with unacceptable high mortality levels. Existing therapies are unable to substitute numerous kidney functions such as metabolic, regulatory, endocrine etc. which can be crucial for the positive dynamics in the therapy. Therefore using bioartificial kidney can be regarded as an attractive approach in solving kidney-related conditions [13,29,34,39]. Overview of the state of the art in the bioartificial kidney development is given in the next section.

2.5. State of the art of bioartificial kidney development

The field of bioartificial kidney (BAK) evolutionary emerged from hemodialysis applications in the late 90s. Two research groups led by A. Saito (Japan) [21,43] and Humes H.D. (USA) [44–46] contributed the most in the early development of BAK. In their work, the authors connected in series BAK device to the hemodialyzer module. Using hemodialyzers to substitute the function of impaired

glomerular filtration is a commonly accepted strategy [24]. By connecting bioreactor unit to the hemodialyzer outlet authors intended to substitute the functions of kidney tubules, such as reabsorption of the nutrients, producing of hormones and cytokines and which is the most important, excretion of the toxins.

Epithelial cells from kidney proximal tubules are of the main interest in BAK applications since they perform the most in the active reabsorption in the nephron. Active reabsorption also includes unidirectional transport of uremic toxins described in section 2.2 (Fig. 2.3) [22,23,47]. Moreover, proximal tubular cells were reported to perform additional metabolic functions, replacing the other physiological functions of kidney. Among such functions are the production of the hormones, paracrine factors and cytokines [48–50]. Naturally the cultivation of the cells is performed in bioreactor conditions. The bioreactor seeded with the proximal tubular cells is traditionally called renal assist device (RAD).

Overall, using hemofilter with connected in series RAD is intended to mimic the functions and the architecture of the nephron (Fig. 2.5). In the following section brief description of the cell types used in BAK will be given. Next, the materials and their modifications applied in bioartificial kidney will be characterized

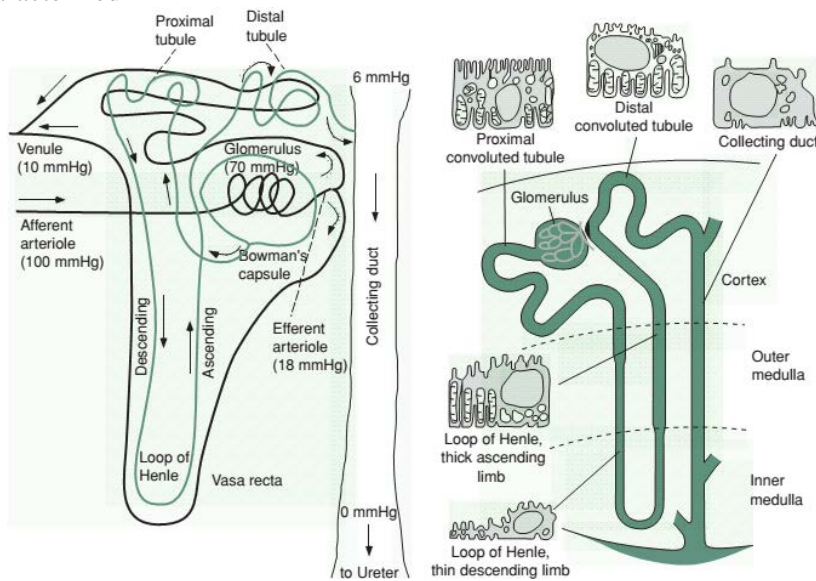


Fig. 2.5. Schematic structure of the nephron [23].

2.5.1. Cell line selection

Most of the research in bioartificial kidney was performed either on human or animal-derived immortalized cell lines or on the primary proximal tubular cells. Early works on BAK were typically completed using immortalized Madin-Darby canine kidney (MDCK) cell line [44,51]. Several advantages of using immortalized cell lines make them a valuable tool for the research applications. Among them is the stability of the cell phenotype, low cost and unlimited proliferative potential. Numerous kidney tubular cell lines exist, however only few of them could be used in BAK applications. For example, transformed HKC cell line developed in 1997 [52] is used to model physiological behavior of tubular cells. However later clones of the cell line fail to form tight junctions. Widely used in BAK human transformed proximal tubular cell line HK-2[53] do not tolerate of being grown to the confluence [20]. Significant number of works have been performed using proximal tubule porcine cell line LLC-PK₁ [54,55]. Both MDCK and LLC-PK₁ cell lines are reported to form confluent functional monolayers and can be grown using simple standard media.

However, the existing strategy always implies using primary culture of human proximal tubular cells (HPTC) in order to confirm the effect obtained for immortal cell lines. Moreover, immortalized cell lines, as it was discussed earlier, commonly do not express crucial physiological characteristics present in the kidney primary cells. Specifically, for the transport functions of epithelial cells it is critical form tight junctions when they are grown in monolayer.

Organic anion transporters, discussed earlier in section 2.2, play critical role in excreting vast majority of the toxins from the bloodstream. Specifically, expression of the transporters OAT1, OAT3 and OAT4 responsible for toxin removal is linked to PDZ (PSD-95, Dg1A, and ZO-1) binding domain proteins, which play role as the scaffolds. In proximal tubular cells these scaffolding proteins are thought to generate cell polarity by forming connections with both tight junction complexes and transporter proteins and the signaling molecules [47]. Therefore failure to form tight junctions would result in impairment of the tubular cell functions. Graphical representation of tight junction complexes, scaffolding proteins (ZO-1) and related cell structures is given in following scheme (Fig. 2.6). As it could be seen from Fig. 2.6 (b) ZO-1 protein is one of the first adapter molecule that connects other scaffolds proteins to the tight junction complex. Therefore ZO-1 protein detection became established technique for investigation of the functional properties of proximal tubular epithelial cells.

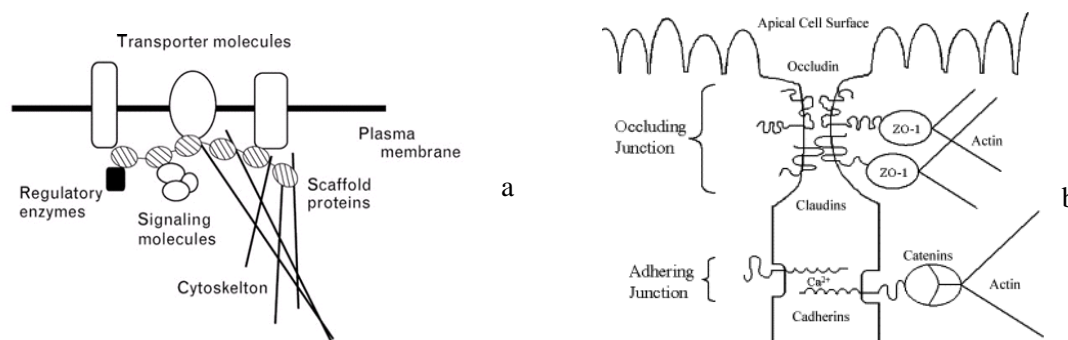


Fig. 2.6. Schematic representation of cellular junctional complexes [47,56].

As it was described above, human and animal-derived, primary and immortalized cell lines are used in BAK development. However, it must be mentioned that primary human derived cells must be used in clinical trials nowadays. Therefore using primary kidney cells of human origin is the necessary step in the development of any renal assist device which is intended to be used in the treatment of the patients. Considering all of above, primary cell line of human proximal tubular cells is used in the current work.

2.5.2. Membranes for bioartificial kidney applications

Considering the contact of BAK membrane with blood, the membranes traditionally used in hemodialysis/hemofiltration are involved in these bioreactors development. Consequently these membranes are generally of hollow fiber configuration having sufficient properties of their hemocompatibility. Despite the diversity of materials used in hemodialysis/hemofiltration, PES/PVP is the membrane material of choice in BAK applications and is used generally as substrate for kidney epithelial cells.

Several requirements must be met for the membranes in BAK applications. As it was already mentioned hemocompatibility is the one of the main prerequisites. In addition to being hemocompatible in the layer contacting with blood, membrane surface must bear sufficient cytocompatibility on the opposite surface interacting with the cells. Next, sufficient immunoisolation of the cell monolayer from the host immune system must be provided. However, at the same time membrane transport properties such as flux, fouling stability etc. must be sufficient to allow optimal performance of the cells.

Specifically, blood compatibility (hemocompatibility) of the membranes is the complex process involving such possible blood-membrane interactions as hemolysis, clotting, membrane fouling, inflammation etc. The membrane properties and material therefore is designed to decrease such negative interactions. The choice of PES/PVP materials in BAK becomes evident when its properties are considered. The balance of nanoscale hydrophilic and hydrophobic domains on the membrane surface is able to provide the optimal hemocompatibility and minimize such processes as clot formation or complement activation [57]. Chemical inertness, resistance to oxidation and action of free radicals, thermal and mechanical stability altogether contribute to the selection of PES/PVP based materials [25,58,59].

Moreover, PES/PVP based membranes provide stable and superior transport properties. Established fabrication methods provide asymmetric membrane structures which can be easily tuned according to the specific requirements. Polyvinylpyrrolidone (PVP) which is commonly used in pharmaceutical applications is added to the PES to introduce the membrane hydrophilicity. Addition of PVP is reported to contribute to improvement of diffusive properties of the membranes and decrease membrane fouling [59–61].

One of the specific membrane requirements for the membrane in BAK applications is their compatibility to the renal epithelial cells. Therefore the dual task must be performed by these membranes. First hydrophilic and antifouling properties are desirable to increase blood compatibility and protein fouling. And second, ECM proteins are required for adequate cell adhesion and contacts which is especially critical when working with sensitive primary tubular epithelial cells. Despite the fact that the sufficient number of successful works is already available on immortalized cell lines of animal and human origin (e.g. MDCK, LLC-PK1 or HK-2) successful cultivation of primary tubular epithelial cells on PES membranes is still limited. In the majority of cases special treatment of the membrane surface was required [44,54,62]. Considering the importance of membrane surface modification for proliferation of human primary tubular cells this topic is described in the following section.

2.5.3. Biomimetic surface modification

Modifications of the polymer surfaces are of great importance in biomedical science and research. And the scientific interest to the field is growing continuously. The main aim of the research is the engineering of the defined extracellular matrix which would be favorable for cell growth, differentiation and proliferation. The need for improving the properties of the carriers is the main prerequisite for the majority of polymeric and inorganic materials in tissue engineering applications [63].

Using the coatings of polycationic synthetic peptide poly-L-lysine was among the first successful strategies to obtain cytocompatible films on the wide range of surfaces. Other polycations such as polyornithine, chitosan etc. can also be used to improve surface biocompatibility, however poly-L-lysine based coating comprise the majority of early works on this topic. Among the examples of such applications could be the work of Orłowski et al [64] for pancreatic cells immunoisolation within alginate membrane. Biocompatibility of alginate/poly-L-lysine system is reviewed in the much later work of Orive et al. in 2006 [65], showing the strong scientific interests to this strategy. Simplicity, ease of use and effectiveness of poly-L-lysine coatings made it the material of choice for many biological applications and for the routine procedures in animal culture labs worldwide [66]. However, pro inflammatory effects of the coating, restricts the use of the compound for in vivo applications or require additional modifications of the coatings by using such glycosaminoglycan as heparin [67].

Another widely applied strategy for creating biocompatible, biomimetic surfaces for wide range of animal cell applications emerged shortly after discovery of integrins and their physiological ligands [68]. Integrins (Fig. 2.7) comprise a large family of heterodimeric glycoprotein receptors that play major roles in cell to ECM adhesion, cytoskeleton organization, intracellular signaling etc. [23,69].

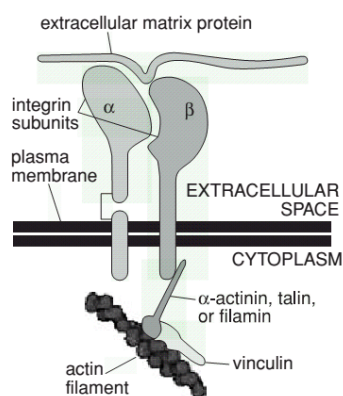


Fig. 2.7. Schematic representation of an integrin receptor [23].

Different types of integrins exhibit various degrees of binding to such extracellular matrix components as collagens, fibronectins, laminins, and cellular receptors such as vascular cell adhesion molecule-1. However, it was discovered that the RGD sequence (standing for tripeptide composed of L-arginine, glycine, and L-aspartic acid) was largely responsible for integrin binding activity in various natural and synthetic compounds that could be used in cell culture applications to improve cell adhesion and promote cell differentiation and proliferation [68–70].

Consequently, the use of natural or synthetic RGD – containing ligands became the most accepted strategy, especially when functionally attached, polarized cell structures are required. Specifically, use of collagen-derived RGD peptides was reported by Jeschke et al. [70] to improve significantly monolayer formation of the chondrocyte cell line.

Taking into account cell type specificity of integrin expression, various coatings were developed to meet the requirements for the particular application. Special attention in the recent years was paid for multilayer coatings using layer-by-layer assembly of polycations and polyanions. Numerous polyelectrolytes could be used in the technique according to the specific goals needed to be achieved. One of the main advantages is the stability of the layer and fine-tuning of the surface properties by varying the number of the layers and their structure [70–73].

Collagen – hyaluronic acid multilayers were reported by Zhang et al. [72] to facilitate chondrosarcoma cell line adhesion and proliferation. Combination of collagen and chondroitin sulfate coatings were known to be used in osteoblast cell culturing. Biomimetic coating of collagen type I and chondroitin sulfate, as it was reported by Vandrovcová et al. [74], improved MG 63 cell adhesion, proliferation and differentiation on poly-(lactide-co-glycolide) polymer surface. Especially promising application of to the multilayer systems is in cultivation of stem cells or muscle cells which are sensitive to the surface stiffness. Richert et al. [75] described in their work the possibility of optimizing the coatings for smooth muscle cell cultivation. Authors exploited fine tuning the properties of poly-L-lysine / hyaluronic acid coatings by changing film thickness and cross-linking ratio and collagen addition. Use of collagen coatings was widely reported for hepatic cell cultivation. In the recent work of [76], authors showed important role of collagen type IV in pancreatic cancer cell proliferation, migration. Use of collagen in engineered systems of hepatic cells for bioartificial liver applications are reported extensively [63,77,78].

Yet another promising strategy for biomimetic coating was introduced by Messersmith research group upon their discovery and publication in Science of their milestone article on mussel-inspired coating of polydopamine in 2007 [79]. The large attention received by the topic of mussel-inspired coatings could be explained by its numerous advantages. First, simple immersion of various substrates in the slightly basic solution of L-DOPA (Fig. 2.8.) results in oxidative self-polymerization and deposition of adherent polymer film. Second, film thickness can be varied from few to hundred nanometers depending on the coating conditions. Next, a distinctive property of the polydopamine film, is its ability to deposit on the vast variety of the organic materials including non-wetting polymer surfaces such as polyethylene, polytetrafluorethylene, polydimethyl-siloxane etc. Inorganic surfaces such as noble metals, metals, metal oxides, mica, silica, ceramics etc. are also reported to be successfully coated with polydopamine. The investigation of the mechanism of spontaneous L-DOPA polymerization and the surface adhesion is still in its progress. Role of catecholic group is thought to be crucial in the adhesive mechanism since concentrations of L-DOPA, dopamine and the other catecholic units prevail in naturally occurring mussel adhesive proteins. Specifically, it is agreed that complexing of TiO₂ nanoparticles with polydopamine involves chelating mechanism with the deprotonation of hydroxyl groups of the catechol molecule as an example. Moreover all catechol molecules readily establish strong non-covalent or covalent interactions with organic substances involving p-electron, hydrogen bonding and Michael interactions. The latter, Michael or nucleophilic interactions will be discussed later in this chapter when describing poly-L-DOPA layer functionalization step [79–83].

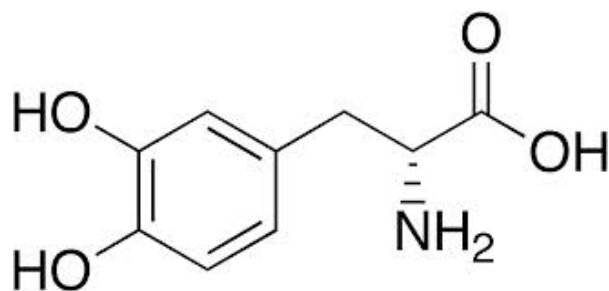


Fig. 2.8. Structural formula of L-3,4-dihydroxyphenylalanine or L-DOPA.

Single poly-L-DOPA or polydopamine coatings are reported to improve and fine tune surface properties to meet the requirements needed for industrial, biomedical or tissue engineering applications. First, poly-L-DOPA layers are known to increase hydrophilization of the surface. The presence of two full charges within the single poly-L-DOPA structure unit is responsible for the effect. Positive and negative charges of cyclo-dopa (Fig. 2.9) establish ionic-dipole interactions with water molecules. Therefore, properties of single poly-L-DOPA coatings are used to obtain anti-fouling membrane surfaces, absorb toxic substances from bulk solutions, fine tune the pore size, scavenge free radicals etc. [82,84].

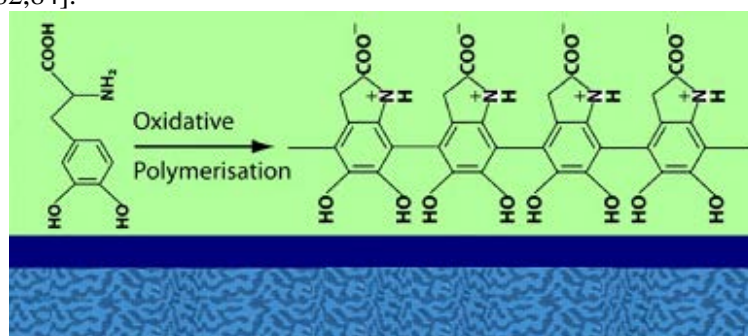


Fig. 2.9. Proposed mechanism of L-DOPA oxidative self-polymerization [84].

Use of the coating of the poly-L-DOPA in the current work for creating bioinspired layer was largely influenced by the cytocompatible properties of the substance and by the ease performing the secondary reactions to create ad-layers to provide desirable functions. Specifically, coating along was shown to promote the proliferative and adhesive behavior of mammalian cells on the example of fibroblast cells [79]. However, the full potential of poly-L-DOPA coatings can be estimated when its functionalization is considered.

The modification of poly-L-DOPA layer is possible through various mechanisms. Particularly in the case of proteins catecholic groups and the products of their oxidation – o-quinones exhibit strong reactivity towards nucleophilic side chain amino acid residues present in peptide chain. Formation of Schiff bases or Michael adducts is reported when reacting mainly with amine and thiol groups of proteins. In this manner, covalent bonding of poly-L-DOPA layer to nucleophiles is thought to be one of the main mechanisms of proteins bioconjugation onto the coating layer. Moreover, such weaker interactions as π -electron delocalization in aryl groups of the molecules, van der Waals forces and hydrogen bonding additionally stabilize the formed double layer [81,82,85].

When protein bioconjugation is considered, special attention must be paid for the preservation of protein native configuration. Promising results were reported when attaching various proteins onto poly-L-DOPA layers. Specifically, Rivera and Messersmith [85] showed in their work 5 to 8- fold increase of enzymatic activity of trypsin when immobilized on polydopamine layer compared to silica or titania monolithic supports. Conjugation of hyaluronic acid was shown by Lee et al. [79] to promote megakaryocytes adhesion. Poh et al. [86] reported immobilization of vascular endothelial growth factor onto the polydopamine film without losing the activity of the protein. Which in turn, promoted human dermal microvascular endothelial cells attachment, viability and proliferation compared to the

unmodified substrate. The osteogenetic differentiation in BRE-Luc C2C12 myoblast stem cells was reported by Kang et al [87] when using L-DOPA assisted bone morphogenic protein conjugation onto titania surface.

Coatings of extracellular matrix have been used extensively by various researchers to improve the performance of renal cells for bioartificial kidney applications. Humes et al. [44] in early 1998 in their pioneering work initiated the strategy for applying biomimetic coatings for renal assist devices (RAD). In their research authors coated polyethersulfone hollow fiber membranes with synthetic RGD-containing protein prolectin-L to facilitate the performance of porcine primary renal proximal tubular cells. Since then, various approaches have been applied to provide sufficient immunoprotection, cell compatibility and the transport properties of the membranes. However, extensive analysis of the extracellular matrix coating on the performance of human renal cells is still missing.

The attempt of such systematic analysis was performed in the research by Zhang et al. [88]. The impact of extracellular matrix coatings on the performance of immortalized human renal cell line HK-2 and primary human proximal tubular cells (HPTC) applied in bioartificial kidneys was investigated in the work. Various coatings of defined composition including such components and the mixtures of ECM as collagen type I, gelatin, collagen type IV, laminin, nidogen, nephronectin, Poly-D-lysine etc were studied. Moreover, effect of using Matrigel – complex mixture of ECM proteins was also investigated. The most promising results were obtained for the coatings consisting of such components of the basal lamina as laminin or collagen IV. Differentiated monolayers of HK-2 and human renal proximal tubular cells were obtained for the specified coatings. However, it must be mentioned that the authors performed their study working with flat, dense surfaces of standard tissue culture polystyrene 24-well plates. Therefore, additional improvement of the coating architecture is required when working with porous hollow fiber polymer surface.

Taking into account all of above using of double coatings of poly-L-DOPA combined with RGD-containing components of the basal membrane could be extremely promising approach. Specifically, this approach was investigated in the work of Ni et al. [54] where the authors tested different membrane materials used in hemodialysis/hemofiltration and coatings as described above. Numerous challenges of the approach arose with using the membranes instead of polystyrene tissue culture plates. Among those were the properties of the bulk materials such as contact angle, surface charge etc, as well as such the properties of the membrane itself such as pore size or membrane roughness. All these factors could play detrimental roles both for applying the coating and for the cell attachment. Authors tested two cell types, immortalized renal cells HK-2 and primary human renal proximal tubular cells. The cell performance was evaluated on native, L-DOPA coated, and L-DOPA + collagen IV coated flat sheet membranes. From the results it can be concluded, that PES/PVP membranes performed the most efficiently compared to the other materials used in hemodialysis application in sustaining renal cell lines. HK-2 cells formed distinctively differentiated and polarized epithelium with clear tight junction formation after 7 days of culturing on PES/PVP L-DOPA coated membranes (Fig. 2.10 a). However, it must be mentioned that the clinical importance of HK-2 cell line is low, therefore human primary cell line experiments are required. As it was shown, in the later studies, human renal proximal tubular cells were not able to proliferate efficiently on native or L-DOPA coated membranes, implying the more demanding nature of the cells for the conditions of their cultivation (Fig. 2.10 b). However some level of tight junction formation and differentiation was obtained by the authors for polysulfone/polyvinylpyrrolidone (PSF/PVP) membrane double coated with L-DOPA and collagen type IV (Fig. 2.10 c).

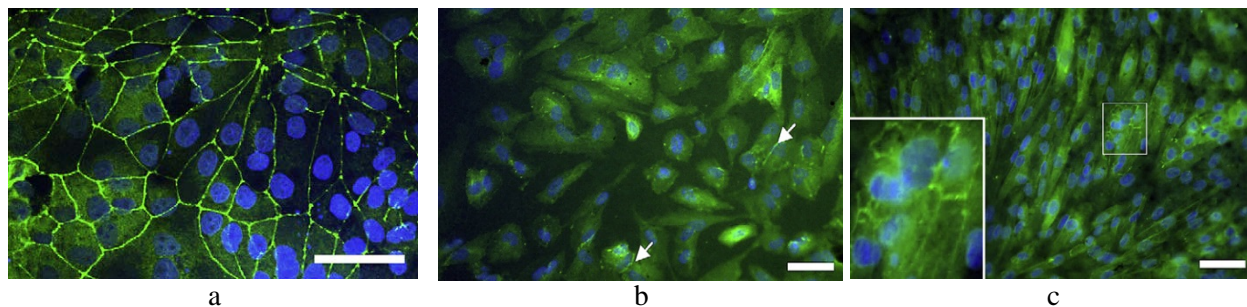


Fig. 2.10. Immunostaining for tight junction ZO-1 protein (green) of renal cells after one week incubation on coated flat synthetic membranes: a – HK-2 cells on PES/PVP flat L-DOPA coated membrane; b – HPTC on L-DOPA coated PES/PVP membrane; c – HPTC on double coated with L-DOPA and collagen IV PSF/PVP membrane [54].

As it can be seen from above, special attention should be paid towards selection of the membrane materials and their coatings. In the current work, the performance of primary culture of human renal proximal tubular cells is described. In addition to the demanding nature of these cells to the ECM conditions and growth factors, outer surface of hollow fiber membranes is chosen as substrate for cell proliferation. Thereby, new parameters such as membrane curvature and the absence of passive, gravity facilitated attachment, as in case with flat membranes, are to be considered.

3. MATERIALS AND METHODS

3.1. Reagents, materials and the supplies

- Two types of commercial PES based membranes were used in the experiments. PES/PVP/PA-based HCO 1100® HD hollow fiber membrane of ultrafiltration range were obtained from Theralite™ hemodialyzer (Gambro, Dialysatoren GmbH, Hechingen, Germany). Also, PES/PVP microfiltration range apheresis membranes MicroPES® TF10 were purchased from Membrana GmbH, Germany (Appendices C, D and E).
- Polyethylene tubes (Rubber BV, Hilversum, The Netherlands) of 6 mm in outer diameter were used as housing for assembly of the mini-modules. Festo push-in T-connections (Brussel, Belgium) or Kartell® polypropylene T-shaped tubing connectors (Kartell, Milan, Italy) were used to provide 4-port architecture of the modules. Two component polyurethane potting (Intercol B.V., Ede, The Netherlands) was applied for potting of the modules (Appendix E).
- Ultrapure water was used for preparing of the solutions, buffers and pure water flux (PWF) experiments unless stated otherwise. All ultrapure water was obtained from a Mili-Q Advantage A10 purifications system (Millipore, Billerica, USA) having 18 MΩ at 25 °C.
- All chemicals used in the work were of analytical or cell culture grade, used as received and stored at 4 °C in the fridge unless stated otherwise. Bovine serum albumin (BSA), 3,4-Dihydroxyphenylalanine (L-DOPA), Tris(hydroxymethyl)aminomethane (Tris), immunoglobulin G (IgG), human collagen type IV were purchased from Sigma-Aldrich (St. Louis, MO, USA).
- Nitrocellulose 0.2 µ Millex® syringe filters were used for filter-sterilization and providing gas exchange in batch bioreactors (Millipore, Billerica, USA).
- The culture of human renal proximal tubular epithelial cells (HRPTEPIC or in short HTPC) used in the experiments, was obtained from ScienCell Research Laboratories, Carlsbad, USA. The cells were supplied in dry ice and stored in liquid nitrogen for cryopreservation. Cell culture was handled and maintained according to the recommendation of the supplier [89].
- Primary polyclonal rabbit anti-ZO-1 antibody was purchased from Invitrogen (Life Technologies, Carlsbad, USA). Alexa Fluor® 488 Goat Anti-Rabbit IgG secondary antibody and DAPI were purchased from Molecular Probes®-Invitrogen (Life Technologies, Carlsbad, USA).
- Clonetics™ renal epithelial basal medium (REBM) and REGM™ BulletKit™ supplements were purchased from Lonza, Basel, Switzerland. Supplements were shipped in dry ice and stored at -20 °C according to the manufacturer's instructions [90].
- Trypsin-EDTA solution, PBS tablets, sterile HBSS supplemented with Ca²⁺/Mg²⁺ and calcium and magnesium free DPBS were obtained from Gibco® (Life Technologies, Carlsbad, USA).
- In current work the following buffer solutions were used. Phosphate buffered saline (PBS), with pH=7.4 was prepared by dissolving the tablets according to the manufacturers instruction. 10mM Tris-HCl buffer was prepared by dissolving TRIS in ultrapure water, and adjusting pH to the value of 8.5 with 1N HCl / 2N NaOH. Such sterile buffer solutions as DPBS, HBSS were used as supplied.
- Other used chemicals were of analytical grade and used without further purification.

3.2. Assembly of the mini-modules

Mini-modules prepared consisted of from 1 to 3 hollow fibers in polypropylene housing. To prepare the modules hollow fiber membranes were first cut to a length of 20 cm. Both ends of the hollow fibers were glued to secure the lumens of the membranes. Polypropylene housing (6 mm outer diameter, 4 mm inner diameter) was cut to the length of 8.5 cm, T-shaped connectors were fitted to the both ends of the housing. Smaller pieces of housing of 5 cm were fitted into the connectors and the membrane fibers introduced into the mini modules. Housings of 3 cm were introduced in the lumen ports of the modules.

Two type of connectors were used in the current work. Reusable Festo push-in T-connections were chosen for the modules for the membrane transport testing. Whereas, dispensable Kartell® polypropylene T-shaped tubing connectors selected for the cell culture experiments.

After having inserted hollow fibers into the modules, potting process started. Two component potting was used. After mixing the components of the potting Pur N and Pur 150 in a ratio of 100:150, then glue was allowed to cure for 3.5 to 4 hours to reach the gel consistency. Outer ends of the modules on the one side were filled with glue with a syringe to occupy the space between the entrance and the connectors, thereby reducing the volume of the dead ends. Glued outlets were sealed with parafilm, to prevent the leaking of the glue out. Modules were kept vertically with the glued end facing downwards for at least 24 h for hardening. The similar potting procedure was performed for the opposite ends of the modules. Active length of the fibers in the modules prepared as described was equal approximately 11 cm, and the exact value was obtained after the modules were disassembled and the fiber lengths were measured. After potting the ends of the modules were cut open. Images of the prepared modules are given in Appendix E.

3.3. Modification of PES-based hollow fiber membranes

Interfacial self-polymerization of dopamine was performed by exposure of the outer surface of the hollow fibers to the dopamine solution. To prepare the solution, L-DOPA was dissolved in 10 mM Tris-HCl buffer, pH=8.5, with the final concentration of 2 g/L of L-DOPA. Solution was kept open to atmospheric oxygen at 37 °C to induce the self-polymerization process for 1 hour and stirred with a magnetic stirrer (190 rpm). After preparing the solution, filtration with 0.2 µ filter was performed and dynamic coating of the hollow fibers with poly-L-DOPA was applied using a multi-channel cartridge peristaltic pump 205U (Watson-Marlow, Wilmington, USA). Prior to coating, after installing the modules into the hydraulic circuit, modules were washed with ultrapure water for 30 min, emptied and equilibrated with Tris-HCL buffer for 30 min at the flow rate 0.8 ml/min and emptied again. Afterwards, coating with p solution was performed at the same flow rate at 37 °C for 2 hours. Next, modules were emptied, and dried for 15 min with following washing with ultrapure water for 30 min. After the coating was performed modules were kept wet at 4°C before using for the maximum duration of 24 hours. When coating the modules for the cell culture experiments, the system and modules were sterilized with 70% EtOH before starting coating process. After ethanol sterilization, 0.2 µ filters were installed in the inlets of the modules to ensure sterile conditions, and the coating was performed as described above.

Double coating with human collagen type IV (Col IV) was applied on the poly-L-DOPA coated membranes according to the literature with some modifications [88,91,92]. Single coated membranes were equilibrated with DPBS before the double coating for 30 min. Amount of 1 ml of Col IV solution diluted in DPBS to concentration 25 µg/ml was injected in the lumen of the modules with a syringe in sterile conditions under LFH and the outlets of the modules were secured with the end cap (Festo, Brussel, Belgium). Thereafter, modules were incubated for 1 h at 37 °C, with the rotation of the modules at 180° after half an hour. After 1 h of the Col IV coating solution was aspirated and the modules were dried overnight at 37 °C in the incubator. Before using in cell culture experiments, the membranes were equilibrated with HBSS for 30 min. Ultrapure water was used for equilibration before performing PWF tests and PBS was used for protein permeation experiments.

3.4. Hollow fiber membranes characterization

3.4.1. Hydraulic permeability experiments

To perform dynamic characterization of hollow fibers performance and to investigate the effect of coatings on the membranes permeation tests were performed. Membrane transport measurements were performed using lab-scale Kross Flo Research Iii system (Spectrumlabs, Houston, USA) and a back pressure valve (KrosFlo® Automatic Backpressure Valve, Spectrumlabs, Houston, USA) were used to provide constant transmembrane pressure during the experiments.

For all permeation experiments membranes were wetted in ultrapure water for at least 2 hours at room temperature. Mini-modules were tested in Kross Flo setup in hemofiltration mode, when fluid was fed in the lumen inlet, retentate was collected from lumen outlet port and permeate was collected from the shell side outlet. Transmembrane pressure (TMP) was regulated using a back pressure valve by pressurizing the retentate stream, and permeate stream was at the atmospheric pressure.

After filling the hydraulic system with water in all streams and equilibrating for 30 min with no TMP applied, TMP of 0.25 bar was used to pre compress the membranes. Afterwards, the permeate flux was measured for subsequently applied pressures of 0.1, 0.15 and 0.2 bar for at least 15 min for each pressure in the steady state conditions. Mass of the permeate was collected with a digital laboratory balance for each time interval. Density of water was assumed to be equal 1 g/cm³ to relate mass and volumetric fluxes. Hydraulic permeability of the membrane L_p was calculated using Darcy's Law [58,93] :

$$J_v = \frac{V}{A \cdot \Delta t} = L_p \cdot TMP \quad (3.1)$$

Where:

V – volume of permeate;

A – membrane area;

L_p – hydraulic permeability;

TMP – transmembrane pressure;

J_v – permeate volumetric flux.

Permeate flux data were calculated with Eq. 3.1 and plotted as a function of TMP. After performing linear regression, membrane hydraulic permeability in L/m²/h/mbar was obtained from a slope of the linear function.

3.4.2. Protein permeation and apparent sieving coefficient determination

Protein solutions in PBS were used in all permeation experiments. Transport of two model solutes was investigated. First, permeation of bovine serum albumin (BSA) in PBS of concentration 1 mg/ml was assumed to model behavior of albumin in hemofiltration in patients. Second, the transport of immunoglobulin G (IgG), the main circulating antibody in humans was investigated. Concentration of IgG in model solution was equal to 0.02 mg/ml. Protein permeation was investigated similarly to the method described in 3.4.1 using Eq. 3.1. with several modifications. Before protein permeation, the membranes were equilibrated with PBS for 30 min. Thereafter, modules were emptied and protein solution was fed to the lumen side of the modules without applying external TMP. After the filling of all hydraulic system with liquids, permeation started for the previously used set of TMP, 0.1, 0.15 and 0.2 bar. After obtaining steady state conditions for each pressure (15 – 20 min) permeate was collected and the weight of it was recorded with a digital laboratory balance for at least 15 min.

Membrane transport properties are commonly described in terms of solute retention and solutes and solvent flux [94]. Describing retention of solute in terms of sieving coefficients are often used. Apparent (observed) sieving coefficient S_o is a fraction of solute that passes through the membrane into permeate stream from feed stream, which could be calculated using following equation [95]:

$$S_o = \frac{C_{perm}}{C_{feed}} \quad (3.2)$$

Where:

S_o – apparent sieving coefficient;

C_{perm} – protein concentration in the permeate;
 C_{feed} – protein concentration in the feed.

Samples from the feed and permeate streams were taken for each TMP value, and protein concentrations were determined spectrophotometrically using (Varian, Cary 300 Scan UV–visible spectrophotometer (Varian, Inc., Palo Alto, USA) at the wavelength 280 nm.

3.4.3. Scanning electron microscopy

Surface morphology of hollow fiber membranes were imaged by field emitting FEI environmental scanning electron microscope XL30 ESEM (FEI, Eindhoven, The Netherlands). Cross sections of the fibers with clear, straight edges were obtained by freeze fracturing in liquid nitrogen. Hollow fiber samples for the side surface investigation as well as the cross-section samples were dried at 37 °C overnight after placing them onto sample holders. After drying the samples were gold sputtered using a BalzersUnion SCD 040 sputter coater (Oerlikon Balzers, Balzers, Liechtenstein) and imaged with the electron microscope.

3.4.4. Coating characterization by ATR-FTIR

Differences in chemical composition of unmodified and coated membranes were investigated using attenuated total reflectance Fourier transform infrared spectroscopy (ATR-FTIR, PerkinElmer, Waltham, USA). Changes in the composition of various functional groups were compared between the spectra of unmodified, L-DOPA coated and L-DOPA + Col IV double coated hollow fibers.

3.5. Cell culture *in vitro*

Primary renal proximal tubular epithelial cells [89] obtained from ScienCell Research Laboratories, Carlsbad, USA, were cultured in renal epithelial basal medium supplemented with Media Clonetics™ REGM™ BulletKit™ containing 0.5% fetal bovine serum, 0.5 ml of Human Epidermal Growth Factor (hEGF), 0.5 ml of hydrocortisone, 0.5 ml of epinephrine, 0.5 ml of insulin, 0.5 ml of triiodothyronine, 0.5 ml of transferrin and of 0.5 ml of gentamicin sulfate/amphotericin-B (GA). Culture and subculture of the cell line were carried out according to the supplier recommendations and the data available from literature [20,54,66,89]. Unless stated otherwise, all cells were propagated using standard tissue culture polystyrene plastic, handled in aseptic conditions in the laminar fume hood (LFH) and incubated at 37 °C in humidified atmosphere with 5% CO₂. Cell counting was performed using Neubauer hemacytometer chamber (Laboroptic Ltd, Lancing, United Kingdom). Cells used in all experiments were of the passages up to V.

3.5.1. Initiating the culture

Cryopreserved cells were used for culture initiation. Vials were thawed in a 37 °C water bath and seeded immediately in the cell culture flask with 5 ml of pre warmed complete renal epithelial growth medium (REGM). Poly-L-lysine (2µg/cm²) coated T-25 culture vessel was used for culture initiation. Seeding density of 10 000 cells/cm² was used. Afterwards, after closing the cap of the vessel, flask was gently rocked to distribute cell even and propagated in the incubator after loosening the cap for the gas exchange. On the next day, media was refreshed to remove residual DMSO from the culture medium. Media refreshment was performed on each 3 days of the culturing or earlier if indicated by the drop of pH reflected in the significant color change of the medium. Cells were cultured until 80 % confluence.

3.5.2. Subculturing

Upon reaching 80 % confluency cells were trypsinized and passaged. Culture medium, DPBS and trypsin solution were pre warmed in a water bath at 37 °C. After aspirating the medium from cell culture flasks cells were washed with DPBS and the trypsin solution was added to the flasks and placed for 2 min in the incubator. Cell detachment was inspected in the inverted microscope. Instantly, culture medium was added to the flask to block the action of trypsin, cell suspension was transferred in the centrifuge tube and centrifuged for 5 minutes at 300 RCF. After centrifugation, supernatant was aspirated and cells were resuspended with the culture medium to the given concentration. Cell

counting was performed using hemacytometer chamber according to the manufacturer instructions [96]. Fluorescent stained cell nuclei were counted using the $100 \times 100 \mu\text{m}$ grid provided by the microscope software. Cells were seeded in the flasks at the density of ~ 5000 cells/cm². After the seeding the flasks were incubated at 37 °C in humidified atmosphere with 5% CO₂. Refreshing of the media was done on the third day of the culture or when indicated by the color change of phenol red pH indicator. Subcultures of cells used in all experiments were of 80% confluency or less. Evaluating of the cell growth rate was performed by calculating population doubling time using the following equations [97]:

$$x = x_0 \cdot e^{\mu \cdot t} \quad (3.3 \text{ a})$$

$$t_d = \frac{\ln(2)}{\mu} \quad (3.3 \text{ b})$$

Where:

x_0 – initial cell density;

x – cell density at time t ;

μ – specific growth rate;

t_d – doubling time.

Characterization of cell morphology was done using inverted light microscope or EVOS® FL fluorescent microscope (Life Technologies, Carlsbad, USA). Amounts of the DPBS, trypsin and culture medium used for cell maintenance are listed in Table 3.1.

Table 3.1. Cell subculture parameters

Cell culture flask	Maintenance medium (REGM), ml	DPBS washing, ml	Trypsin solution, ml	Trypsin blocking solution (REGM), ml
T25	5	5	1.5	5
T75	15	10	3	10
T175	30	15	5	15

3.6. Bioreactor conditions

HCO 1100 and MicroPES TF10 membranes were used to serve as cell scaffold in semi batch type membrane bioreactor. The membrane area available to the cells in the mini-modules was estimated as ~ 1 cm². Before the cell seeding modules were treated with 70% EtOH for 30 min for sterilization and coated as described in 3.3. Coated membranes and control samples were afterwards washed with HBSS 3 times for 10 min. Afterwards, cells were trypsinized and cell suspensions with $5 \cdot 10^5$ cells was seeded into each of the modules. Outlets of the modules from the shell side were secured with the syringe filters, lumen outlets with push-in caps. Thereafter modules were placed in the incubator at 37 °C for cell attachment for 1 hour, with the rotation on 180° after 30 min. Conditionally, to facilitate cell adhesion, the negative pressure was applied in the shell side by suction the fluid from the lumen of the fibers with a syringe for a short period of time. Upon module rotation after 30 min, the procedure was repeated. After 1 hour, cell suspension was removed from the modules and replaced with equal amount of culture medium. Modules were placed statically in the incubator, with media refreshment and 180° rotation each 24 hours.

3.6. Direct and indirect fluorescent staining

To investigate cell properties, morphology and the viable cells density fluorescent staining techniques were performed to the cells attached to the hollow fiber membranes. In all experiments, after modules disassembly membranes were washed with HBSS and fixed in the solution of 2 % paraformaldehyde and 4% sucrose in HBSS for 5 min.

Indirect immunostaining for zonula occludens protein-1 was performed to investigate cell polarization and monolayer confluency. After fixating membranes were washed for 5 min in 4% FBS in HBSS. Thereafter, cells were permeabilized with 0.3% Triton solution in HBSS. Permeabilized cells were incubated in block solution for 30 min which consisted of 2% of BSA, 2% of FBS and 0.1% of Tween20 in HBSS. The described block solution was also used to prepare dilutions of primary and secondary antibodies. After blocking, the solution of primary polyclonal rabbit anti-ZO-1 antibody of concentration 5 µg/ml in block solution was applied and the samples were kept overnight in the fridge at 4°C. Subsequently, the cells were washed with 4% FBS in HBSS 3 times for 10 min and secondary Alexa Fluor® 488 goat anti-rabbit IgG, diluted to the concentration 10µg/ml in block solution (1:200 dilution) was applied on the samples for 30 minutes at the room temperature in the dark environment. After binding of the secondary antibodies the samples were washed with 4% FBS in HBSS 3 times for 10 min.

Direct immunofluorescence technique with fluorescent DNA-binding molecule - DAPI was applied to estimate cell density and viability. Pre washed with HBSS samples were used for the staining. DAPI diluted in HBSS to the 300 nM concentration was applied onto the samples for 10 min. Thereafter samples were washed with HBSS 3 times for 10 min, and kept in the dark environment.

3.7. Attachment of cells to hollow fiber membranes

Adherence of the cells to membrane scaffolds was investigated using DAPI staining technique, described previously in 3.6., and cell detachment with trypsin. Following the disassembly of the modules, hollow fiber membranes of defined lengths were washed with DPBS and placed in 0.5 ml of trypsin solution. Cells were incubated for 10 min at 37 °C to perform trypsinization and 1.5 ml of culture medium was added to inactivate action of the enzyme. After centrifugation at 5000 RCF and aspirating of supernatant, cells were resuspended in 0.1 ml of culture medium.

3.8. Cell imaging

After fluorescent staining, samples were imaged using epifluorescent EVOS® FL fluorescent microscope (Life Technologies, Carlsbad, USA) or laser confocal microscope (Zeiss LSM 510, Carl Zeiss AG, Oberkochen, Germany). Inverted light microscope was used for cell density and morphology observation during subculturing.

3.9 Statistical analysis

Raw data calculation and processing and imaging were done with Microsoft® Excel (Microsoft Corp., Redmond, USA) and OriginPro (OriginLab® Corp., Northampton, USA). Statistical analysis was performed using OriginPro software. First, the data sets were evaluated for containing the outliers with Grubb's test. Consequently, the difference between the groups was detected by comparing the group means using Student's t-test. Significance level of 0.05 was used for the analysis.

4. RESULTS AND DISCUSSION

In this chapter, two types of commercial membranes were characterized and examined on their ability to serve as the scaffolds for the human primary kidney cell culture. First, membrane surface topography, roughness, pore size, etc., were investigated with scanning electron microscopy. Effect of coatings and membrane transport properties were examined using such dynamic characterization techniques as pure water and protein permeation tests. And finally, cell culture experiments were performed.

4.1. Surface characterization of hollow fiber membranes

Surface topography is one of the most important parameters for the successful cell attachment and proliferation. Both membranes, HCO 1100 and MicroPES TF10 were used in clinical practice for blood and plasma separation applications and have excellent hemo- and cytocompatibility [35,59,98,99].

SEM images of the polyethersulfone based HCO 1100 and MicroPES TF10 membranes are shown in Figs. 4.1 and 4.2 respectively. From images it can be established that HCO 1100 membrane is characterized by the typical asymmetric structure. It can be clearly seen in the Figs. 4.1 a-f, that HCO membranes possess a dense selective skin layer in the lumen side of the fiber. Finger-type macrovoids are present in the membrane support layer, and sponge-type structures with the smaller pores underlie the polyamide skin selective layer of the lumen side.

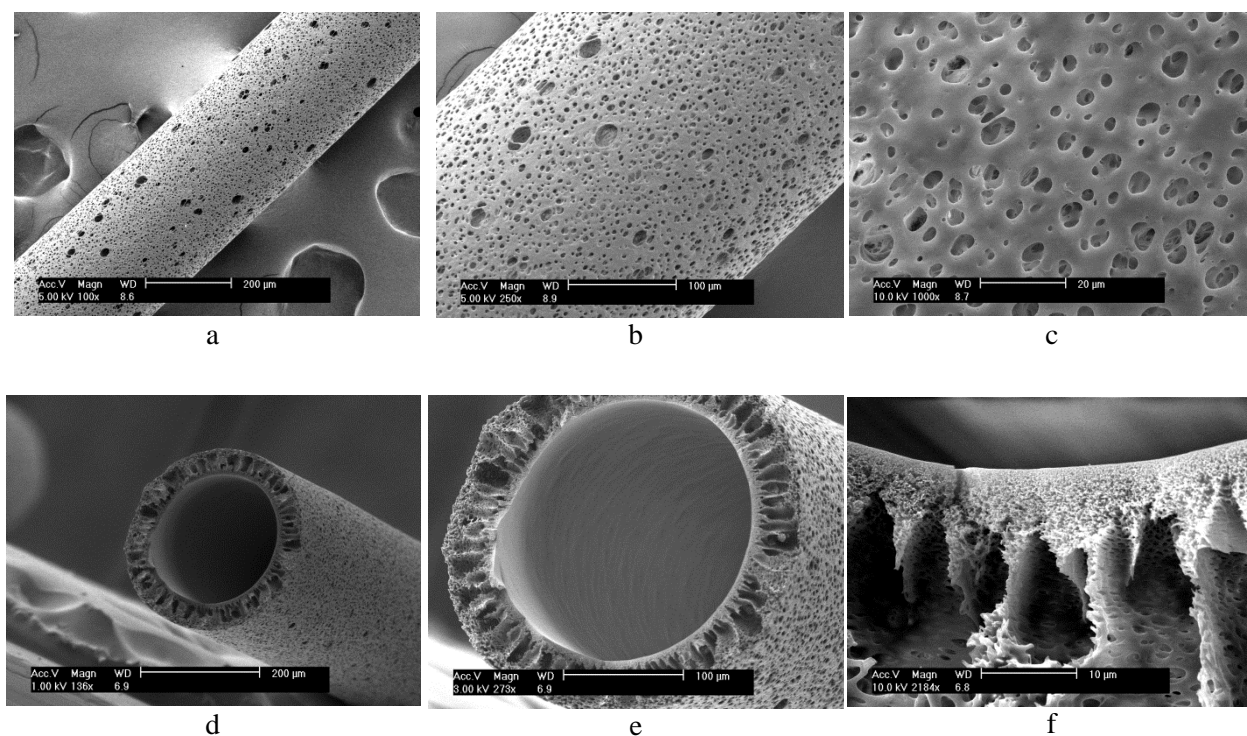


Fig. 4.1. Scanning electron microscopy images of lateral surface (a, b, c) and the cross sections (d, e, f) of HCO 1100 hollow fiber membranes.

MicroPES membranes, on the contrary, did not contain macrovoids or microporous selective skin layer. Sponge-like structure was present throughout the whole length of the membrane wall. As shown in Fig 4.2 pore size distribution of the MicroPES membrane is more narrow compared to HCO 1100 membrane. Macropores of the size $\sim 0.1 - 0.5 \mu$ are present on both skin and shell surface of hollow fibers. Comparing the lateral surface morphology of the membranes at high magnifications (Fig. 4.1 (c) and 4.2 (c)) it can be seen that MicroPES TF10 membrane has increased roughness compared to HCO 1100 membrane, whereas the later, possess smooth outer surface. Also it can be concluded that HCO 1100 membrane has larger macropores or wide distribution on its outer surface

whereas, as it was already mentioned macropores of MicroPES TF10 membrane are the of more uniform size.

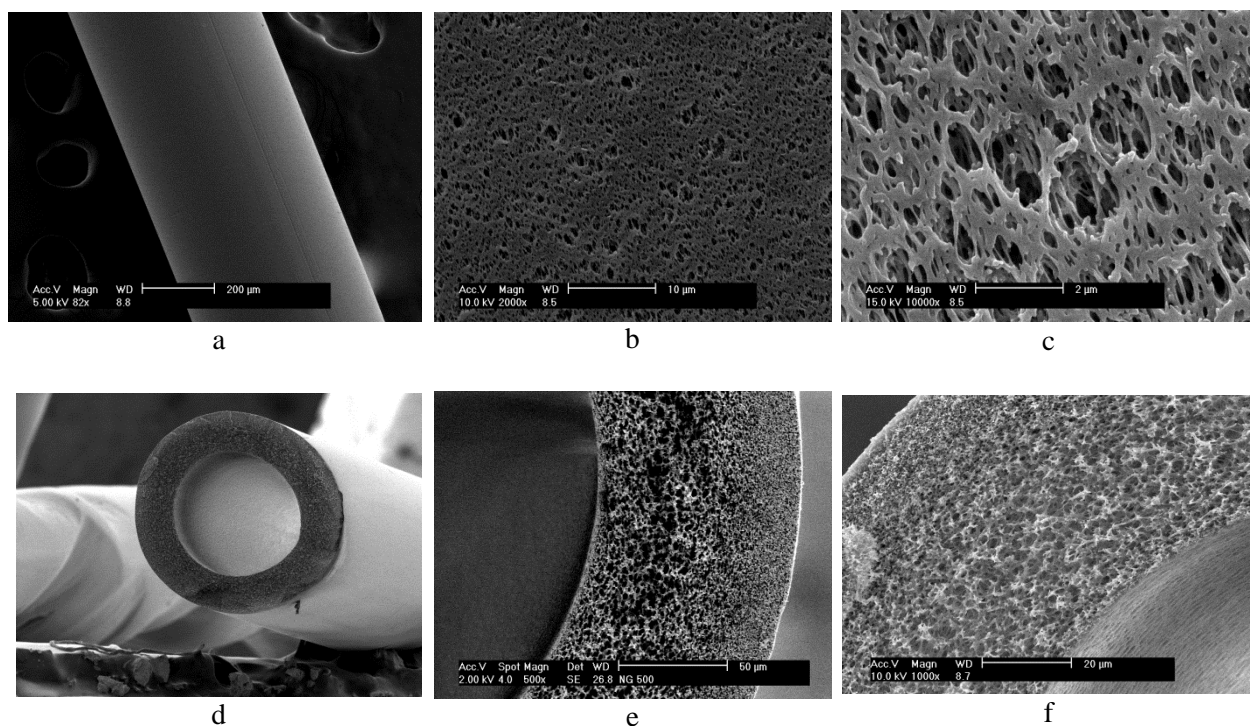


Fig. 4.2. Scanning electron microscopy images of lateral surface (a, b, c) and the cross sections (d, e, f) of MicroPES hollow fiber membranes.

The obtained results reflect the data present in literature and correspond to the application fields of the both membranes. Thus, HCO membrane was designed to achieve permeability of the middle molecules of molecular weight 15 – 45 kDa [100] and provide adequate retention of the large molecules such as albumin (67 kDa) in haemofiltration treatment. Moreover, since the membrane is used clinically for HD therapy, it should minimally interact with plasma proteins to reduce membrane fouling to provide stable membrane permeability during the treatment of the patients. According to Ronco et al. [59] such three-layer structure optimizes the transport and permeability properties of the membrane.

On the contrary, plasma separation MicroPES TF10 membranes were designed to allow the passage of all blood protein and to retain the blood cells. Membranes nominal pore size was equal to 0.2 μ (Appendix D) which is correlated to the size of the human cells. At the same time, protein open, microfiltration type structure of MicroPES TF10 membrane would imply the risk of the membrane fouling due to pore plugging [101]. But again, taking into account that the membrane initially was designed to be used in plasma separation applications, which normally run in the batch mode, this effect might not impact significantly overall efficiency of the process. Moreover, since in the current work MicroPES TF10 membrane is intended to be used as a cell scaffold, these properties could have positive overall effect on the membrane performance. First, the size of the pores is uniformised to retain and concentrate the blood cells for the further use. And second, having a monolayer of cells on the hollow fiber surface would decrease dramatically convective properties of the membrane, which in turn would alter pore plugging with proteins [99,98,102].

Overall, it could be concluded from the obtained microphotographs and the literature data that according to their pore size the two membranes can be classified into ultrafiltration and microfiltration types. Pore size of MicroPES TF10 membranes is adjusted to the size of human cells. However, the surface of MicroPES TF10 membranes possesses roughness in the nano scale, which could increase or decrease cells attachment and proliferation when comparing to HCO 1100 membrane, which should be further investigated.

It must be also mentioned, that no difference in SEM microphotographs was observed for the membranes coated according to the procedure described in the section 3.3. Apparently, more sensitive technique is required to detect the nanoscale changes in membrane structure. Therefore such attempt was performed using attenuated total reflectance Fourier transform infrared spectroscopy (ATR-FTIR). Transmittance spectra of coated and virgin HCO 1100 and MicroPES TF10 membranes are given in Figs. 4.3 a and 4.3 b respectively.

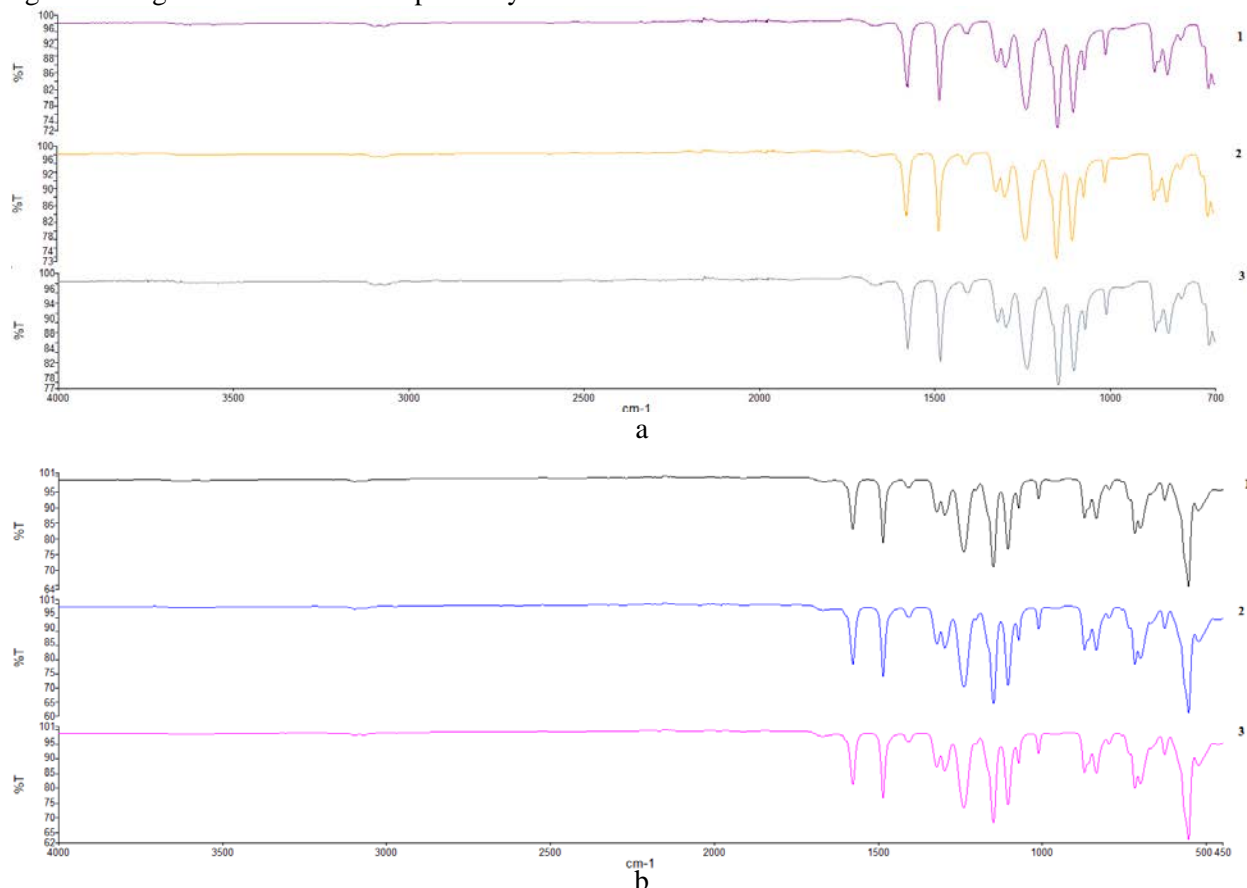


Fig. 4.3. ATR-FTIR spectra of HCO 1100 (a) and MicroPES TF10 (b) membranes: 1 – virgin membrane; 2 – L-DOPA coated membrane; 3 – L-DOPA and Col IV coated membrane.

It can be seen from the graphs that no significant differences is observed. In fact, when analyzed with Spectrum for Windows software, spectra 1-3, within the same membrane type showed more than 99% similarity and no separate distinctive peaks can be observed in the modified membranes compared to the native one. Despite the fact that, L-DOPA coating on the surface of the hollow fibers was visually observed (Appendix E) chemical group analysis did not vary significantly.

When comparing the results with the data present in literature, it becomes clear that the spectra provided for polydopamine or poly-L-DOPA coatings were obtained from the flat membrane samples coated for at least 24 h in static conditions [103,104]. Therefore, the obtained results signify that layer thickness of poly-L-DOPA deposited in the dynamic conditions for 2 h on the surface of hollow fiber membranes was not sufficient to be detected by the ATR-FTIR technique.

4.2 Transport properties of the membranes

Morphology related parameters of the membranes were described in previous chapter. However, “dynamic” characterization techniques are always necessary since they involve only active pores. Among such techniques flow and rejection measurements are among the most relevant ones to the current project. First, pure water flux experiments were used to investigate the effect of the coatings. And second, rejections of such proteins as BSA and IgG were studied to model the behavior of the coated membranes in the bioreactor conditions.

Pure water flux test is a robust, sensitive, easily reproducible and established “dynamic” technique used for membrane characterization. Pure water fluxes of the unmodified and coated HCO 1100 and MicroPES TF10 membranes are presented in Figs. 4.4 and 4.5 respectively.

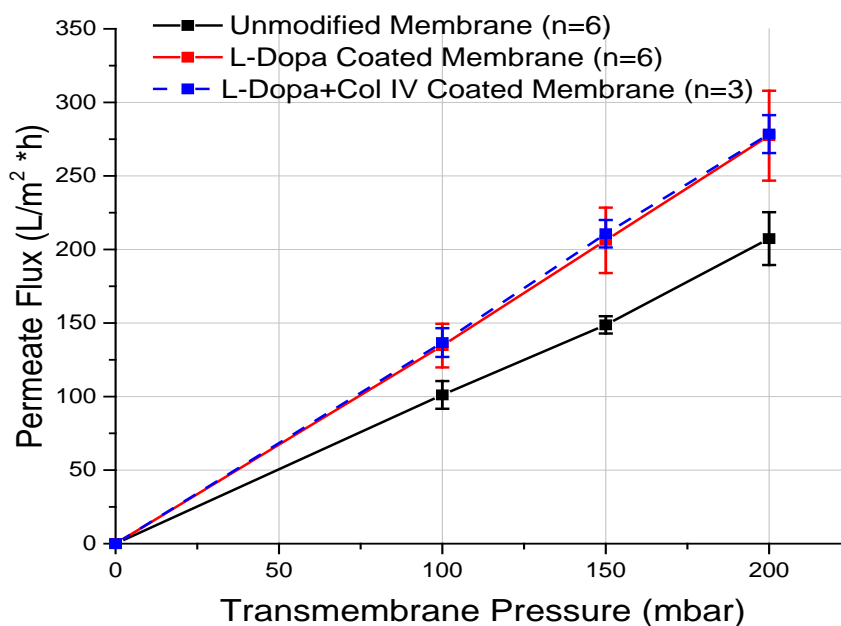


Fig. 4.4. Pure water flux of HCO 1100 membranes.

Transmembrane pressure range for the experiments selected was 100 – 200 mbar which correlates to the pressure diapasons used in haemofiltration treatments [24]. It can be seen from the graph, that for HCO 1100 membrane the increase in the fluxes of the coated membranes was observed. The increase of the fluxes, in fact, indicates that the alteration in the hydraulic radiuses of the pores resulted from coatings do not contribute to the extent it could be recognized by this technique. Instead, such alterations in the chemical structure, such as hydrophilization of the surface, in particular, could determine membrane behavior.

Such assumptions in the above are supported by the literature data available on the polydopamine coatings. In fact from the recent studies provided by the different authors [79,84,104] it can be estimated that the coating layer thickness under the performed conditions (see 3.3) could not exceed 5 nm. Since only the outer surface of the membranes was subjected to coatings without applying TMP, selective skin layer of the membrane is expected to be mainly not affected by poly-L-DOPA the coating. Coating effect on the skin layer will be mainly discussed when describing protein rejection measurements in this chapter below. Charge effects of the poly-L-DOPA coatings, according to the paper of Azari and Zou [84] were also considered to be negligible, for the same reason as it was discussed above, since the nanometer scale coatings could not contribute significantly to the net overall charge. On the other hand, even the very thin nanoscale coatings of polydopamine are reported to contribute to surface hydrophilization. Positively and negatively charged moieties of the deposited layer establish ionic interactions with water molecules dipoles, as described in section 2.5.3.

Consequently, data showed in Fig. 4.5 for permeate flux of native and modified MicroPES TF10 membranes is consistent with the above considerations. As it could be seen from the graph, hydraulic permeability of the membranes exceed the corresponding data for HCO 1100 membrane on one order of magnitude, which is also expected for a microfiltration range membrane. However the effect of the coating on MicroPES TF10 membrane could not be detected by means of the pure water flux technique since the changes in the permeability caused by the coating could be regarded as negligible when applied on the much more open, microfiltration range membranes.

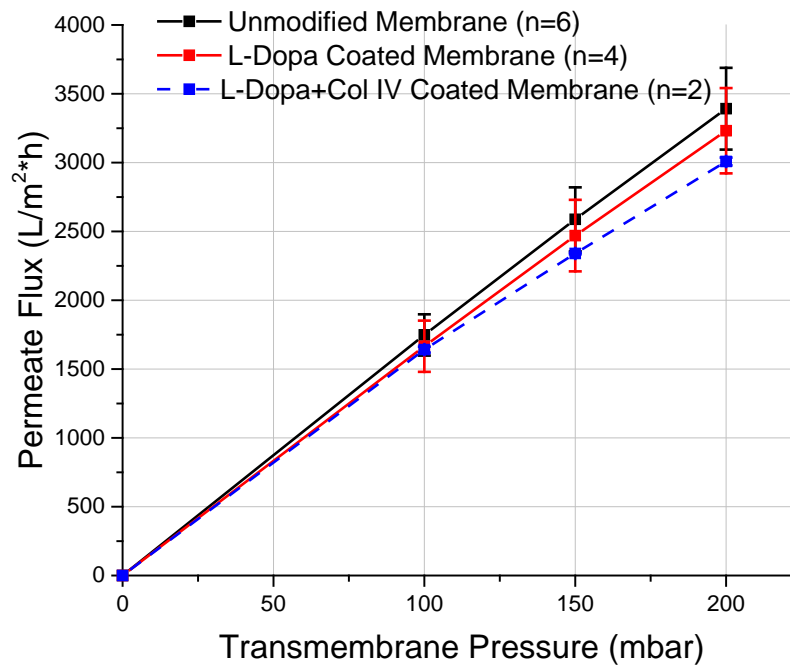


Fig. 4.5. Pure water flux of MicroPES TF10 membranes.

Numeric values of hydraulic permeabilities were calculated using Eq. 3.1 after performing linear regression and one sample t-Test on the obtained data. Consequently, numeric value of hydraulic permeability of HCO 1100 membranes were equal to $0.997 \pm 0.036 \frac{L}{m^2 \cdot h \cdot mbar}$ for unmodified membrane compared to the values of 1.352 ± 0.156 and $1.393 \pm 0.066 \frac{L}{m^2 \cdot h \cdot mbar}$ for L-DOPA coated and L-DOPA/Col IV double coated membrane respectively. Pairwise comparison between the permeability values obtained for virgin and single or double coated HCO 1100 membranes was performed using two sample one tailed t-Test. One tailed test was used since it was evident (Fig. 4.5) that hydraulic permeabilities of the both single and double coated membranes were higher compared to the native membrane. After assuming equal variances, p-values for the tests were calculated and were equal to $1.43 \cdot 10^{-4}$ ($n_1=n_2=6$) and $2.46 \cdot 10^{-4}$ ($n_1=6, n_2=3$) respectively, which is in the both cases less than the significance value 0.05. Therefore, with the significance level 0.05 it could be stated that single and double coatings of HCO 1100 membranes resulted in the increase of its hydraulic permeability.

Similar data treatment was performed for the results obtained for MicroPES TF10 membranes. Hydraulic permeabilities for virgin, single coated and double coated MicroPES TF10 membranes were equal to 17.12 ± 1.51 , 16.32 ± 1.65 , 15.52 ± 0.19 respectively. Two sample two tailed t-Test was performed to compare the data for virgin and coated membranes. No statistically significant difference was observed when comparing permeabilities of virgin and single coated membrane ($p=0.450, n_1=6, n_2=4$) or virgin and double coated membrane ($p=0.60, n_1=6, n_2=2$). The values of hydraulic permeability for coated and unmodified membranes is given in the following diagrams (Fig. 4.6).

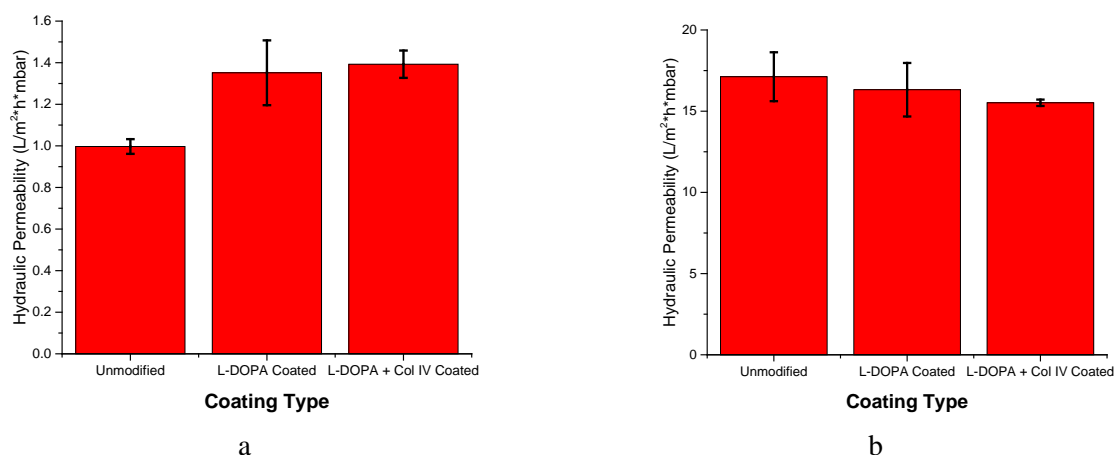


Fig. 4.6. Hydraulic permeabilities of virgin and coated HCO 1100 (a) and MicroPES TF10 (b) membranes.

The membranes behavior in hemofiltration conditions was estimated with the model solutions of 1 mg/ml of BSA and 0.02 mg/ml IgG in PBS. Typical protein ultrafiltration curve depicting permeate flux vs. TMP was obtained for HCO 1100 membranes for both protein solutions (Fig. 4.7).

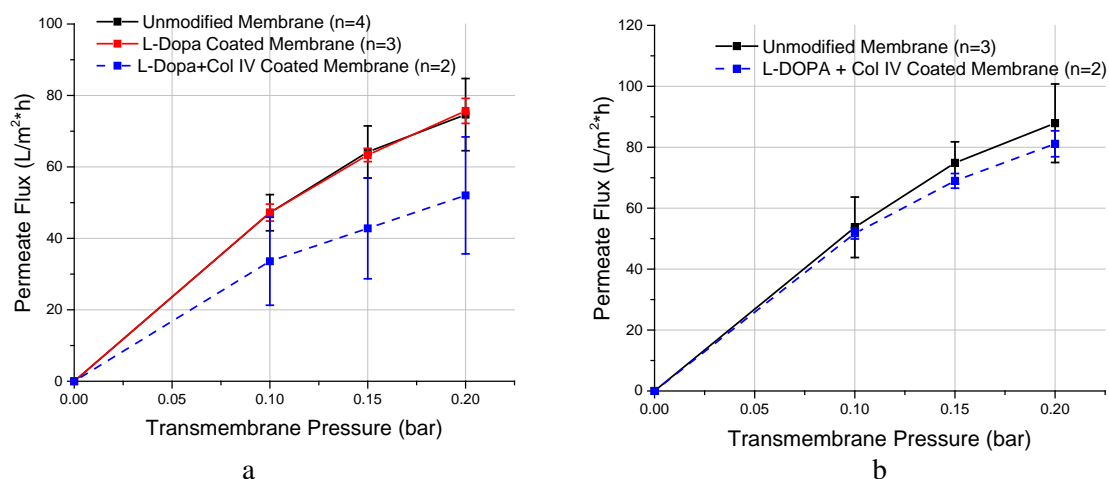


Fig. 4.7. Operational curve of HCO 1100 membrane for filtration of BSA (a) and IgG (b) solutions.

In a tangential flow filtration operation permeate flux increases with increasing TMP up to a point (operating point or critical) when it levels off. In the cases of both proteins this value is estimated as 0.15 bar. The part before this point is defined as pressure dependent regime and part of the graph to the right of the operating point is called pressure independent regime. As it could be seen from the graphs, flux curve is reaching the pressure independent or plateau region at 0.2 bar. Therefore, the presented results enable us to conclude that the operation curves of coated and native PES membranes are consistent with the behavior of typical PES ultrafiltration membranes [95].

However, when analyzing protein filtration curves it could be denoted that the increase of the flux no longer took place for single and double coated membranes in case of protein solution ultrafiltration. This fact could be stated by overlapping of confidence intervals in the graph, that the single coating of L-DOPA did not affect the permeate flux. Moreover, in the case of double coated with L-DOPA and collagen IV HCO 1100 membranes a decrease of permeate flux was observed. The

latter effect can be correlated with the decrease in hydraulic radiuses of the pores resulting from collagen IV immobilization.

Different assumption could be made to establish the mechanism of the phenomena. In such attempt intrinsic fouling of the membrane could be considered [105,106]. First of all, the presence of collagen IV immobilized in the membrane wall would naturally reduce hydraulic radiuses of the pores. Additionally it could serve as secondary adsorption site for proteins transported to the permeate side, increasing the overall effect on the hydraulic radius. However, additional experiments are required to investigate the effect of coating on active pore size distribution of the membrane.

Utterly different behavior of the flux curve of MicroPES TF10 (Fig. 4.8) membrane was observed for filtration of the same protein solutions. Dramatic flux decrease was observed when operating at higher pressures in the case of both proteins filtration which is indicated by the negative overall negative slope of operation curves. However, even in its lower points (at the highest TMP value), permeate fluxes obtained for MicroPES TF10 membranes were significantly higher compared to HCO 1100.

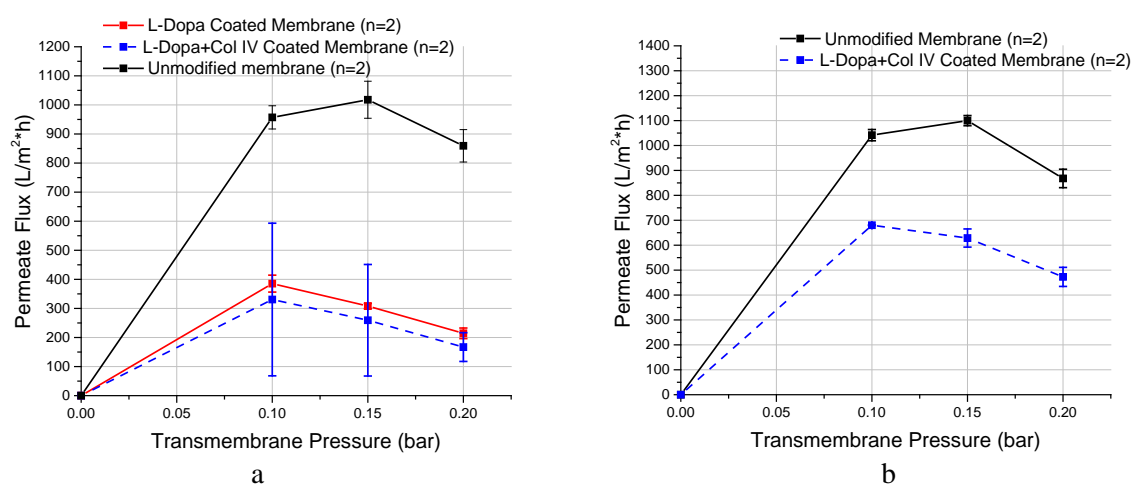


Fig. 4.8. Permeate flux of MicroPES TF10 membranes during filtration of BSA(a) and IgG (b) solutions.

Analyzing the data available in literature [107,108], the probable explanation of the effect, as well as the behavior of the filtration curve itself is the deposition of aggregated/denaturated proteins on the membrane surface. Protein concentration in the bulk, operating conditions, protein and solvent properties play critical role in the process. Specifically, similar behavior of the flux curve of 0.16 μm PES microfiltration membrane during the filtration of BSA solution in PBS was reported by Kelly et al. [108]. Taking into account that the active pore size of MicroPES TF10 membrane is equal to 0.2 μm , the proposed model could be used to explain observed phenomenon. According to the authors, protein aggregates or denaturated proteins tend to form deposited layers on the relatively open structures of PES microfiltration membranes. Alternatively, formation of thiol-disulfide linkages in protein molecules during microfiltration, according to Kelly and Zydney [109] was greatly responsible for protein aggregation. Higher permeate fluxes (~ 2 fold) observed during IgG microfiltration support the above considerations. Moreover, the decrease in permeate flux for the coated MicroPES TF10 membranes is well aligned with the described models. The ability of poly-L-DOPA layer to form conjugates with proteins was discussed in section 2.5.3. Therefore, it is highly probable that the coating of the membranes decrease the fouling resistance of MicroPES TF10 membranes.

Rejection properties of modified and native membranes were evaluated with apparent sieving coefficient during protein filtration using Eq. 3.2. For native, single coated and double coated HCO 1100 membrane these values were equal to 0.234 ± 0.005 , 0.231 ± 0.0329 and 0.069 ± 0.0195 respectively. Assuming the equal variances two sample two tailed t-Tests were performed to establish statistical difference of the data. At the level of 0.05, the difference between BSA sieving coefficients of virgin and L-DOPA coated membrane was not established ($p=0.9008$, $n_1=n_2=3$). However, BSA

sieving coefficient was significantly different at when comparing virgin and double coated HCO 1100 membranes ($p=0.0073$, $n_1=3$, $n_2=2$).

Membrane sieving properties for IgG permeation were similar for the previous data. Decrease in IgG sieving coefficient from 0.353 ± 0.037 to 0.114 ± 0.019 was observed when comparing virgin and double coated HCO 1100. Statistical significant difference was observed using t-Test as described above ($p=0.0039$, $n_1=3$, $n_2=2$). Observed sieving coefficients for both protein solutions obtained with virgin and coated HCO 1100 membranes are visualized in the following graph.

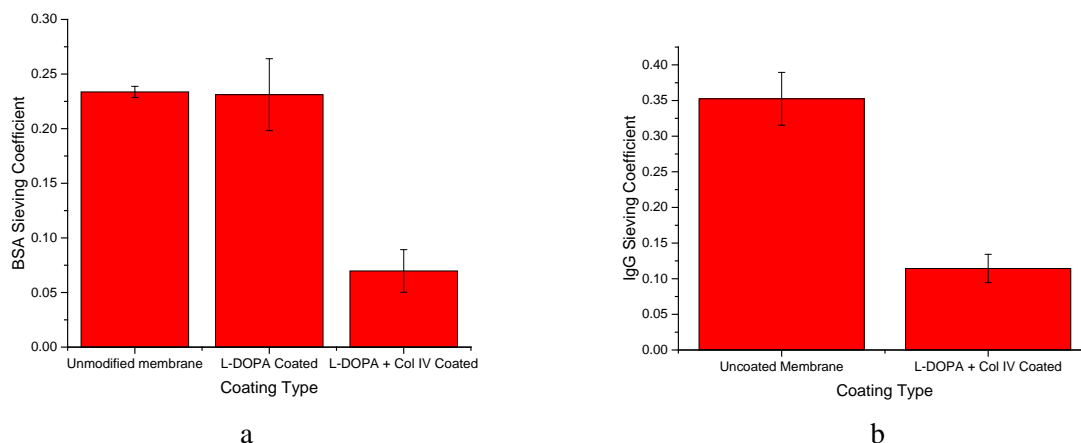


Fig. 4.9. BSA (a) and IgG (b) sieving coefficients of HCO 1100 membranes.

Microfiltration range MicroPES TF10 membranes are of significantly more open structure compared to HCO 1100 and are transparent to the proteins (Appendix D) [99,98]. Therefore main interest in protein sieving experiments was in the effect of the double coating, which was intended to use for cell culture experiments. Results obtained from the permeation tests, however, showed that BSA sieving coefficients of single or double coated MicroPES TF10 membranes were equal to 0.967 ± 0.0116 and 0.967 ± 0.005 respectively which is comparable to the data found in literature.

IgG sieving coefficients of virgin and coated with L-DOPA and collagen IV MicroPES TF10 membranes were also determined. Obtained respective values of 0.97 ± 0.021 and 0.875 ± 0.015 were statistically different when the sets of data had been compared with two sample t-Test ($p=0.0367$, $n_1=n_2=2$). Sieving coefficients for the MicroPES TF10 membranes are shown in Fig. 4.10.

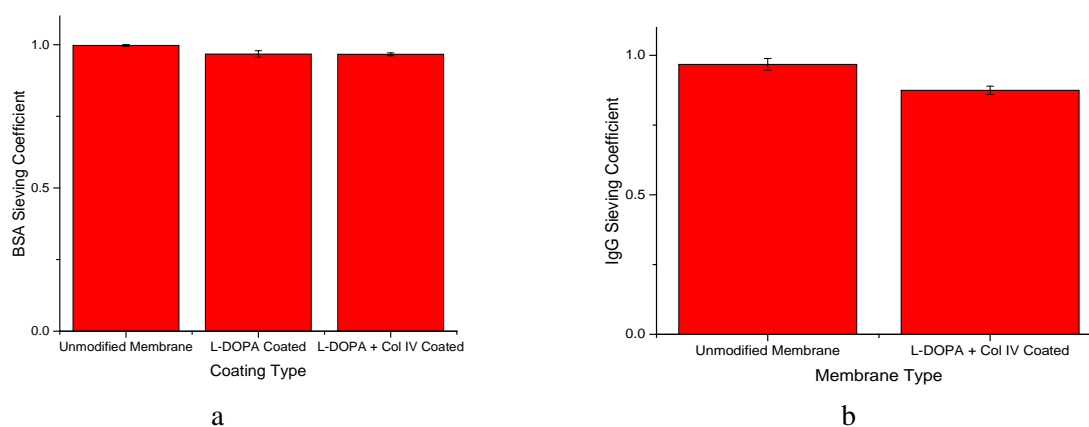


Fig. 4.10. BSA (a) and IgG (b) sieving coefficients of MicroPES TF10 membranes.

In general, sieving coefficients data is consistent and well aligned with the above consideration concerning membrane permeabilities towards protein solutions. On the example of HCO 1100 and to less extent MicroPES TF10 membranes it could be established that double coating resulted in decrease of sieving coefficient or increase of membrane rejection. The effect was much less pronounced for MicroPES TF10 membranes, however, the data from literature [110] provides information that protein-fouled microfiltration membrane obtain ultrafiltration rejection properties in temporal perspective.

4.3 Cells attachment and proliferation

Prior to the bioreactor assembly, seeding and incubation investigation of growth parameters of the subculture of human proximal tubular cells was performed. The common technique for studying proliferation behavior of the cell is the growth curve. From a growth curve it is possible to estimate doubling time of the cells in culture and also cell density at the confluence level. Moreover, during the experiments it is possible to investigate cell morphology and the growth patterns. Thereafter, using the obtained information of the cell behavior and literature data

4.3.1. Preliminary characterization of the cell line

In order to build the growth curve of the culture of human proximal tubular cells standard tissue culture 12-well plates were used. Cell suspension of different cell densities were seeded in the plate and harvested after the defined periods of time. Three seeding cell densities were used: 5400 cells/cm², 16200 cells/cm² and at nearly confluent 54000 cells/cm². Cell performance can be visualized in the following graph.

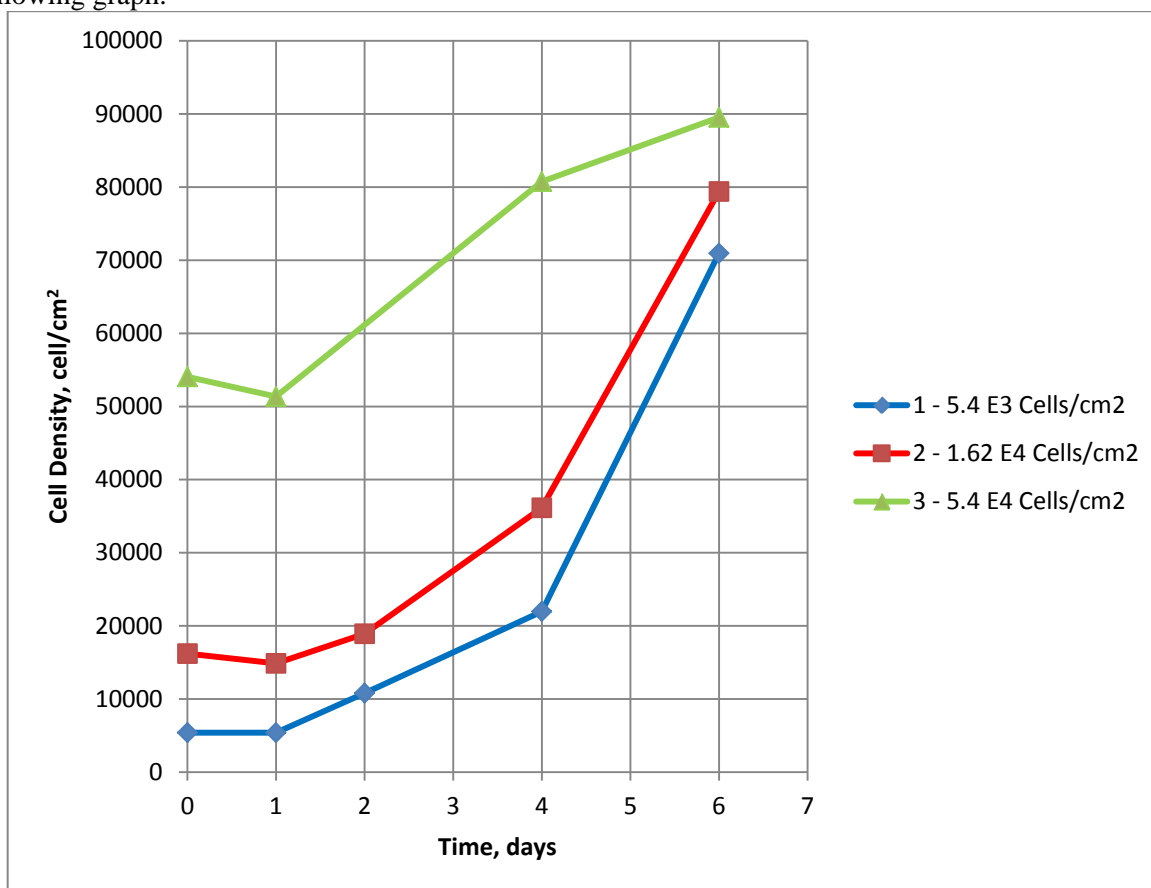


Fig. 4.11. Human proximal tubular cells growth curve.

After observing the graph it could be noticed that in the all cases before the cell proliferation lag phase occurred in the period of 0 - 24 hours of the culturing. Next, lag phase was followed by the region of exponential growth. The data obtained for the period could be used to estimate the doubling time of the population. Finally, the third terminal plateau region could be distinguished when

analyzing the curve with the highest seeding density. Density limitation or contact inhibition is the commonly accepted explanation for the phenomenon for the cultures of renal primary cell lines [111].

Moreover, as it can be observed from the transmitted light microphotographs (Appendix F), that after reaching the confluence the cells formed superconfluent multilayer structures under the conditions applied. Formation of dome-shaped multilayer structures was observed in this case. Again, such behavior of renal primary cell lines was previously described in literature and can be controlled by varying the composition of the growth factors and nutrients. Serum free defined growth media are typically preferred in this respect [112,113]. Therefore when quantifying the confluent cell density the both cells counts and microscopy observations are required.

Important parameters for the further were established in the cell line characterization stage. Overall, typical behavior for monolayer culture growth curve was observed in Fig. 4.11 [66]. Doubling time of the cell populations seeded with different cell densities was calculated according to the Eqs. 3.3. First, regions of the growth curves corresponding to the exponential growth were fitted exponentially to obtain the values of the specific growth rates. Values of μ obtained from exponential fit for the curves 1 – 3 were equal 0.0205 ($R^2=0.987$), 0.014 ($R^2=0.993$) and 0.0062 h^{-1} ($R^2=1$) respectively. Consequently the corresponding doubling times for the curves (Eq. 3.3 b) were calculated as 34, 49 and 110 hours. The obtained results are consistent with the above considerations, as the highest growth rate was obtained for the smallest seeding density and contact inhibition effects were the lowest.

Confluency levels of the cell populations were determined using cell counts and microscopy observations as discussed earlier. For this reason the data obtained for growth curve No. 3 was excluded from the calculation as the multilayer structures were determined in the last days of cultivation. The obtained value of confluent cell density was thereby determined as $75.2 \cdot 10^3 \pm 5.9 \cdot 10^3$ cells/cm². However, it must also be mentioned that the results that were obtained for tissue culture multiwell plates could not be directly extrapolated onto such systems as cell culture flask or bioreactors. Access for oxygen, nutrients and the growth factors in the investigated system would differ when culture flask are used, for example. Such effect seems evident since volumes of the medium per unit surface are proportionally higher for multiwell plates.

Information of the lag-phase duration, as it is shown later will be used for the further experiments. Furthermore, microscopy observations during the cell attachment process to the tissue culture plates surface after seeding indicated that the cells were able adhere during 1 h after the seeding. During the specified time rounded suspended cells started to elongate upon the contact with the surface and were immobilized. These results, lag phase duration data, confluency level and doubling time will be used afterwards when developing the strategy for seeding and maintaining bioreactor system.

It should be also mentioned, that when culturing the cell for the large number of passages (up to 7th) loss of the phenotype of the cells was observed. In such conditions, cells tend to form elongated structures, typical for fibroblasts cultures [113]. Therefore in the performed experiments HPTCs were used up to passage V.

Thereafter the performance of the human proximal tubular cells was evaluated using flat coated 50 kDa PES membranes (Sartorius Stedim Biotech, Gettingen, Germany). Seeding protocol on the flat membranes was adapted from the work of the partners on Bioart Consortium [114] which was developed for culturing of immortalized renal cell line ciPTEC [115] and is currently being prepared for publications. In short, small exposure times when applying single or double coatings were used since the process was facilitated by the gravity and the flatness of the surface further contributed to homogenous coating formation. Results of the experiments were evaluated with the immunostaining for ZO-1 protein, indicator of tight junction formation in monolayer structure and shown in Fig 4.12.

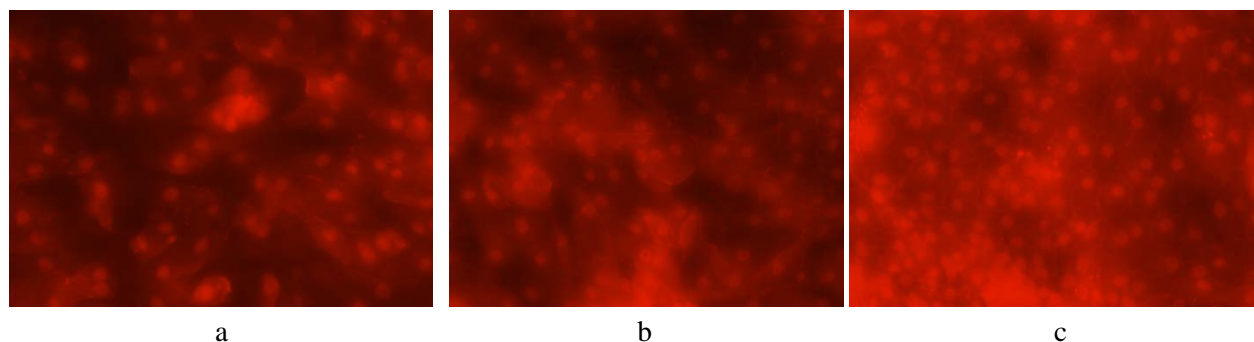


Fig. 4.12. Immunostaining for tight junction ZO-1 protein (red) of primary tubular proximal cells after one week incubation on unmodified (a), L-DOPA coated (b) and double coated with L-DOPA and Col IV flat PES membranes. Staining for rabbit ZO-1 antibody was performed with goat anti-rabbit Texas Red labeled secondary antibody.

As it could be seen from the photographs, the optimal performance of the cells was detected when double coated flat PES membranes were used. Chicken wire-like structures could be recognized in Fig. 4.12 (c) which signified proper tight junction formation within the monolayer. Upon the applying of single L-DOPA coating the cells performed better comparing to the virgin membranes, as the formation of tight junctions could still be detected, however the pattern of its formation was no longer regular. Overall these results are well aligned with the considerations described on biomimetic coatings in section 2.5.3.

4.3.2 Cell attachment in hollow fiber bioreactors

Adhesion of the primary cell to the surface of hollow fiber membranes was among one of the first challenges needed to overcome in order to obtain homogenous confluent monolayers. In case of monolayer formation on the flat surface, adhesion process is facilitated by the gravity forces and the properties of the surface. Therefore obtaining promising results in cell attachment could be the first step for the monolayer formation strategy in the hollow fiber membranes.

Several approaches were used to facilitate cell attachment. For example, application durations of single and double coatings in hollow fiber bioreactors (see section 3.3) were increased significantly compared to the procedures performed for flat fiber membranes. First, L-DOPA coatings were applied in the dynamic flow conditions allowing easy scale up. And second, drying, washing and collagen IV adsorptions steps were also adjusted in respect to the hollow fiber module system.

Further, the application of short-term negative pressure in the cell suspension compartment was assumed to facilitate the cell attachment. Therefore, considering the results of the described above experiments and the literature data, human proximal tubular cell performance were tested in data in the bioreactor conditions with double coated HCO 1100 and MicroPES hollow fiber membranes. Unmodified membranes served as a negative control.

Inner surface area of the hollow fiber module available for the cell attachment was estimated as $\sim 10 \text{ cm}^2$. However only $\sim 1 \text{ cm}^2$ corresponded to the surface area of the PES membranes and the rest of the inner area of the module was related to the surface of the housing. Therefore it was decided to perform seeding with suspension of relatively high cell concentration ($5 \cdot 10^5$ cells/ml) which corresponded to the total estimated seeding density $\sim 5 \cdot 10^4$ cells/cm². Which, in turn, is in the range of the seeding cell density depicted by curve No. 3 in Fig. 4.11. Of course, the specified seeding density in hollow fiber membranes do not imply 100% attachment to the surface as it can be expected in flat surfaces.

Also it was decided to discard the cell suspension after 1 hour interval which was estimated as the minimal time required for cell attachment. In this manner, the excess of the suspended cells or the cells that could not attach to the polypropylene housing was removed from the bioreactor. Attachment of cells to the hollow fiber membranes of both types evaluated 24 hours after seeding by fluorescent DNA staining with 4',6-diamidino-2-phenylindole (DAPI) is shown in the following figure.

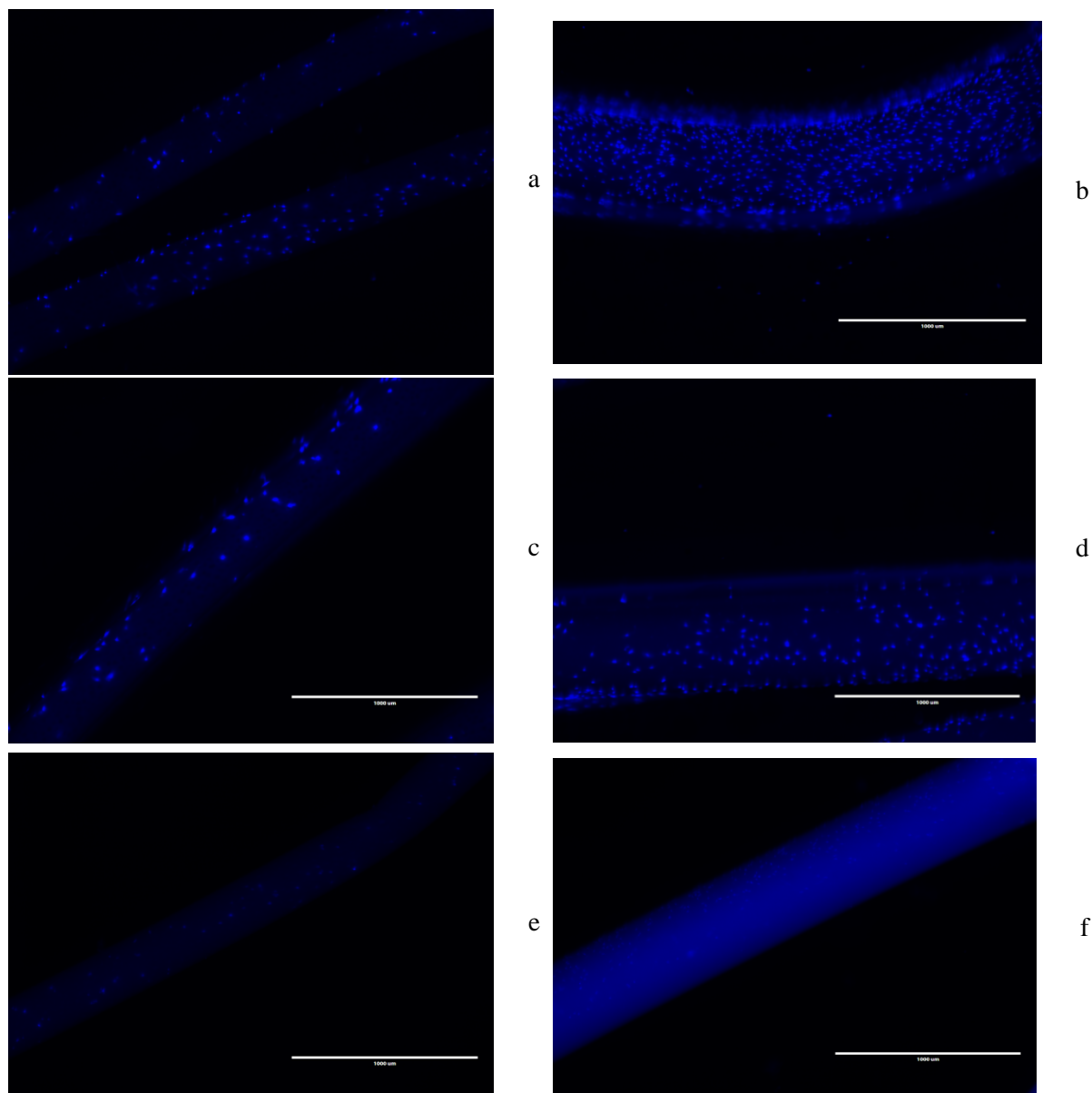


Fig. 4.13. DAPI fluorescent staining for the nuclei of cells attached to the surface of HCO 1100 (a, c, e) and MicroPES TF10 (b, d, f) membranes: a, b – negative pressure applied, double coated membranes; c, d – passive adsorption, double coated membranes; e, f – passive adsorption, unmodified membranes.

From the figure it could be recognized that the highest cell densities and more homogeneous cell distributions were observed when negative pressure was applied. Passive cell attachment for the coated membrane also yielded sufficient results, and significantly reduced cell numbers attached to the native membranes were observed. Another feature that can be observed from Fig. 4.14 is the MicroPES TF10 membrane was more favorable for the cell attachment in all three conditions applied as the higher cell densities were observed compared to the respected HCO 1100 samples.

To quantify and evaluate cell viability after attachment cells adherent to hollow fibers were trypsinized and harvested according to the procedure described in section 3.7. Cell harvesting trypsinization and harvesting step is required to confirm fluorescent technique, since cell density and distribution could be affected by the staining procedure. This is especially significant when the cells were only 24 hours after the seeding, since the young cells do not yet establish maximal adhesion with the substrate.

The results of the cell harvesting and counts are presented in Table 4.1. As it could be seen from the table the results are consistent with the ones presented in Fig. 4.13. However the error of cell

counting with haemocytometer chamber is related to significant error and more sensitive method of cell counting may be considered for future applications.

Table 4.1. Cell densities on the hollow fiber membranes 24 h after the seeding

	Cell density, $\cdot 10^3 \text{cell/cm}^2$	
	HCO 1100	MicroPES TF10
Negative pressure applied, double coated membranes	27 \pm 13	48 \pm 1.7
Passive adhesion, double coated membranes	18 \pm 3.4	21.4 \pm 5.6
Passive adhesion, unmodified membranes	8.0 \pm 1.0	13 \pm 3.2

Summarizing the obtained results, it becomes evident that applying negative pressure facilitated the cell adhesion. However, passive cell attachment onto the surface of the double coated membranes showed also satisfactory results. MicroPES TF10 membranes scored better than HCO 1100 in all the conditions tested. Such result, most probably related to the surface morphology of the membrane, which was adapted to retain blood cells and have dimensions of the pores comparable to the cell size.

4.3.3 Investigation of monolayer formation in batch bioreactor conditions

Cells were cultivated in semi-batch type conditions as described in section 3.6 for 7 days. First, after module disassembly fibers were removed and prepared for fluorescent analysis. Cell density on the hollow fibers was established using fluorescent staining for nuclei with DAPI. As it could be seen from Table 4.2 cell densities on the coated fibers exceeded near-confluency levels determined for tissue culture multiwell plate.

Table 4.2. Cell densities on the hollow fiber membranes after 7 days in culture

	Cell density, $\cdot 10^3 \text{cell/cm}^2$	
	HCO 1100	MicroPES TF10
Negative pressure applied, double coated membranes	60 \pm 23	46 \pm 28
Passive adhesion, double coated membranes	106 \pm 25	92 \pm 37
Passive adhesion, unmodified membranes	24 \pm 21	77 \pm 32

Number of nuclei indicating viable cells were counted in 10 different areas of $100 \times 100 \mu\text{m}$ grid and thereafter averaged. When analyzing the obtained data it becomes evident that cell counts are generally higher than the counts obtained for the attachment assay indicating the cell growth. Surprisingly, the cell density on both membranes at passive adhesion conditions exceeded the confluency levels estimated for multiwell plates and no multilayer structures were detected. The most probable explanation for the phenomenon is in the more hydrophilic nature of the modified membranes compared to tissue culture polystyrene. Consequently, cell spreading is significantly reduced in hydrophilic surfaces. Differentiation of epithelial layer and formation of the brush border layer could also contribute to the increased cell density compared to the conditions present on tissue culture polystyrene. Increase of vertical dimension of the cells is expected in this case [116]. Fluorescent DAPI staining showing the nuclei of the cells attached to hollow fiber membranes are given in the following photographs.

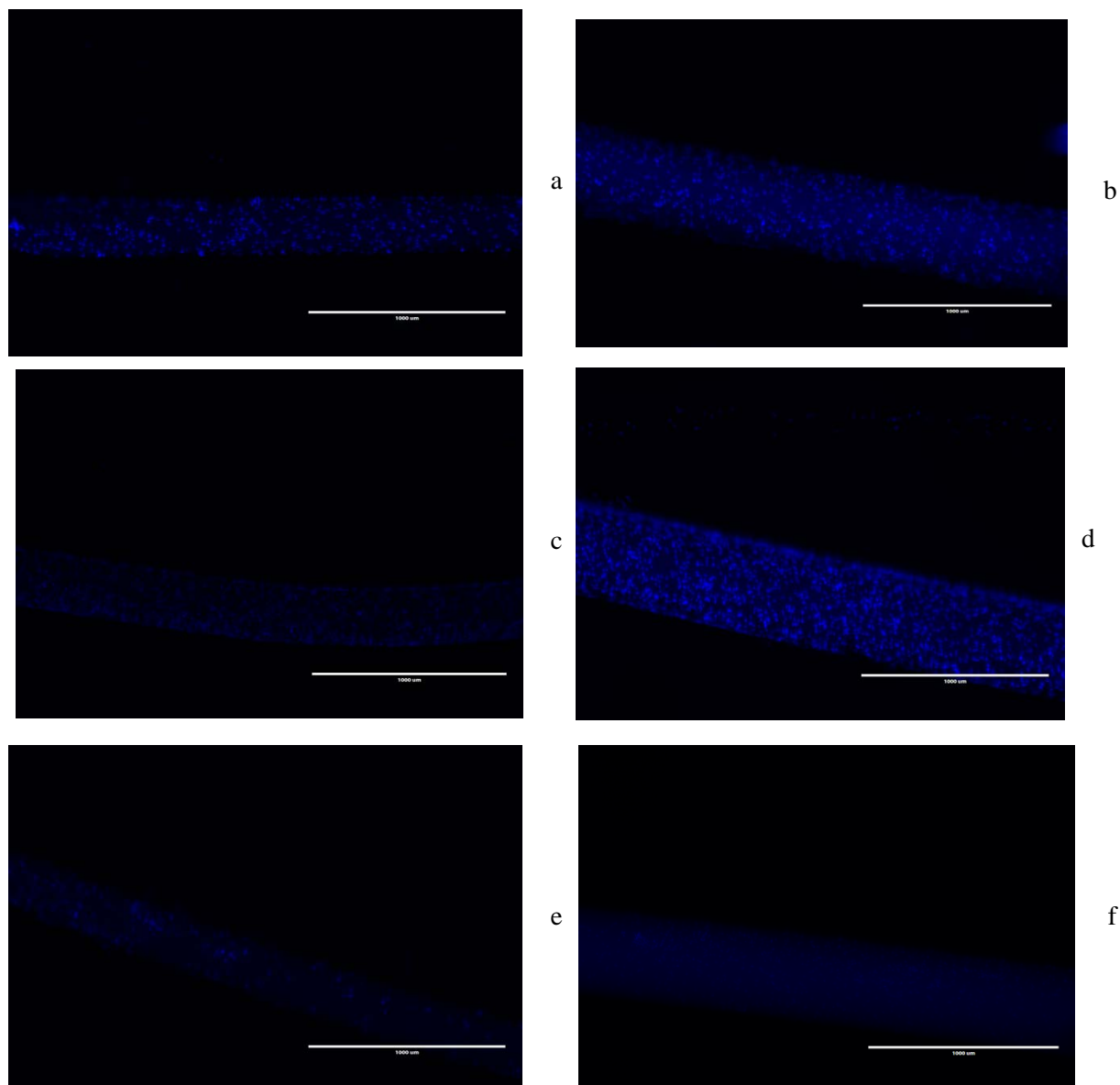


Fig. 4.14. DAPI fluorescent staining for the nuclei of cells attached to the surface of HCO 1100 (a, c, e) and MicroPES TF10 (b, d, f) membranes after 7 days of culture: a, b – negative pressure applied, double coated membranes; c, d – passive adsorption, double coated membranes; e, f – passive adsorption, unmodified membranes.

As showed in Fig. 4.14. the highest cell density is observed for double coated membranes when no negative pressure was applied. The cells were homogeneously distributed in both hollow fibers. Less homogeneous cell distribution is observed for the samples with applying the negative pressure, and irregular pattern of cell growth was observed for the native membranes. As indicated by cell counts, amounts of cells proliferated on the native MicroPES membranes are higher compared with the HCO 1100 counterpart, which is well aligned with the previous results.

From the detailed view of the graph it could be also recognized that the nuclei of irregular shape are present in Figs. 4.14 (a) and (b). Such conditions could indicate loss of the cell viability. As a contrast, in the rest of the photographs the majority of the nuclei were of the rounded oval shape [117].

For further investigation of the cell properties immunostaining for tight junction component – ZO-1 protein was performed. First, the conditions with passive adhesion of the cells onto double coated membranes are presented (Figs. 4.15 – 4.16).

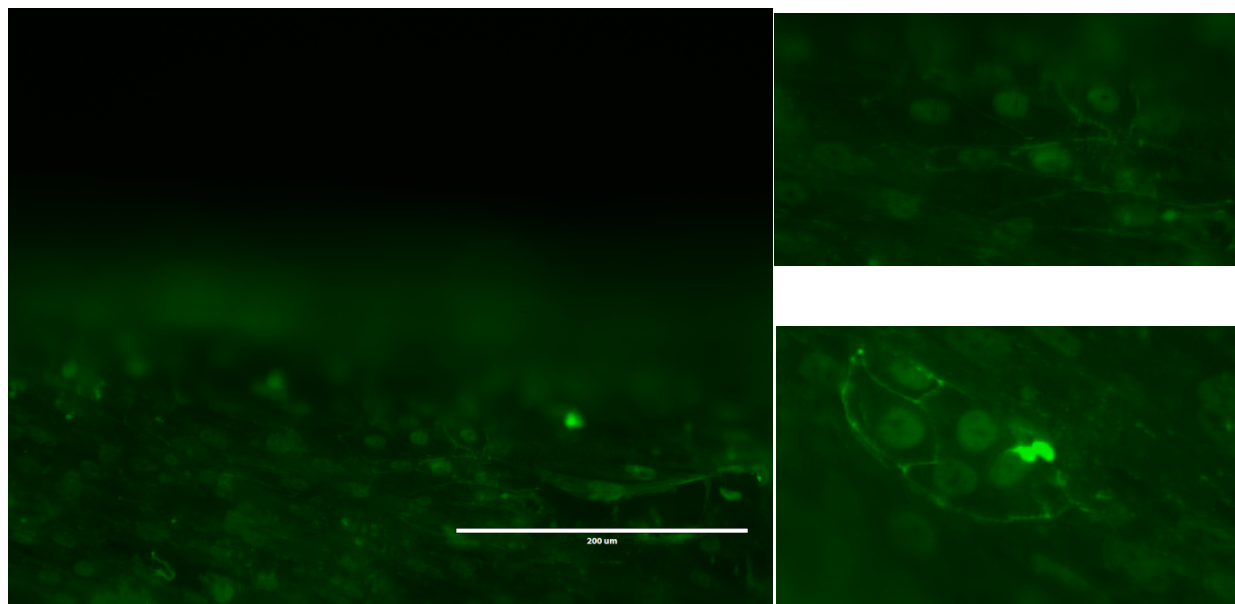


Fig. 4.15. Immunostaining for tight junction ZO-1 protein (green) of primary tubular proximal cells after one week incubation on double coated with L-DOPA and Col IV hollow fiber HCO 1100 membranes. Staining for rabbit ZO-1 antibody was performed with goat anti-rabbit Alexa 488 labeled secondary antibody.

As it could be noticed from the picture, the formed cell monolayers expressed tight junctions which indicates functional differentiation. Despite no visible gaps between the cells was observed in the microscope, tight junction formation pattern only in some regions repeats chicken wire-like structures indicating the formation of the contacts on the perimeter of the cell. Whereas in some regions ZO-1 protein could only be partly recognized. However, the expression levels and patterns of ZO-1 protein of the HPTCs cultivated on double coated HCO 1100 membranes were comparable or even superior to the results obtained for the flat PES membranes (Fig. 4.12) or literature data (Fig. 2.10 (c)) [54]. Also it must be noticed that aligned in the direction of the fiber more elongated cell morphologies were observed when compared to the cells cultivated on the flat membranes. Hollow fiber curvature could play a role in this alignment and is connected with up-regulating of cell differentiation [117].

Cell density counts obtained for MicroPES TF10 membranes after 7 days culture were surprisingly lower compared with HCO 1100 counterpart (Table 4.2). However the cell density registered and the cell distribution still imply the formation of the functional monolayer. Tight junction formation in double coated MicroPES TF10 membrane is depicted in Fig. 4.16.

As it could be seen from the picture levels of ZO-1 expression are lower compared to the previously described. Formation of chicken wire-like structures are more rare and the ZO-1 patterns tend to be more irregular. Cells have still elongated shape, however their orientation is no longer in the direction of the fiber but rather at the sharp angle to it. Such behavior is observed throughout the length of the fiber. As it was discussed previously increased membrane curvature of HCO 1100 membranes could play major role in the phenomenon. Therefore the effect of membrane curvature could play one of the detrimental roles in epithelial cell differentiation and needs to be further investigated.

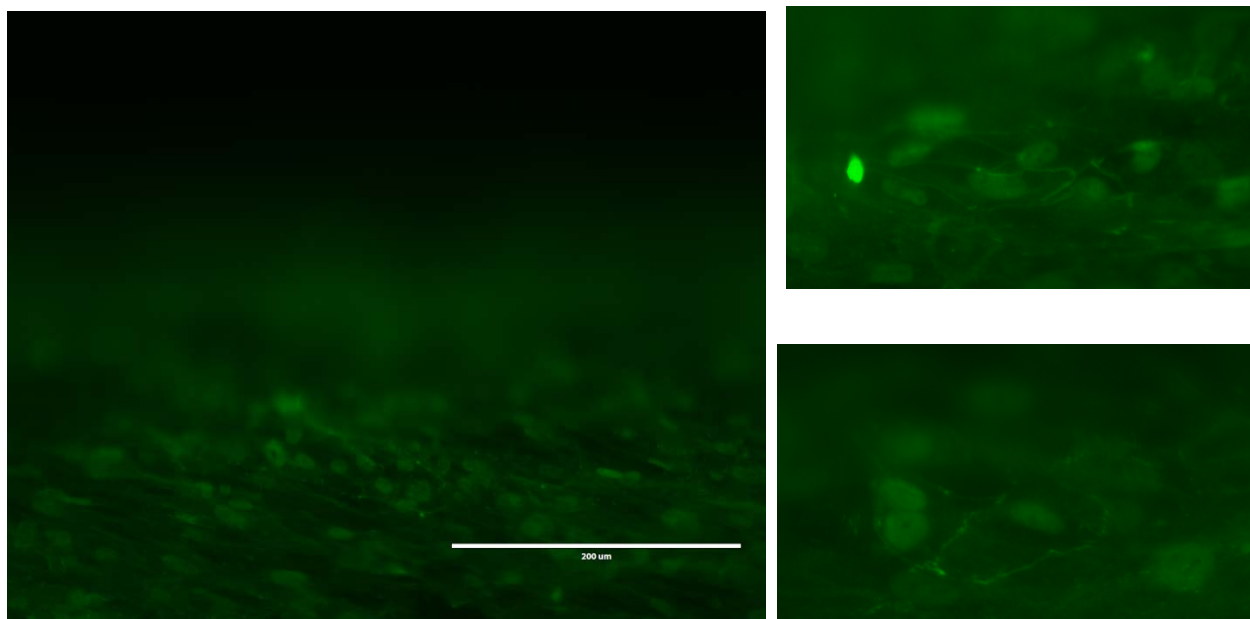


Fig. 4.16. Immunostaining for tight junction ZO-1 protein (green) of primary tubular proximal cells after one week incubation on double coated with L-DOPA and Col IV hollow fiber MicroPES membranes. Staining for rabbit ZO-1 antibody was performed with goat anti-rabbit Alexa 488 labeled secondary antibody.

Next, properties of monolayers for the conditions with applying negative pressure were investigated. The results of the fluorescent staining for the cellular tight junctions are presented in Fig. 4.17.

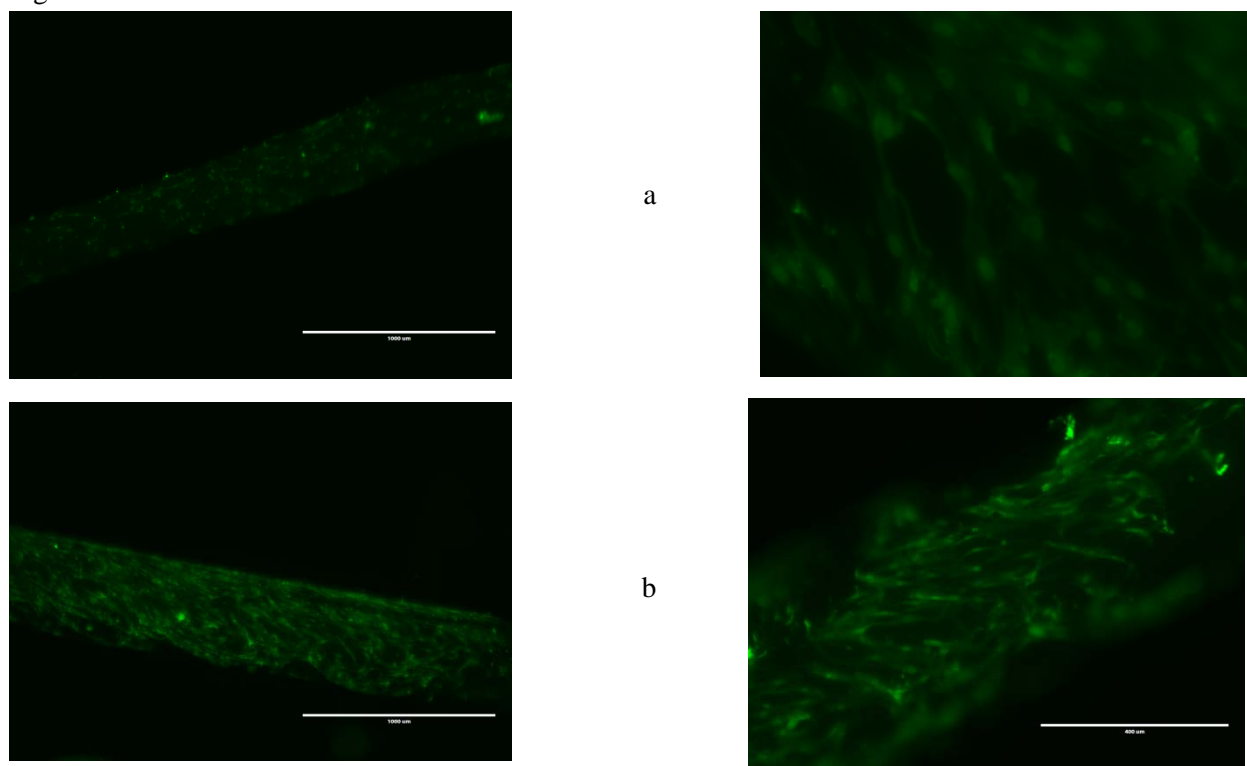


Fig. 4.17. Immunostaining for tight junction ZO-1 protein (green) of primary tubular proximal cells after one week incubation on double coated with L-DOPA and Col IV HCO 1100 (a) and MicroPES (b) membranes. Negative pressure applied for the seeding.

As it could be seen from the Fig. 4.17, no confluent monolayer formation was detected. At higher magnifications (Fig. 4.17 a) gaps in the cell structure could be recognized. Tight junction formation also was significantly reduced and no chicken wire-like structures were present. All of above could indicate impaired properties of the cells present on the membranes. Cell counts data before and after cultivation indicate that ~ 2-fold increase in cell density, which is significantly lower than ~ 5 times increase for the bioreactors seeded with passive cell adhesion. Two factors could be responsible for the effect. First, seeding density that resulted from applying of the pressure was too high, and the cells experienced contact inhibitions, and were unable to spread and form tight junctions [66]. Second, the cells were damaged under applying of the pressure [99]. Therefore the both effects need to be further investigated by applying range of regulated pressures and using seeding suspensions of lower cell concentrations.

According for the nuclei staining data cell monolayers in the bioreactors with unmodified membranes were not formed. Which was indicated by the cell densities and their distribution. Staining for ZO-1 protein confirmed previous results (Fig. 4.18).

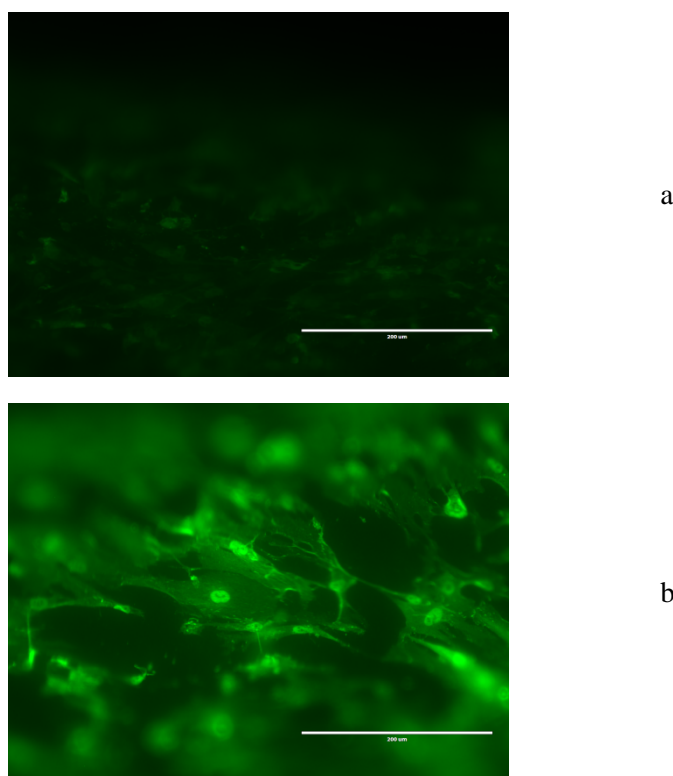


Fig. 4.18. Immunostaining for tight junction ZO-1 protein (green) of primary tubular proximal cells after one week incubation on virgin HCO 1100 (a) and MicroPES (b) membranes.

The results obtained for unmodified membranes are consistent with the cell counts and the literature data, indicating that PES surface modification is required for successful cell attachment and proliferation.

Specific strategies could be applied to improve the monolayer properties. If nutrients or oxygen levels were the limiting factor, using the flow system with recirculation could improve these parameters. Also according to the literature [44,88] up to 14 days was needed to obtain differentiated monolayers, therefore cultivation time could be also increased and its effect investigated.

Optimization of the coatings could be another strategy to improve cell adhesion and performance. Two approaches could be distinguished in this topic. First, optimization of the parameters of application existing components namely collagen type IV and L-DOPA could be performed. Concentration of collagen IV applied for performing the double coating could be increased and in the cell performance tested for example in the range of 25 – 200 µg/ml. Another approach would include enlarging the number of components used in ECM coating. Among the strategies that could be performed on the hollow fiber membranes are using cell feeder layers with following decellularization

[20], using complex ECM protein mixture such as Matrigel [88] or using different defined compositions of ECM proteins. The last option in the list is preferable since in the defined ECM composition it would be possible to investigate the effect of each component on cell proliferation.

5. CONCLUSIONS AND FUTURE PERSPECTIVES

Biomimetic coatings were developed and applied on the outer surface of two commercial hollow fiber membranes HCO 1100 and MicroPES TF10. The properties the coated membranes were investigated in the current work and the results of the investigation showed that:

- Increase in pure water permeability of the coated HCO 1100 membranes was observed. Membrane surface hydrophilization was assumed as the major factor responsible for the experimental effect;
- Protein permeation experiments revealed that significant decrease in permeate flux for double coated membranes of the both types;
- Rejection properties of the membranes could be tuned with applying the double coating. Specifically BSA and IgG sieving coefficients of HCO 1100 hollow fibers decreased from 0.214 ± 0.037 and 0.352 ± 0.0370 respectively for the native membrane compared to the values of 0.069 ± 0.019 and 0.114 ± 0.019 for the double coated membranes. Small effect of the double coating applied on MicroPES TF10 membranes in protein sieving was observed;
- Significant increase in cell attachment onto the surface of double coated hollow fiber membranes of both types was demonstrated;
- Functional confluent monolayers of human primary tubular cells were obtained on the outer surface of double coated hollow fiber membranes when cultivated in semi batch bioreactors. Higher degree of cell polarization was indicated for HCO 1100 membrane compared to MicroPES TF10 counterpart.

However, after achieving initial objectives further investigations are required to unravel and to confirm the exact mechanisms underlying the observed phenomena. Specifically, future strategies could be categorized in the two groups. First, additional tests are required to characterize the properties of double coated membranes and cell monolayers in the bioreactors. Strategies in the second category are intended to provide dynamic characterization of obtained BAK.

Specifically, among the characterization methods could be distinguished the following:

- Develop direct methods of detection and poly-L-DOPA coating. Using UV-vis spectrometry, ellipsometry could be applied ;
- Characterization methods of coated membrane should be extended with wettability and surface charge measurements;
- MWCO of the coated membranes could be detected by using dextrans/latex beads to obtain precise information on the effect of coating on the hydraulic radiuses of the pores;
- Investigate the homogeneity and structure of collagen IV coating in double coated membranes. Fluorescent techniques could be applied.
- Fluorescent cell viability assays may be applied to investigate investigate cell viability upon different conditions.

As the next stage of BAK development bioreactor modules should be used and tested in dynamic perfusion conditions. After applying the dynamic conditions next investigations of the monolayers could be performed:

- Investigate monolayer integrity using inulin permeation technique;
- Perform the analysis of toxin removal by the BAK system.

Improvement of the membrane coatings of the bioreactors could be considered separately. Obtained results could be considered as a starting point which can be used to compare effect of new coating formulations. Specifically increase of concentration of applied Col IV could improve cell polarization. Applying of different components of extracellular matrix, specifically glycosaminoglycan could increase viability of the cells in renal assist device.

6. REFERENCES

- [1] <http://www.adqi.net/>.
- [2] R. Bellomo, C. Ronco, J.A. Kellum, R.L. Mehta, P. Palevsky, Acute Dialysis Quality Initiative workgroup, Acute renal failure - definition, outcome measures, animal models, fluid therapy and information technology needs: the Second International Consensus Conference of the Acute Dialysis Quality Initiative (ADQI) Group, *Crit Care*. 8 (2004) R204–212. doi:10.1186/cc2872.
- [3] <http://www.akinet.org/>.
- [4] R.L. Mehta, J.A. Kellum, S.V. Shah, B.A. Molitoris, C. Ronco, D.G. Warnock, et al., Acute Kidney Injury Network: report of an initiative to improve outcomes in acute kidney injury, *Critical Care*. 11 (2007) R31. doi:10.1186/cc5713.
- [5] C. Ronco, R. Bellomo, J.A. Kellum, Acute kidney injury, Karger, Basel; New York, 2007.
- [6] Z. Ricci, D.N. Cruz, C. Ronco, Classification and staging of acute kidney injury: beyond the RIFLE and AKIN criteria, *Nature Reviews Nephrology*. 7 (2011) 201–208. doi:10.1038/nrneph.2011.14.
- [7] H. Husi, M. Sanchez-Niño, C. Delles, W. Mullen, A. Vlahou, A. Ortiz, et al., A combinatorial approach of Proteomics and Systems Biology in unravelling the mechanisms of acute kidney injury (AKI): involvement of NMDA receptor GRIN1 in murine AKI, *BMC Systems Biology*. 7 (2013) 110. doi:10.1186/1752-0509-7-110.
- [8] R. Bellomo, J.A. Kellum, C. Ronco, Acute kidney injury, *The Lancet*. 380 (2012) 756–766. doi:10.1016/S0140-6736(11)61454-2.
- [9] A. Jörres, C. Ronco, J.A. Kellum, Management of acute kidney problems, Springer, Heidelberg, 2010. <http://site.ebrary.com/id/10374962>.
- [10] S. Uchino, J.A. Kellum, R. Bellomo, G.S. Doig, H. Morimatsu, S. Morgera, et al., Acute renal failure in critically ill patients: a multinational, multicenter study, *JAMA*. 294 (2005) 813–818. doi:10.1001/jama.294.7.813.
- [11] S. Herget-Rosenthal, G. Glorieux, J. Jankowski, V. Jankowski, Uremic Toxins in Acute Kidney Injury, *Seminars in Dialysis*. 22 (2009) 445–448. doi:10.1111/j.1525-139X.2009.00598.x.
- [12] R. Vanholder, R. De Smet, G. Glorieux, A. Argilés, U. Baurmeister, P. Brunet, et al., Review on uremic toxins: classification, concentration, and interindividual variability, *Kidney Int*. 63 (2003) 1934–1943. doi:10.1046/j.1523-1755.2003.00924.x.
- [13] T. Niwa, Uremic toxins, John Wiley & Sons, Hoboken, N.J., 2012. <http://search.ebscohost.com/login.aspx?direct=true&scope=site&db=nlebk&db=nlabk&AN=484923>.
- [14] T. Niwa, Uremic toxicity of indoxyl sulfate, *Nagoya J Med Sci*. 72 (2010) 1–11.
- [15] R. D’Hooge, G. Van de Vijver, P.-P. Van Bogaert, B. Marescau, R. Vanholder, P.P. De Deyn, Involvement of voltage- and ligand-gated Ca²⁺ channels in the neuroexcitatory and synergistic effects of putative uremic neurotoxins, *Kidney Int*. 63 (2003) 1764–1775. doi:10.1046/j.1523-1755.2003.00912.x.
- [16] A.J. Cardounel, H. Cui, A. Samouilov, W. Johnson, P. Kearns, A.-L. Tsai, et al., Evidence for the pathophysiological role of endogenous methylarginines in regulation of endothelial NO production and vascular function, *J. Biol. Chem*. 282 (2007) 879–887. doi:10.1074/jbc.M603606200.
- [17] A.F. Perna, D. Ingrosso, C. Lombardi, F. Acanfora, E. Satta, C.M. Cesare, et al., Possible mechanisms of homocysteine toxicity, *Kidney Int. Suppl.* (2003) S137–140.
- [18] G.L. Glorieux, A.W. Dhondt, P. Jacobs, J. Van Langeraert, N.H. Lameire, P.P. De Deyn, et al., In vitro study of the potential role of guanidines in leukocyte functions

- related to atherogenesis and infection, *Kidney Int.* 65 (2004) 2184–2192. doi:10.1111/j.1523-1755.2004.00631.x.
- [19] Y. Miyamoto, Y. Iwao, K. Mera, H. Watanabe, D. Kadowaki, Y. Ishima, et al., A uremic toxin, 3-carboxy-4-methyl-5-propyl-2-furanpropionate induces cell damage to proximal tubular cells via the generation of a radical intermediate, *Biochemical Pharmacology*. 84 (2012) 1207–1214. doi:10.1016/j.bcp.2012.07.033.
- [20] C.C. Sharpe, M.E.C. Dockrell, Primary culture of human renal proximal tubule epithelial cells and interstitial fibroblasts, *Methods Mol. Biol.* 806 (2012) 175–185. doi:10.1007/978-1-61779-367-7_12.
- [21] K.-I. Inui, S. Masuda, H. Saito, Cellular and molecular aspects of drug transport in the kidney, *Kidney International*. 58 (2000) 944–958. doi:10.1046/j.1523-1755.2000.00251.x.
- [22] A. Enomoto, T. Niwa, Roles of Organic Anion Transporters in the Progression of Chronic Renal Failure, *Therapeutic Apheresis and Dialysis*. 11 (2007) S27–S31. doi:10.1111/j.1744-9987.2007.00515.x.
- [23] W.M. Saltzman, *Biomedical Engineering Bridging Medicine and Technology.*, Cambridge University Press, Leiden, 2009.
- [24] B.A. Warady, *Pediatric dialysis*, Springer, New York, 2011.
- [25] E. Drioli, L. Giorno, *Comprehensive membrane science and engineering*, Elsevier Science, Amsterdam; London, 2010.
<http://public.eblib.com/EBLPublic/PublicView.do?ptiID=625314> (accessed December 25, 2012).
- [26] C. Ronco, A. Brendolan, A. Lupi, G. Metry, N.W. Levin, Effects of a reduced inner diameter of hollow fibers in hemodialyzers, *Kidney Int.* 58 (2000) 809–817. doi:10.1046/j.1523-1755.2000.00230.x.
- [27] N. Jourde-Chiche, L. Dou, C. Cerini, F. Dignat-George, R. Vanholder, P. Brunet, Protein-Bound Toxins-Update 2009, *Seminars in Dialysis*. 22 (2009) 334–339. doi:10.1111/j.1525-139X.2009.00576.x.
- [28] M. Roche, P. Rondeau, N.R. Singh, E. Tarnus, E. Bourdon, The antioxidant properties of serum albumin, *FEBS Lett.* 582 (2008) 1783–1787. doi:10.1016/j.febslet.2008.04.057.
- [29] M. Piroddi, D. Bartolini, S. Ciffolilli, F. Galli, Nondialyzable uremic toxins, *Blood Purif.* 35 Suppl 2 (2013) 30–41. doi:10.1159/000350846.
- [30] P.J. Thornalley, N. Rabbani, Protein damage in diabetes and uremia--identifying hotspots of proteome damage where minimal modification is amplified to marked pathophysiological effect, *Free Radic. Res.* 45 (2011) 89–100. doi:10.3109/10715762.2010.534162.
- [31] J. Himmelfarb, E. McMonagle, Albumin is the major plasma protein target of oxidant stress in uremia, *Kidney Int.* 60 (2001) 358–363. doi:10.1046/j.1523-1755.2001.00807.x.
- [32] Y. Matsuyama, H. Terawaki, T. Terada, S. Era, Albumin thiol oxidation and serum protein carbonyl formation are progressively enhanced with advancing stages of chronic kidney disease, *Clin. Exp. Nephrol.* 13 (2009) 308–315. doi:10.1007/s10157-009-0161-y.
- [33] Y. Itoh, A. Ezawa, K. Kikuchi, Y. Tsuruta, T. Niwa, Protein-bound uremic toxins in hemodialysis patients measured by liquid chromatography/tandem mass spectrometry and their effects on endothelial ROS production, *Anal Bioanal Chem.* 403 (2012) 1841–1850. doi:10.1007/s00216-012-5929-3.
- [34] T. Niwa, Removal of protein-bound uraemic toxins by haemodialysis, *Blood Purif.* 35 Suppl 2 (2013) 20–25. doi:10.1159/000350843.

- [35] C.A. Hutchison, A.R. Bradwell, M. Cook, K. Basnayake, S. Basu, S. Harding, et al., Treatment of Acute Renal Failure Secondary to Multiple Myeloma with Chemotherapy and Extended High Cut-Off Hemodialysis, *Clinical Journal of the American Society of Nephrology*. 4 (2009) 745–754. doi:10.2215/CJN.04590908.
- [36] C.H. Jonee, Continuous Renal Replacement Therapy in Acute Renal Failure: Membranes for CRRT, *Artificial Organs*. 22 (1998) 2–7. doi:10.1046/j.1525-1594.1998.06071.x.
- [37] P. Fabbrini, S. Sirtori, E. Casiraghi, F. Pieruzzi, S. Genovesi, D. Corti, et al., Polymethylmethacrylate membrane and serum free light chain removal: enhancing adsorption properties, *Blood Purif*. 35 Suppl 2 (2013) 52–58. doi:10.1159/000350849.
- [38] R. Vanholder, U. Baurmeister, P. Brunet, G. Cohen, G. Glorieux, J. Jankowski, et al., A Bench to Bedside View of Uremic Toxins, *Journal of the American Society of Nephrology*. 19 (2008) 863–870. doi:10.1681/ASN.2007121377.
- [39] D.F. Stamatialis, B.J. Papenburg, M. Gironés, S. Saiful, S.N.M. Bettahalli, S. Schmitmeier, et al., Medical applications of membranes: Drug delivery, artificial organs and tissue engineering, *Journal of Membrane Science*. 308 (2008) 1–34. doi:10.1016/j.memsci.2007.09.059.
- [40] T.W. Meyer, J.W.T. Peattie, J.D. Miller, D.C. Dinh, N.S. Recht, J.L. Walther, et al., Increasing the clearance of protein-bound solutes by addition of a sorbent to the dialysate, *J. Am. Soc. Nephrol*. 18 (2007) 868–874. doi:10.1681/ASN.2006080863.
- [41] M.S.L. Tijink, M. Wester, G. Glorieux, K.G.F. Gerritsen, J. Sun, P.C. Swart, et al., Mixed matrix hollow fiber membranes for removal of protein-bound toxins from human plasma, *Biomaterials*. 34 (2013) 7819–7828. doi:10.1016/j.biomaterials.2013.07.008.
- [42] K. Kikuchi, Y. Itoh, R. Tateoka, A. Ezawa, K. Murakami, T. Niwa, Metabolomic search for uremic toxins as indicators of the effect of an oral sorbent AST-120 by liquid chromatography/tandem mass spectrometry, *J. Chromatogr. B Analyt. Technol. Biomed. Life Sci*. 878 (2010) 2997–3002. doi:10.1016/j.jchromb.2010.09.006.
- [43] A. Saito, T. Aung, K. Sekiguchi, Y. Sato, D.M. Vu, M. Inagaki, et al., Present status and perspectives of bioartificial kidneys, *J Artif Organs*. 9 (2006) 130–135. doi:10.1007/s10047-006-0336-1.
- [44] H.D. Humes, D.A. Buffington, S.M. MacKay, A.J. Funke, W.F. Weitzel, Replacement of renal function in uremic animals with a tissue-engineered kidney, *Nat. Biotechnol*. 17 (1999) 451–455. doi:10.1038/8626.
- [45] W.H. Fissell, J. Kimball, S.M. MacKay, A. Funke, H.D. Humes, The role of a bioengineered artificial kidney in renal failure, *Ann. N. Y. Acad. Sci*. 944 (2001) 284–295.
- [46] H.D. Humes, D. Buffington, A.J. Westover, S. Roy, W.H. Fissell, The bioartificial kidney: current status and future promise, *Pediatric Nephrology*. (2013). doi:10.1007/s00467-013-2467-y.
- [47] N. Anzai, P. Jutabha, Y. Kanai, H. Endou, Integrated physiology of proximal tubular organic anion transport, *Curr. Opin. Nephrol. Hypertens*. 14 (2005) 472–479.
- [48] D.R. Fraser, E. Kodicek, Unique biosynthesis by kidney of a biological active vitamin D metabolite, *Nature*. 228 (1970) 764–766.
- [49] R.N. Boswell, B.A. Yard, E. Schrama, L.A. van Es, M.R. Daha, F.J. van der Woude, Interleukin 6 production by human proximal tubular epithelial cells in vitro: analysis of the effects of interleukin-1 alpha (IL-1 alpha) and other cytokines, *Nephrol. Dial. Transplant*. 9 (1994) 599–606.
- [50] S.E. Gould, M. Day, S.S. Jones, H. Dorai, BMP-7 regulates chemokine, cytokine, and hemodynamic gene expression in proximal tubule cells, *Kidney Int*. 61 (2002) 51–60. doi:10.1046/j.1523-1755.2002.00103.x.

- [51] H.D. Humes, S.M. Mackay, A.J. Funke, D.A. Buffington, Tissue engineering of a bioartificial renal tubule assist device: In vitro transport and metabolic characteristics, *Kidney International*. 55 (1999) 2502–2514. doi:10.1046/j.1523-1755.1999.00486.x.
- [52] L.C. Racusen, C. Monteil, A. Sgrignoli, M. Lucskay, S. Marouillat, J.G. Rhim, et al., Cell lines with extended in vitro growth potential from human renal proximal tubule: characterization, response to inducers, and comparison with established cell lines, *J. Lab. Clin. Med.* 129 (1997) 318–329.
- [53] M.J. Ryan, G. Johnson, J. Kirk, S.M. Fuerstenberg, R.A. Zager, B. Torok-Storb, HK-2: an immortalized proximal tubule epithelial cell line from normal adult human kidney, *Kidney Int.* 45 (1994) 48–57.
- [54] M. Ni, J.C.M. Teo, M.S.B. Ibrahim, K. Zhang, F. Tasnim, P.-Y. Chow, et al., Characterization of membrane materials and membrane coatings for bioreactor units of bioartificial kidneys, *Biomaterials*. 32 (2011) 1465–1476. doi:10.1016/j.biomaterials.2010.10.061.
- [55] N. Ozgen, M. Terashima, T. Aung, Y. Sato, C. Isoe, T. Kakuta, et al., Evaluation of long-term transport ability of a bioartificial renal tubule device using LLC-PK1 cells, *Nephrol. Dial. Transplant.* 19 (2004) 2198–2207. doi:10.1093/ndt/gfh399.
- [56] W.C. Prozialeck, J.R. Edwards, P.C. Lamar, C.S. Smith, Epithelial barrier characteristics and expression of cell adhesion molecules in proximal tubule-derived cell lines commonly used for in vitro toxicity studies, *Toxicology in Vitro*. 20 (2006) 942–953. doi:10.1016/j.tiv.2005.11.006.
- [57] R. Deppisch, H. Göhl, L. Smeby, Microdomain structure of polymeric surfaces--potential for improving blood treatment procedures, *Nephrol. Dial. Transplant.* 13 (1998) 1354–1359.
- [58] L.J. Zeman, A.L. Zydney, *Microfiltration and ultrafiltration : principles and applications*, M. Dekker, New York, 1996.
- [59] C. Ronco, Evolution of synthetic membranes for blood purification: the case of the Polyflux family, *Nephrology Dialysis Transplantation*. 18 (2003) 10vii–20. doi:10.1093/ndt/gfg1073.
- [60] S.B. Teli, S. Molina, E.G. Calvo, A.E. Lozano, J. de Abajo, Preparation, characterization and antifouling property of polyethersulfone–PANI/PMA ultrafiltration membranes, *Desalination*. 299 (2012) 113–122. doi:10.1016/j.desal.2012.05.031.
- [61] S.A. Al Malek, M.N. Abu Seman, D. Johnson, N. Hilal, Formation and characterization of polyethersulfone membranes using different concentrations of polyvinylpyrrolidone, *Desalination*. 288 (2012) 31–39. doi:10.1016/j.desal.2011.12.006.
- [62] H. Ueda, J. Watanabe, T. Konno, M. Takai, A. Saito, K. Ishihara, Asymmetrically functional surface properties on biocompatible phospholipid polymer membrane for bioartificial kidney, *J Biomed Mater Res A*. 77 (2006) 19–27. doi:10.1002/jbm.a.30606.
- [63] U. Meyer, *Fundamentals of tissue engineering and regenerative medicine*, Springer, Berlin, 2009. <http://public.eblib.com/EBLPublic/PublicView.do?ptiID=428772> (accessed November 16, 2013).
- [64] T. Orłowski, E. Sitarek, K. Tatarkiewicz, M. Sabat, M. Antosiak, Comparison of two methods of pancreas islets immunoisolation, *Int J Artif Organs*. 20 (1997) 701–703.
- [65] G. Orive, S.K. Tam, J.L. Pedraz, J.-P. Hallé, Biocompatibility of alginate-poly-L-lysine microcapsules for cell therapy, *Biomaterials*. 27 (2006) 3691–3700. doi:10.1016/j.biomaterials.2006.02.048.
- [66] R.I. Freshney, *Culture of animal cells: a manual of basic technique and specialized applications*, 6th ed, Wiley-Blackwell, Hoboken, N.J, 2010.
- [67] C.M. Bünger, C. Gerlach, T. Freier, K.P. Schmitz, M. Pilz, C. Werner, et al., Biocompatibility and surface structure of chemically modified immunoisolating

- alginate-PLL capsules, *J Biomed Mater Res A*. 67 (2003) 1219–1227.
doi:10.1002/jbm.a.10094.
- [68] R.O. Hynes, Integrins: bidirectional, allosteric signaling machines, *Cell*. 110 (2002) 673–687.
- [69] R. Zent, A. Pozzi, eds., *Cell-Extracellular Matrix Interactions in Cancer*, Springer New York, New York, NY, 2010. <http://www.springerlink.com/index/10.1007/978-1-4419-0814-8> (accessed July 3, 2014).
- [70] B. Jeschke, J. Meyer, A. Jonczyk, H. Kessler, P. Adamietz, N.M. Meenen, et al., RGD-peptides for tissue engineering of articular cartilage, *Biomaterials*. 23 (2002) 3455–3463. doi:10.1016/S0142-9612(02)00052-2.
- [71] C.J. Detzel, A.L. Larkin, P. Rajagopalan, Polyelectrolyte multilayers in tissue engineering, *Tissue Eng Part B Rev*. 17 (2011) 101–113. doi:10.1089/ten.TEB.2010.0548.
- [72] J. Zhang, B. Senger, D. Vautier, C. Picart, P. Schaaf, J.-C. Voegel, et al., Natural polyelectrolyte films based on layer-by layer deposition of collagen and hyaluronic acid, *Biomaterials*. 26 (2005) 3353–3361. doi:10.1016/j.biomaterials.2004.08.019.
- [73] M. Sailer, K. Lai Wing Sun, O. Mermut, T.E. Kennedy, C.J. Barrett, High-throughput cellular screening of engineered ECM based on combinatorial polyelectrolyte multilayer films, *Biomaterials*. 33 (2012) 5841–5847. doi:10.1016/j.biomaterials.2012.05.001.
- [74] M. Vandrovcová, T. Douglas, D. Hauk, B. Grössner-Schreiber, J. Wiltfang, L. Bačáková, et al., Influence of collagen and chondroitin sulfate (CS) coatings on poly-(lactide-co-glycolide) (PLGA) on MG 63 osteoblast-like cells, *Physiol Res*. 60 (2011) 797–813.
- [75] L. Richert, A.J. Engler, D.E. Discher, C. Picart, Elasticity of Native and Cross-Linked Polyelectrolyte Multilayer Films, *Biomacromolecules*. 5 (2004) 1908–1916. doi:10.1021/bm0498023.
- [76] D. Öhlund, O. Franklin, E. Lundberg, C. Lundin, M. Sund, Type IV collagen stimulates pancreatic cancer cell proliferation, migration, and inhibits apoptosis through an autocrine loop, *BMC Cancer*. 13 (2013) 154. doi:10.1186/1471-2407-13-154.
- [77] L. De Bartolo, G. Jarosch-Von Schweder, A. Haverich, A. Bader, A Novel Full-Scale Flat Membrane Bioreactor Utilizing Porcine Hepatocytes: Cell Viability and Tissue-Specific Functions, *Biotechnology Progress*. 16 (2000) 102–108. doi:10.1021/bp990128o.
- [78] S. Diekmann, A. Bader, S. Schmitmeier, Present and Future Developments in Hepatic Tissue Engineering for Liver Support Systems: State of the art and future developments of hepatic cell culture techniques for the use in liver support systems, *Cytotechnology*. 50 (2006) 163–179. doi:10.1007/s10616-006-6336-4.
- [79] H. Lee, S.M. Dellatore, W.M. Miller, P.B. Messersmith, Mussel-Inspired Surface Chemistry for Multifunctional Coatings, *Science*. 318 (2007) 426–430. doi:10.1126/science.1147241.
- [80] Q. Ye, F. Zhou, W. Liu, Bioinspired catecholic chemistry for surface modification, *Chemical Society Reviews*. 40 (2011) 4244. doi:10.1039/c1cs15026j.
- [81] H. Lee, J. Rho, P.B. Messersmith, Facile Conjugation of Biomolecules onto Surfaces via Mussel Adhesive Protein Inspired Coatings, *Adv. Mater. Weinheim*. 21 (2009) 431–434. doi:10.1002/adma.200801222.
- [82] M.E. Lynge, R. van der Westen, A. Postma, B. Städler, Polydopamine—a nature-inspired polymer coating for biomedical science, *Nanoscale*. 3 (2011) 4916. doi:10.1039/c1nr10969c.

- [83] H. Lee, N.F. Scherer, P.B. Messersmith, Single-molecule mechanics of mussel adhesion, *Proceedings of the National Academy of Sciences*. 103 (2006) 12999–13003. doi:10.1073/pnas.0605552103.
- [84] S. Azari, L. Zou, Using zwitterionic amino acid l-DOPA to modify the surface of thin film composite polyamide reverse osmosis membranes to increase their fouling resistance, *Journal of Membrane Science*. 401-402 (2012) 68–75. doi:10.1016/j.memsci.2012.01.041.
- [85] J.G. Rivera, P.B. Messersmith, Polydopamine-assisted immobilization of trypsin onto monolithic structures for protein digestion: Sample Preparation, *Journal of Separation Science*. 35 (2012) 1514–1520. doi:10.1002/jssc.201200073.
- [86] C.K. Poh, Z. Shi, T.Y. Lim, K.G. Neoh, W. Wang, The effect of VEGF functionalization of titanium on endothelial cells in vitro, *Biomaterials*. 31 (2010) 1578–1585. doi:10.1016/j.biomaterials.2009.11.042.
- [87] J. Kang, S. Tada, T. Kitajima, T.I. Son, T. Aigaki, Y. Ito, Immobilization of Bone Morphogenetic Protein on DOPA- or Dopamine-Treated Titanium Surfaces to Enhance Osseointegration, *BioMed Research International*. 2013 (2013) 1–6. doi:10.1155/2013/265980.
- [88] H. Zhang, F. Tasnim, J.Y. Ying, D. Zink, The impact of extracellular matrix coatings on the performance of human renal cells applied in bioartificial kidneys, *Biomaterials*. 30 (2009) 2899–2911. doi:10.1016/j.biomaterials.2009.01.046.
- [89] <http://www.sciencellonline.com/site/productsheets/4100.pdf>.
- [90] http://bio.lonza.com/uploads/tx_mwaxmarketingmaterial/Lonza_BenchGuides_Clonetics_renal_epithelial_cell_systems.pdf.
- [91] <http://www.wicell.org/product-files/cultureProtocols/lt2e-h9cagfp%20protocol.pdf>.
- [92] Z.Y. Oo, R. Deng, M. Hu, M. Ni, K. Kandasamy, M.S. bin Ibrahim, et al., The performance of primary human renal cells in hollow fiber bioreactors for bioartificial kidneys, *Biomaterials*. 32 (2011) 8806–8815. doi:10.1016/j.biomaterials.2011.08.030.
- [93] A. Idris, N. Mat Zain, M.Y. Noordin, Synthesis, characterization and performance of asymmetric polyethersulfone (PES) ultrafiltration membranes with polyethylene glycol of different molecular weights as additives, *Desalination*. 207 (2007) 324–339. doi:10.1016/j.desal.2006.08.008.
- [94] M. Mulder, *Basic principles of membrane technology*, 2nd ed., Kluwer Academic, Dordrecht; Boston, 1996.
- [95] Millipore, *Protein Concentration and Diafiltration by Tangential Flow Filtration*, Millipore Technical Publications. (2003).
<http://www.millipore.com/techpublications/tech1/tb032>.
- [96] <http://www.lo-laboroptik.de/englisch/info/info.html>.
- [97] P.M. Doran, *Bioprocess engineering principles*, 2nd ed, Elsevier/Academic Press, Amsterdam ; Boston, 2013.
- [98] http://www.membrana.com/jdownloads/Products/Healthcare%20Applications/New%20Therapies%20and%20iv-Filtration/micropes_tf10.pdf.
- [99] K.V. Peinemann, S.P. Nunes, *Membranes for life sciences*, Wiley-VCH, Weinheim, 2008.
- [100] http://www.gambro.com/Global/Globalweb/Products/Myeloma/Dialyzers/Theralite/Documents/HCE5586_1%20Theralite_Low.pdf?epslanguage=en.
- [101] N. Maximous, G. Nakhla, W. Wan, Comparative assessment of hydrophobic and hydrophilic membrane fouling in wastewater applications, *Journal of Membrane Science*. 339 (2009) 93–99. doi:10.1016/j.memsci.2009.04.034.
- [102] R.D. Noble, S.A. Stern, *Membrane separations technology : principles and applications*, Elsevier, Amsterdam; New York, 1995.

- [103] J.-H. Jiang, L.-P. Zhu, X.-L. Li, Y.-Y. Xu, B.-K. Zhu, Surface modification of PE porous membranes based on the strong adhesion of polydopamine and covalent immobilization of heparin, *Journal of Membrane Science*. 364 (2010) 194–202. doi:10.1016/j.memsci.2010.08.017.
- [104] C. Cheng, S. Li, W. Zhao, Q. Wei, S. Nie, S. Sun, et al., The hydrodynamic permeability and surface property of polyethersulfone ultrafiltration membranes with mussel-inspired polydopamine coatings, *Journal of Membrane Science*. 417–418 (2012) 228–236. doi:10.1016/j.memsci.2012.06.045.
- [105] M. Cheryan, *Ultrafiltration and microfiltration handbook*, Technomic Publishing Company, Lancaster, Pa., 1998.
- [106] N. Krishnakumar, M. Yea, M. Cheryan, Ultrafiltration of soy protein concentrate: performance and modelling of spiral and tubular polymeric modules, *Journal of Membrane Science*. 244 (2004) 235–242. doi:10.1016/j.memsci.2004.06.056.
- [107] G. Belfort, R.H. Davis, A.L. Zydney, The behavior of suspensions and macromolecular solutions in crossflow microfiltration, *Journal of Membrane Science*. 96 (1994) 1–58. doi:10.1016/0376-7388(94)00119-7.
- [108] S.T. Kelly, W. Senyo Opong, A.L. Zydney, The influence of protein aggregates on the fouling of microfiltration membranes during stirred cell filtration, *Journal of Membrane Science*. 80 (1993) 175–187. doi:10.1016/0376-7388(93)85142-J.
- [109] S.T. Kelly, A.L. Zydney, Effects of intermolecular thiol-disulfide interchange reactions on bsa fouling during microfiltration, *Biotechnol. Bioeng.* 44 (1994) 972–982. doi:10.1002/bit.260440814.
- [110] S. Mochizuki, A.L. Zydney, Sieving Characteristics of Albumin Deposits Formed during Microfiltration, *Journal of Colloid and Interface Science*. 158 (1993) 136–145. doi:10.1006/jcis.1993.1239.
- [111] H. Toutain, N. Vauclin-Jacques, J.P. Fillastre, J.P. Morin, Biochemical, functional, and morphological characterization of a primary culture of rabbit proximal tubule cells, *Exp. Cell Res.* 194 (1991) 9–18.
- [112] M.R. Rosenberg, G. Michalopoulos, Kidney proximal tubular cells isolated by collagenase perfusion grow in defined media in the absence of growth factors, *Journal of Cellular Physiology*. 131 (1987) 107–113. doi:10.1002/jcp.1041310116.
- [113] J.P. Mather, ed., *Mammalian Cell Culture*, Springer US, Boston, MA, 1984. <http://www.springerlink.com/index/10.1007/978-1-4615-9361-4>.
- [114] <http://www.bioart-fp7.eu/>.
- [115] J. Jansen, C.M.S. Schophuizen, M.J. Wilmer, S.H.M. Lahham, H. a. M. Mutsaers, J.F.M. Wetzels, et al., A morphological and functional comparison of proximal tubule cell lines established from human urine and kidney tissue, *Exp. Cell Res.* 323 (2014) 87–99. doi:10.1016/j.yexcr.2014.02.011.
- [116] K.-J. Jang, A.P. Mehr, G.A. Hamilton, L.A. McPartlin, S. Chung, K.-Y. Suh, et al., Human kidney proximal tubule-on-a-chip for drug transport and nephrotoxicity assessment, *Integr Biol (Camb)*. 5 (2013) 1119–1129. doi:10.1039/c3ib40049b.
- [117] C. Shen, Q. Meng, G. Zhang, Increased curvature of hollow fiber membranes could up-regulate differential functions of renal tubular cell layers, *Biotechnol. Bioeng.* 110 (2013) 2173–2183. doi:10.1002/bit.24874.
- [118] W. Beck, J. Bosch, Method for Treating Anemia in Hemodialysis Patients, Google Patents, 2012. <http://www.google.com/patents/US20120305487>.

APPENDICES

Appendix A

Comparison between the parameters of RIFLE and AKIN criteria [6]

System	Serum creatinin criteria	Urine output criteria
RIFLE Class		
Risk	Serum creatinine increase to 1.5-fold OR GFR decrease >25 % from baseline	<0.5 ml/kg for 6 h
Injury	Serum creatinine increase to 2-fold OR GFR decrease >50 %	<0.5 ml/kg for 12 h
Failure	Serum creatinine increase to 3-fold OR GFR decrease >75 % from baseline OR serum creatinine $\geq 340 \mu\text{mol/l}$ with acute increase of at least $44 \mu\text{mol/l}$	Anuria for 12 h
AKIN Stage		
1	Serum creatinine increase $\geq 26.5 \mu\text{mol/l}$ or increase to 1.5 – 2.0-fold from baseline	<0.5 ml/kg for 6 h
2	Serum creatinine increase to 2.0 – 3.0-fold from baseline	<0.5 ml/kg for 12 h
3	Serum creatinine increase to > 3.0-fold from baseline OR serum creatinine $\geq 340 \mu\text{mol/l}$ with acute increase of at least $44 \mu\text{mol/l}$ OR need for RRT	<0.3 ml/kg for 24 h OR anuria for 12 h OR need for RRT

Appendix B

Different groups of uremic toxins [12]

Free water-soluble low-molecular-weight solutes ($N = 45$)

Solute	C _N	C _U	C _{MAX}	MW	Group
1-methyladenosine $\mu\text{g/L}$	17.1±5.1/10	104.0 ± 56.2/17	216.4	281	Ribonucleosides
1-methylguanosine $\mu\text{g/L}$	13.7±16.9/10	41.6 ± 23.8/17	89.2	297	Ribonucleosides
1-methylinosine $\mu\text{g/L}$	13.5±3.9/10	620.4 ± 203.4/14	1027.2	282	Ribonucleosides
ADMA mg/L	0.2±0.06/6	1.6 ± 1.2/10	7.3 ^a	202	Guanidines
α -keto- δ -guanidinovaleric acid $\mu\text{g/L}$	<30.2/66	—	140.4 ^a	151	Guanidines
α -N-acetylarginine $\mu\text{g/L}$	18.1±24.8/16	328.3 ± 142.6/13	4580.0 ^a	216	Guanidines
Arab(in)itol mg/L	<0.6/33	15.0 ± 9.0/12	33.0	152	Polyols
Argininic acid $\mu\text{g/L}$	<77.0/66	80.5 ± 56.0/11	197.8 ^a	175	Guanidines
Benzylalcohol mg/L	—	27.0 ± 50.7/17	187.9 ^a	108	
β -guanidinopropionic acid $\mu\text{g/L}$	<3.3/24	28.8 ± 18.3/29	65.4	131	Guanidines
β -lipotropin ng/L	<55.3/10	62.7/22	108.8 ^a	461	Peptides
Creatine mg/L	9.7±3.3/24	134.0 ± 30.3/29	235.8 ^a	131	Guanidines
Creatinine mg/L	<12.0/23	136.0±46.0/19746	240.0 ^a	113	Guanidines
Cytidine $\mu\text{g/L}$	<468.0	683.3±287.8/7	1263.6 ^a	234	Purines
Dimethylglycine $\mu\text{g/L}$	<381.1/33	576.8/18	1040.3 ^a	103	
Erythritol mg/L	<0.7/33	9.8±14.0/12	37.0 ^a	122	Polyols
γ -guanidinobutyric acid $\mu\text{g/L}$	<3.6/24	33.3±16.0/30	1750.0 ^a	145	Guanidines
Guanidine $\mu\text{g/L}$	<11.8/16	172.9±83.8/13	800.0 ^a	59	Guanidines
Guanidinoacetic acid $\mu\text{g/L}$	222.3±79.6/24	383.8 ± 143.9/29	693.8 ^a	117	Guanidines
Guanidinosuccinic acid mg/L	0.03±0.01/16	6.5 ± 3.4/13	47.0 ^a	175	Guanidines
Hypoxanthine mg/L	1.5±0.5/145	2.0 ± 1.6/65	5.3	136	Purines
Malondialdehyde $\mu\text{g/L}$	257.7±81.7/30	428.8 ± 170.4/16	769.6	71	
Mannitol mg/L	<1.3/33	26.0 ± 25.0/12	76.0	182	Polyols
Methylguanidine $\mu\text{g/L}$	<7.3/24	773.8 ± 508.8/5	1820.0 ^a	73	Guanidines
Myoinositol mg/L	<10.0/8	94.0 ± 69.0/12	232.0	180	Polyols
N ² ,N ² -dimethylguanosine $\mu\text{g/L}$	9.0±4.7/10	236.4 ± 89.7/14	415.8	311	Ribonucleosides
N ⁴ -acetylcytidine $\mu\text{g/L}$	57.0±17.1/10	159.6 ± 30.8/14	221.2	285	Ribonucleosides
N ⁶ -methyladenosine $\mu\text{g/L}$	18.5±8.4/10	70.3 ± 53.3/17	176.9	281	Ribonucleosides
N ⁶ -threonylcarbamoyladenosine $\mu\text{g/L}$	35.5±27.2/10	378.0 ± 151.2/17	680.4	378	Ribonucleosides
Orotic acid mg/L	0.5±1.4/30	6.7 ± 16.0/22	38.7	174	Pyrimidines
Orotidine mg/L	1.2±1.6/30	20.2 ± 13.5/22	47.2	288	Pyrimidines
Oxalate mg/L	0.3±0.1/8	4.9 ± 1.4/8	7.6	90	
Phenylacetylglutamine mg/L	<4.7	53.3 ± 44.7/6	120.6 ^a	264	
Pseudouridine mg/L	0.5±5.8/30	13.1±21.4/7	86.6 ^a	244	Ribonucleosides
SDMA $\mu\text{g/L}$	76.1±21.0/66	640.3±212.1/38	1232.2 ^a	202	Guanidines
Sorbitol mg/L	<0.4/33	3.1±2.1/12	7.3	182	Polyols
Taurocyamine $\mu\text{g/L}$	<52.2/24	—	121.8 ^a	174	Guanidines
Threitol $\mu\text{g/L}$	<319.6/33	990.0±920.0/12	5697.4 ^a	122	Polyols
Thymine mg/L	—	2.8±4.2/22	11.2	126	Pyrimidines
Uracil $\mu\text{g/L}$	<224.0	252.0±154.6/7	448.0 ^a	112	Purines
Urea g/L	<0.4/23	2.3±1.1/16	4.6 ^a	60	
Uric acid mg/L	<67.2	83.4±44.5/7	146.7 ^a	168	Purines
Uridine mg/L	1.5±1.3/30	9.8±11.4/22	32.6	244	Pyrimidines
Xanthine mg/L	0.5±1.4/180	1.5±0.8/65	3.0	152	Purines
Xanthosine $\mu\text{g/L}$	23.9±12.8/10	96.6±62.9/11	222.4	284	Ribonucleosides

Protein-bound solutes ($N = 25$)

Solute	C _N	C _U	C _{MAX}	MW	Group
2-methoxyresorcinol $\mu\text{g/L}$	—	19.6±81.2/17	322.0 ^a	140	Phenols
3-deoxyglucosone mg/L	0.3 ± 0.1/30	1.7 ± 1.0/27	3.5	162	AGE
CMPF mg/L	7.7 ± 3.3/7	61.0 ± 16.5/15	94.0 ^a	240	
Fructoselysine mg/L	—	58.1 ± 10.8/10	79.7	308	AGE

Glyoxal $\mu\text{g/L}$	67.0 \pm 20.0	221.0 \pm 28.0/ <u>20</u>	277.0	58	AGE
Hippuric acid mg/L	<5.0	247.0 \pm 112.0/ <u>7</u>	471.0	179	Hippurates
Homocysteine mg/L	<1.7/ <u>24</u>	8.1 \pm 1.6/ <u>7</u>	26.4 ^a	135	
Hydroquinone $\mu\text{g/L}$	—	50.6 \pm 84.7/ <u>17</u>	286.0 ^a	110	Phenols
Indole-3-acetic acid $\mu\text{g/L}$	17.5 \pm 17.5/ <u>7</u>	875.0 \pm 560.0/ <u>42</u>	9076.9 ^a	175	Indoles
Indoxyl sulfate mg/L	0.6 \pm 5.4/ <u>40</u>	53.0 \pm 91.5/ <u>20</u>	236.0	251	Indoles
Kinurenine $\mu\text{g/L}$	<391/ <u>7</u>	686.4 \pm 178.9/ <u>21</u>	952.6	208	Indoles
Kynurenic acid mg/L	<1.0	—	9.5 ^a	189	Indoles
Leptin $\mu\text{g/L}$	8.4 \pm 6.7/ <u>56</u>	72.0 \pm 60.6/ <u>8</u>	490.0 ^a	16000	Peptides
Melatonin ng/L	26.5 \pm 7.1/ <u>35</u>	175.8 \pm 130.2/ <u>13</u>	436.2	126	Indoles
Methylglyoxal $\mu\text{g/L}$	47.0 \pm 12.0/ <u>15</u>	110.0 \pm 18.0/ <u>20</u>	146.0	72	AGE
Nϵ-(carboxymethyl)lysine mg/L	1.1 \pm 0.3/ <u>24</u>	4.3 \pm 1.3/ <u>44</u>	6.9	204	AGE
p-cresol mg/L	0.6 \pm 1.0/ <u>12</u>	20.1 \pm 10.3/ <u>20</u>	40.7	108	Phenols
Pentosidine $\mu\text{g/L}$	51.6 \pm 18.8/ <u>19</u>	896.0 \pm 448.0/ <u>24</u>	2964.0 ^a	342	AGE
Phenol mg/L	0.6 \pm 0.2/ <u>12</u>	2.7 \pm 3.9/ <u>10</u>	10.5	94	Phenols
P-OHhippuric acid mg/L	—	18.3 \pm 6.6/ <u>13</u>	31.5	195	Hippurates
Putrescine $\mu\text{g/L}$	21.1 \pm 7.9/ <u>10</u>	77.4 \pm 27.3/ <u>25</u>	132.0	88	Polyamines
Quinolinic acid mg/L	0.1 \pm 0.05/ <u>10</u>	1.5 \pm 0.9/ <u>54</u>	3.3	167	Indoles
Retinol-binding protein mg/L	<80	192.0 \pm 78.0/ <u>112</u>	369.2 ^a	21200	Peptides
Spermidine $\mu\text{g/L}$	—	97.2 \pm 45.0/ <u>25</u>	187.2	145	Polyamines
Spermine $\mu\text{g/L}$	—	18.2 \pm 16.2/ <u>25</u>	66.7 ^a	202	Polyamines

Middle molecules ($N = 22$)

Solute	C_N	C_U	C_{MAX}	MW	Group
Adrenomedullin ng/L	13.2 \pm 4.6/ <u>17</u>	41.8 \pm 19.7/ <u>29</u>	81.2	5729	Peptides
Atrial natriuretic peptide ng/L	28.0 \pm 12.2/ <u>23</u>	202.0 \pm 117.3/ <u>27</u>	436.6	3080	Peptides
β_2-microglobulin mg/L	<2.0	55.0 \pm 7.9/ <u>10</u>	100.0 ^a	11818	Peptides
β-endorphin ng/L	<173.3/ <u>10</u>	301.5/ <u>22</u>	492.0 ^a	3465	Peptides
Cholecystokinin ng/L	<20.0	45.9 \pm 32.3/ <u>38</u>	131.5 ^a	3866	Peptides
Clara cell protein (CC16) mg/L	<0.1	3.3 \pm 2.0/ <u>112</u>	12.5 ^a	15800	Peptides
Complement factor D mg/L	1.9 \pm 0.5/ <u>5</u>	19.8 \pm 4.1/ <u>5</u>	26.0 ^a	23750	
Cystatin C mg/L	<1.6	11.8 \pm 3.0/ <u>112</u>	20.0 ^a	13300	Peptides
Degranulation inhibiting protein I^c $\mu\text{g/L}$	321.7 \pm 59.7/ <u>23</u>	713.7 \pm 390.0/ <u>125</u>	1631.4 ^a	14100	Peptides
Delta-sleep inducing peptide $\mu\text{g/L}$	—	1.5 \pm 0.9/ <u>7</u>	3.3	848	Peptides
Endothelin ng/L	20.8 \pm 3.8/ <u>23</u>	63.0 \pm 33.2/ <u>12</u>	129.4	4283	Peptides
Hyaluronic acid $\mu\text{g/L}$	<124.0/ <u>86</u>	215.0 \pm 257.0/ <u>184</u>	1843.0 ^a	25000	Peptides
Interleukin-1$\mu\text{ng/L}$	<160.0/ <u>15</u>	428.0 \pm 134.0/ <u>29</u>	1700.0	32000	Cytokines
Interleukin-6 ng/L	13.3 \pm 3.1/ <u>28</u>	92.3 \pm 117.9/ <u>230</u>	328.1	24500	Cytokines
κ-Ig light chain mg/L	34.0 \pm 15.0/ <u>15</u>	70.0 \pm 60.9/ <u>104</u>	287.0 ^a	25000	Peptides
λ-Ig light chain mg/L	31.0 \pm 11.2/ <u>15</u>	87.0 \pm 60.9/ <u>104</u>	328.0 ^a	25000	Peptides
Leptin $\mu\text{g/L}$	8.4 \pm 6.7/ <u>56</u>	72.0 \pm 60.6/ <u>8</u>	490.0 ^a	16000	Peptides
Methionine-enkephalin ng/L	<18.3/ <u>10</u>	32.2/ <u>22</u>	75.5 ^a	555	Peptides
Neuropeptide Y ng/L	<80.0	64.9 \pm 25.5/ <u>19</u>	115.9	4272	Peptides
Parathyroid hormone $\mu\text{g/L}$	<0.06	1.2 \pm 0.6/ <u>10</u>	2.4	9225	Peptides
Retinol-binding protein mg/L	<80	192.0 \pm 78.0/ <u>112</u>	369.2 ^a	21200	Peptides
Tumor necrosis factor-$\mu\text{ng/L}$	13.3 \pm 3.0/ <u>28</u>	114.0 \pm 147.0/ <u>230</u>	408.0	26000	Cytokines

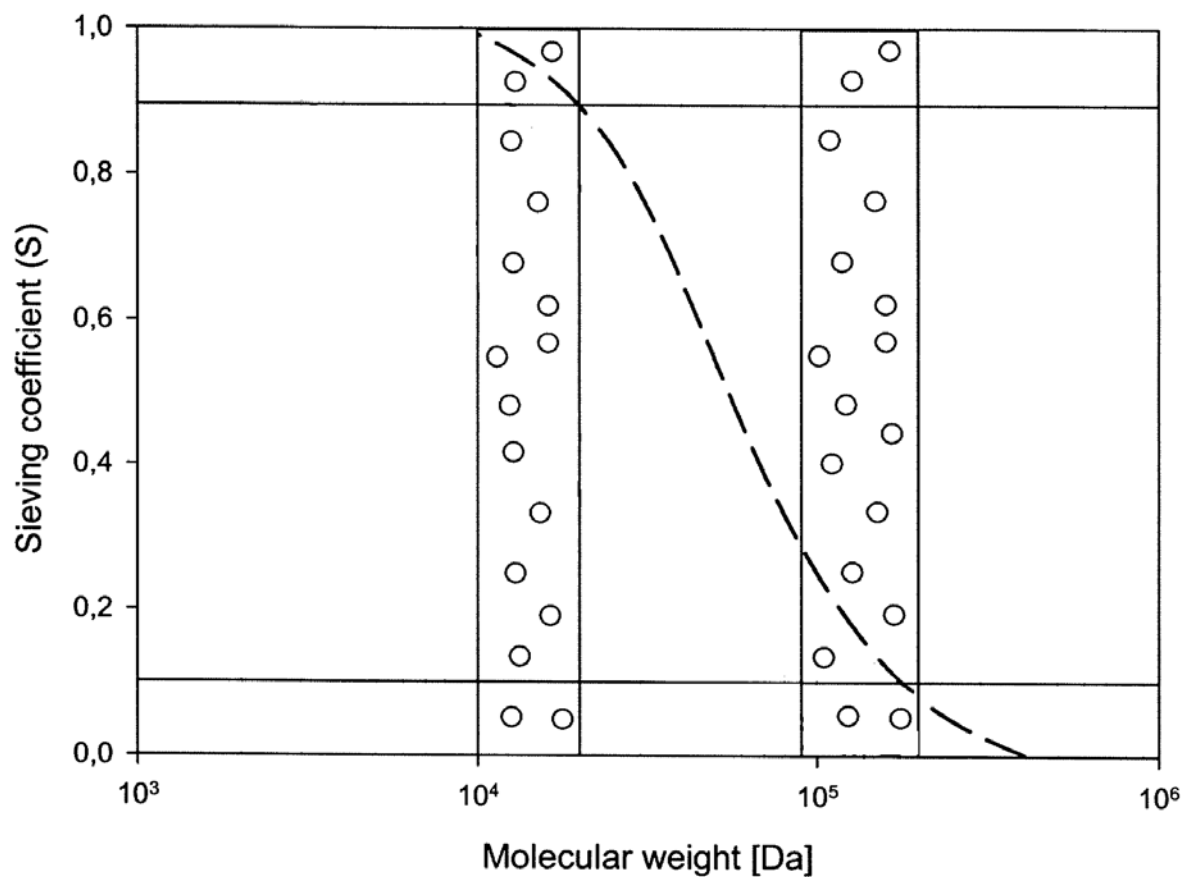
Abbreviations are: C_N , normal concentration; C_U , mean/median uremic concentration; C_{MAX} , maximal uremic concentration; MW, molecular weight, ; CMPF, 3-carboxy-4-methyl-5-propyl-2-furanpropionic acid; AGE, advanced glycation end products, ADMA, asymmetrical dimethylarginine; SDMA, symmetrical dimethylarginine. The underlined numbers behind the slash point to the number of data on which the means or medians have been obtained. No underlined number indicates that no data about the number of samples were available. No number indicates that no n value was given. Normal values are reported as mean \pm SD, or in the case of a single value as a maximum (accompanied by <); uremic values are reported as mean \pm SD or, in the case of a single value, as a median.

Appendix C

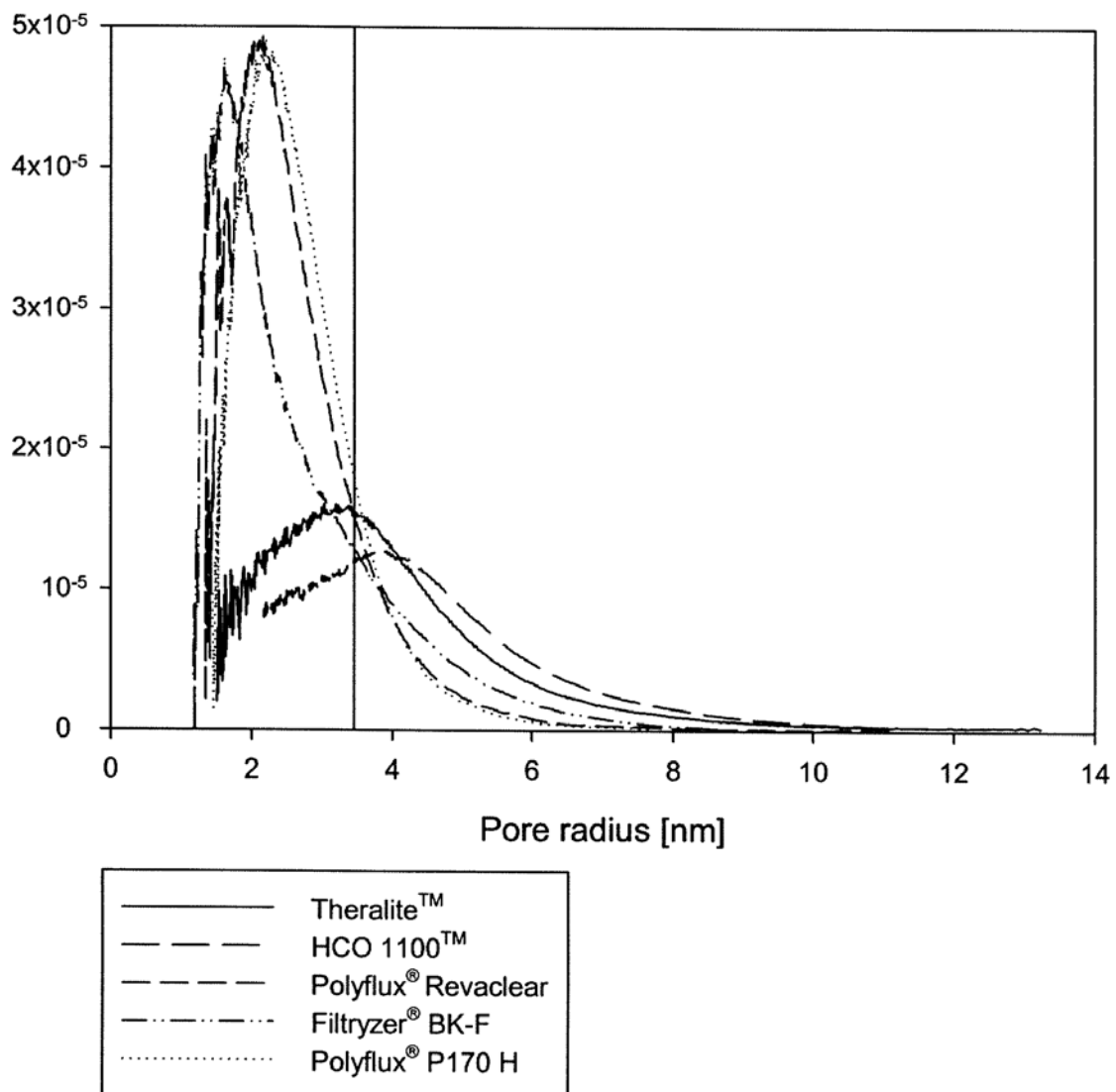
HCO 1000 membrane specification [100,118]

Membrane Specifications	
Ultrafiltration coefficient, ml/(h*mmHg)	52
Inner diameter, μm	300
Wall thickness, μm	100
Pore size in selective skin layer, nm	8 - 12
Membrane Performance	
C_L urea, ml/min	199 - 390
C_L phosphate, ml/min	195 - 354
C_L myoglobin, ml/min	126 - 170
S_0 Vitamin B ₁₂	1.0
S_0 Inulin	1.0
S_0 Myoglobin	0.95
S_0 Albumin	0.2

Dextran sieving curve of HCO 1100 membrane [118]



Selective skin layer pore size distribution of several hemodialysis membranes [118]

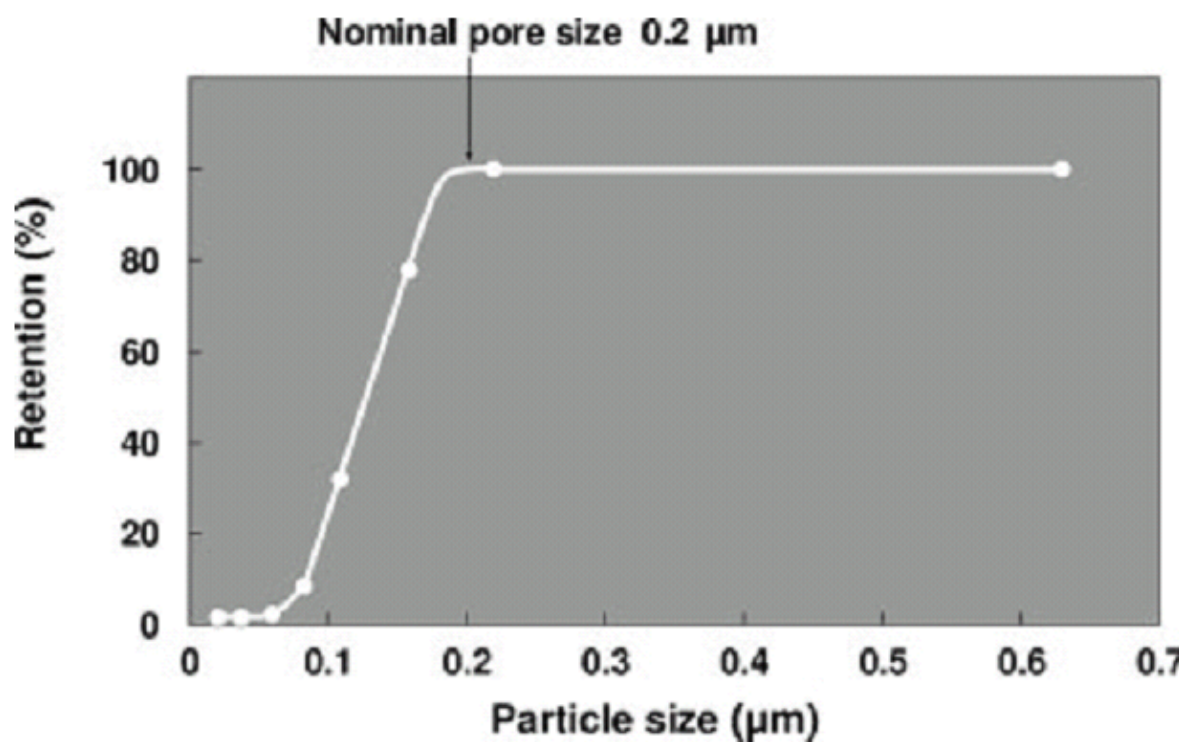


Appendix D

MicroPES TF10 membrane specification [99,98]

Membrane Specifications	
Inner diameter, μm	300
Wall thickness, μm	100
Maximum pore size, μm	0.5
Nominal pore size, μm	0.2
Membrane Performance	
S ₀ Albumin	0.99
S ₀ IgG	0.97
S ₀ Fibrinogen	0.88
S ₀ High Density Lipoprotein	1
S ₀ IgM	0.99
S ₀ Low Density Lipoprotein	0.97
S ₀ Cholesterol	0.97

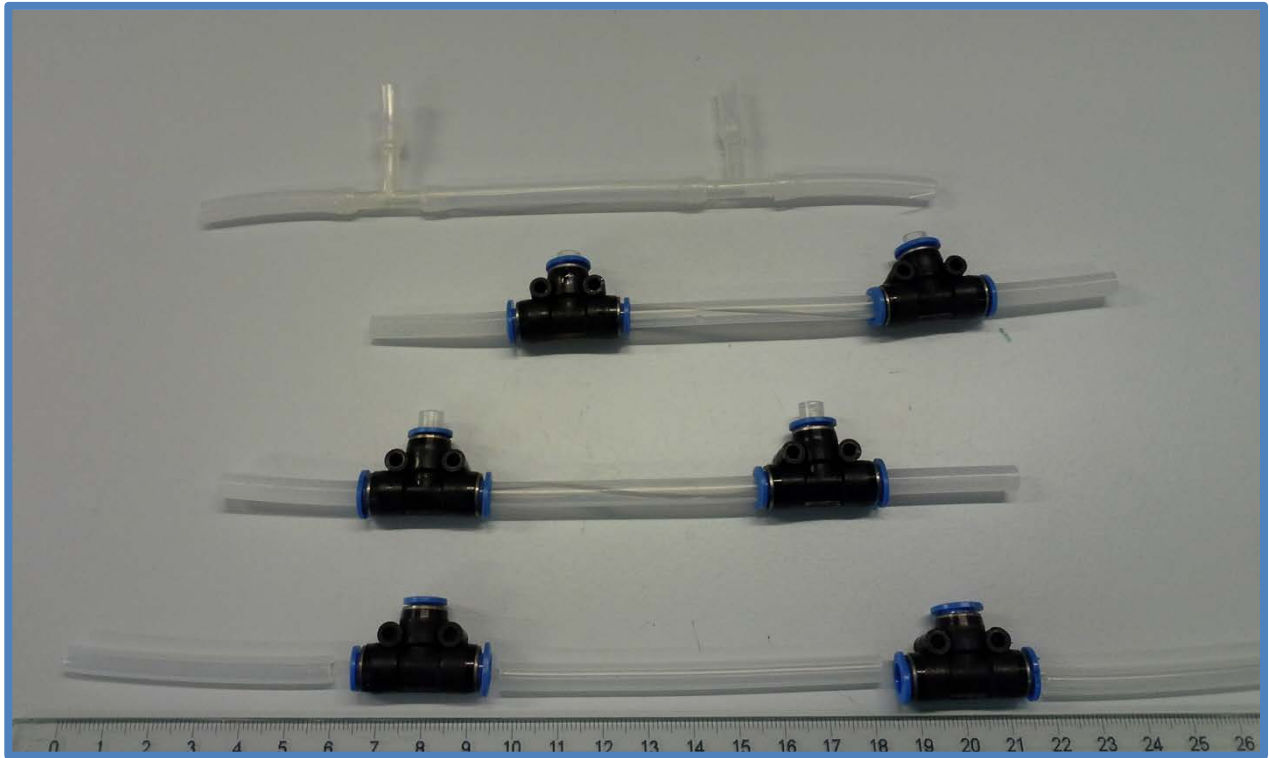
Latex beads sieving curve of MicroPES TF10 membrane [99]



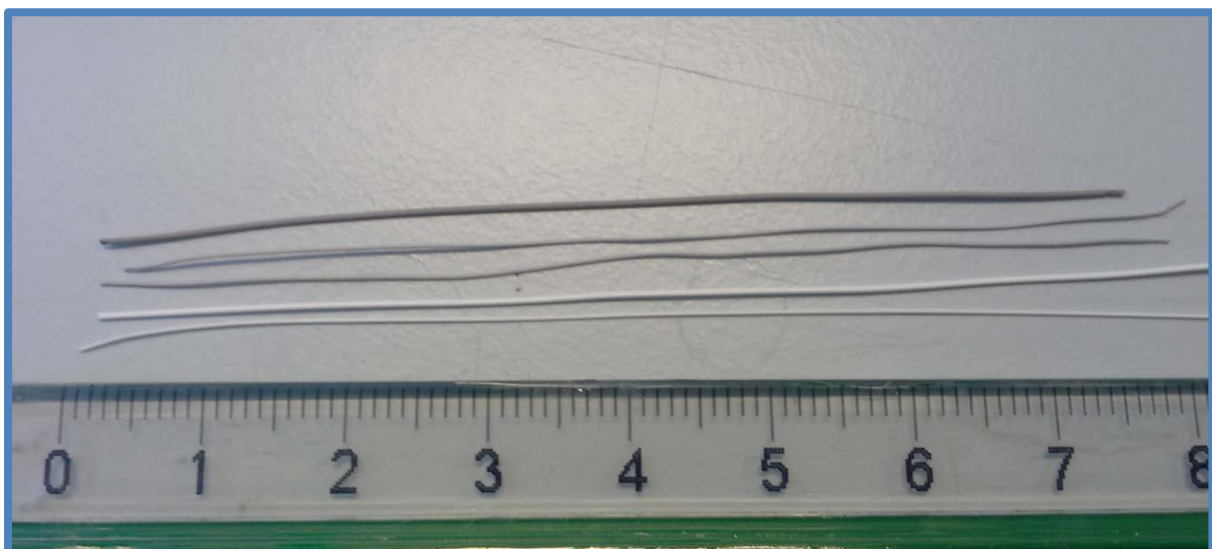
Appendix E

Membranes, mini-modules and the setup used in the current work

Mini modules assembled with reusable and dispensable T-shape connectors



Virgin (white) and L-DOPA coated (darker) HCO 1100 and MicroPES TF10 hollow fiber membranes

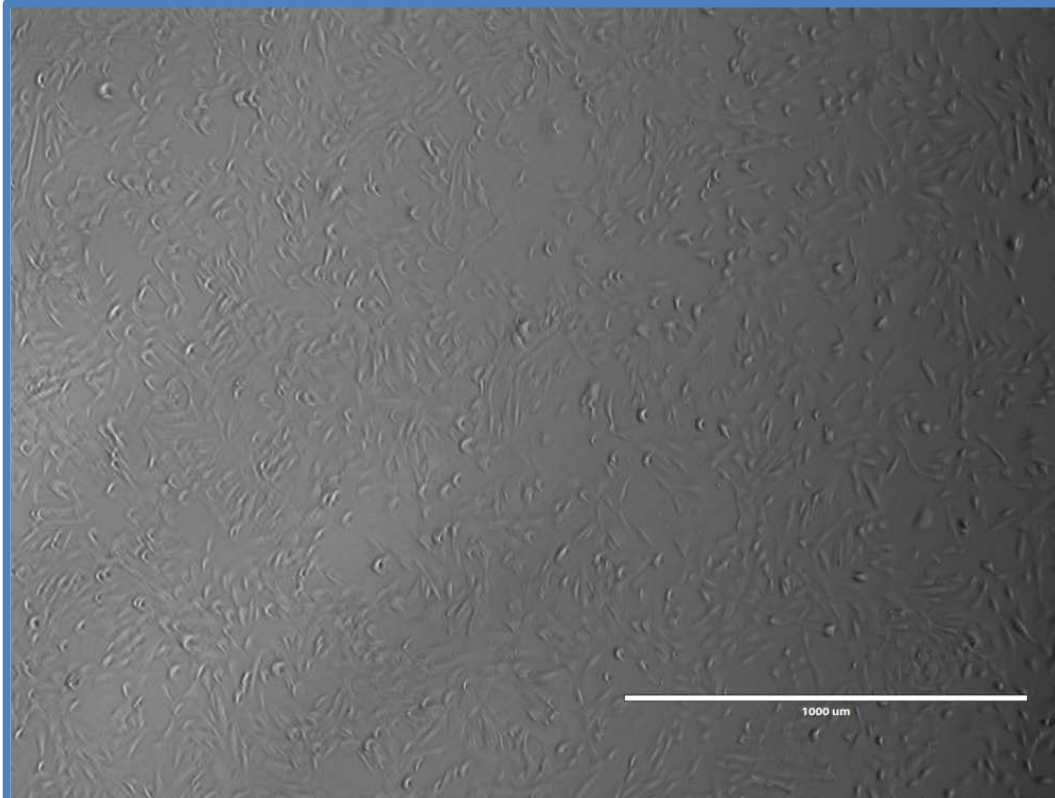


Setup for membrane transport measurements

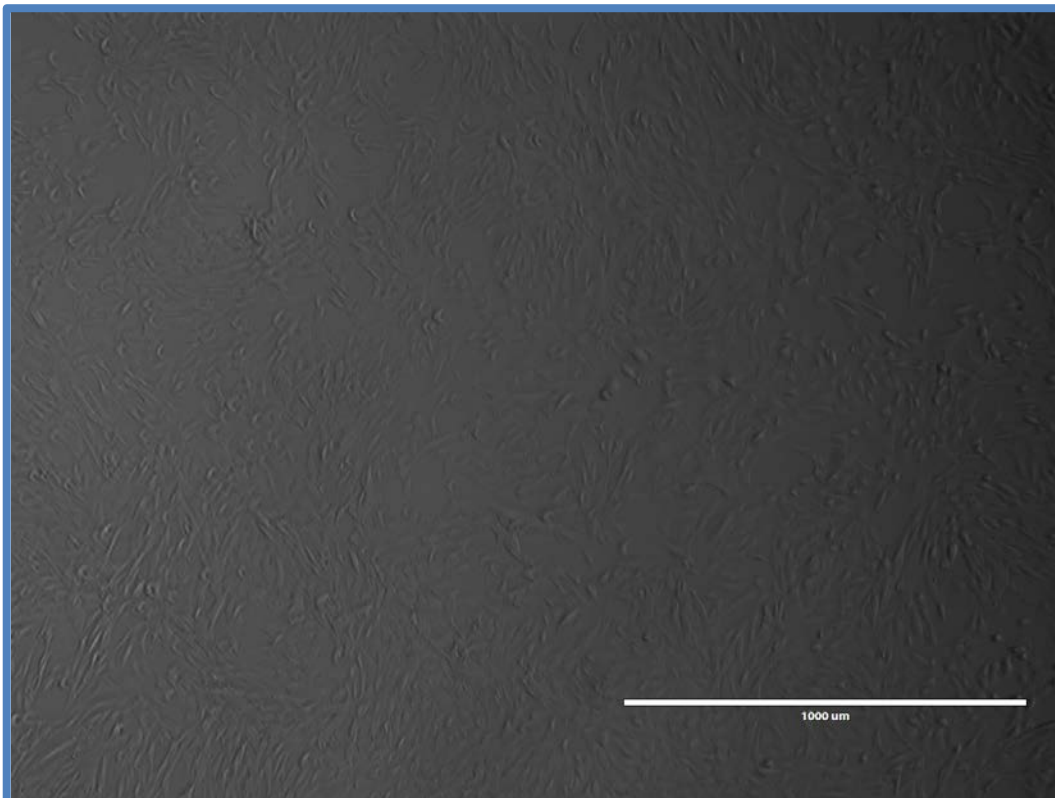


Appendix F

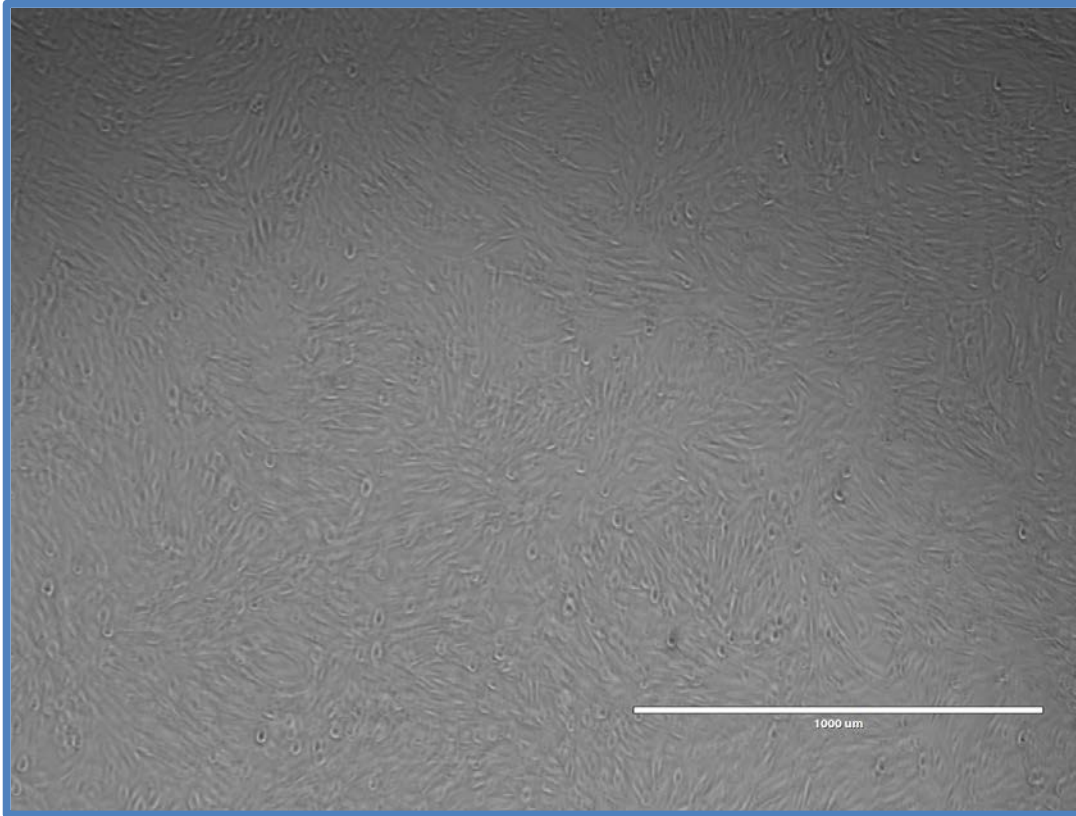
Morphology and growth patterns of subconfluent (a), near confluent (b) and superconfluent (c) human proximal tubular cells



a



b



c